MEANDERLINE NETWORKS INCORPORATING P.I.N. DIODES FOR DIGITAL MULTIPLEXING APPLICATIONS

Thesis submitted to the University of Warwick
for the award of the degree of Ph.D in
Telecommunication Engineering

By

GREG NWACHUKWU ONOH

Department of Engineering

June 1982

To my mother: MAMA NAGU

Your continuous prayers and hard works to give your children a good education was the inspiring factor behind me throughout this work. It is my wish that the successful completion of this work should serve as an answer to your prayers.

CONTENTS

LIST OF FIGURES

FIGURES

FIGURES

ACKNOWLEDGEMENT

I wish to express my sincere thanks and gratitude to my supervisor Dr H.V. Shurmer for his guidance and advice throughout the entire period of this project. I also wish to thank Professor J.L. Douce, Chairman of the Department, for the facilities provided for conducting the investigations and Dr M.K. McPhun for many useful discussions.

In the Engineering Department, my gratitude goes to Mr. W.R. Davies, G. Beesley and S.M. Tran. Same goes to Mr. A. Hulme of the Computer Unit and Mr. L. Bulmer of the Library Centre whose patience and understanding during my late night consultations are well appreciated.

No project could ever take off successfully if funds and material were not available. To this end, I wish to thank the Federal Government of Nigeria and the British Council for their financial support, and the AEI Semiconductor Lincoln who supplied the diodes used in the project.

Finally, I wish to thank my wife for her moral support and help during the difficult days.

DECLARATION

Unless otherwise stated, I claim the credit for the research carried out in this thesis.

The work of the thesis has not been submitted to any other University or Institution. However, part of the thesis may be submitted for publication in technical journals.

SUMMARY

The design of a two-state multiplexer is presented in this project. The design is based on the switching actions of a p.i.n. diode and the filtering characteristics of a meanderline. The diodes used are MEDL types DC 2518G and DC 2418A. The diodes were characterized and the elements of the equivalent circuit found using an insertion loss technique. Effective biasing and driving of the diodes were achieved using a three element low-pass filter and a two-stage transistor driver respectively.

The design of the meanderline networks was based on a new technique developed by the author. The technique involves the evaluation of the coupling and susceptance loading parameters of the meanderlines. These parameters were evaluated from the quasi-static consideration using a function sub-program, fifteen meanderline circuits were designed. The response of the circuits showed an isolation of 12.2dB in the stop-band an insertion loss of only 0.8dB in the passband for an 11-turns meanderlines. Comparison of the measured and computed results showed a disparity less than 5%.

Five categories of digital filters were designed. The basic circuit is a meanderline having p.i.n. diode terminated stubs inside the meander-loops. The diodes serve as ideal transmission-reflection devices, providing either short or open circuit terminations to the stubs depending on the bias applied to them. When a TTL 'O' is driving the diodes a bandpass filter results, but when the drive is a TTL '1', the bandpass filter is converted to a bandstop filter. The maximum transmission coefficient in the 'O' state was $|S_{21}| = 0.95$ and in the '1' state the minimum transmission coefficient was $|S_{21}| = 0.0135$. The maximum bandwidth measured was 39.5%.

These filters were cascaded to form a two and three channel multiplexers. For the diplexer, an assymmetric Y-junction was used in the design. The measured isolation between the two channels was 25.4dB. For the triplexer, a matched cross-junction was used as the common junction. The isolation between channels 1 and 2 was 21dB, while between 2 and 3 it was 10.45 dB.

LIST OF SYMBOLS

Tan δ	Loss tangent
α	Attenuation constant
β	Phase constant
γ	Propagation constant
ε_r	Relative permitivity
θ	Electrical length
λ_g	Guide wavelength
λ_o	Free space wavelength
π	A constant (3.1416)
Γ, ρ	Reflection coefficient
$\Delta \phi$	Differential phase shift
δ	Susceptance parameter
KEFF	Effective dielectric constant
KFE	Even mode coupling parameters
KFO	Odd mode coupling parameters
KM	Mutual coupling
Z_{oe}, Z_{oo}	Mode impedance
Z_o	Characteristic impedance
h	Dielectric height
ξ_o	Free space permitivity
μ_o	Free space permeability

CHAPTER I

INTRODUCTION

Over the past few years, a class of microwave control components is being speedily integrated in many microwave applications. These devices differ from earlier components in that they are electronically controlled as opposed to mechanically controlled devices. The application of these microwave components has been extended to all phases of microwave control systems. At present, components of this sort have been designed and fabricated to operate in the frequency range from VHF to as high as Ku band and above and with power levels extending from milliwatts to kilowatts.

The features of these semiconductor control devices which make them attractive in many microwave systems include their moderate control power requirements (typically 50 milliwatts or less), their high response speed which is less than 20 nanoseconds, their compactness and light weight and most important their long life and high reliability provided by their solid state nature.

Recent technological advances in the use of microwave frequencies for communications, navigation, air surveillance and other aspects of telecommunications

have promoted a growing interest in the integration of semiconductor controlled devices in r.f. filters designed to provide frequency discrimination and signal selection. Such systems make it possible for a single sweep frequency signal generator to cover frequencies of several bands. This is accomplished through the multiplexing of several communication channels operating within a certain frequency band and then switching them so that any of the frequency bands can be obtained.

At lower frequencies, such filters are usually designed using MOS devices in a "switched capacitor" approach. Because of the high speed and power capability required in most microwave applications, this approach is not used above L-band. At microwave frequencies, the technique normally used is to insert a microwave switch at the input or output of the r.f. filter. This means that the switch and the filter have to be designed separately. The drawback to this approach is that when the two are combined together, extra optimization had to be carried out to match their VSWR. Moreover the technique cannot be used in systems where the filters are connected in series.

In this project, a design technique which combats the above drawbacks is presented. The aim is to use the parasitic elements of the semiconductor device in

the filter design. This objective was achieved by incorporating p.i.n. diodes inside the loops of a meanderline. The p.i.n. diode parameters were designed into the circuit in such a way that when a TTL '1' is driving the diode a bandpass filter was obtained but when the drive is a TTL '0', the bandpass filter is converted to a bandstop filter. Using a cascade of these filters, a switchable multi-channel multiplexer was readily realized.

The advantage of this technique is that the diode is an integral part of the filter circuit. Its parameters were used in the filter design. Hence in addition to their normal switching operations, the diodes also serve a purpose in the frequency multiplexing and demultiplexing operations. The diodes used were supplied by AEI Semiconductor Lincoln - types MEDL DC 2518G and DC 2418A.

Strip transmission lines were used throughout this project. Recent years have seen the rapid rise in importance of these miniature structures. At microwave frequencies these transmission lines because of their light weight, small dimensions and easy processing capabilities are being increasingly used in most network design. The design criteria for these types of transmission lines is given in Chapter 2. The production process used is the vacuum evaporation technique. All the necessary steps involved in this

process are given in the same chapter.

Strip transmission lines are invariably accompanied by discontinuities of one type or another. A complete understanding and design of these lines require the characterization of the various discontinuities included in the circuit. The major discontinuities encountered in the project were characterized in Chapter 2. The chapter also presents a new technique of compensating for the effects of the T-junction parasitic reactances.

Errors in the s-parameter measurement of any passive or active circuit make it difficult to obtain an accurate measurement at microwave frequencies. Such an accurate measurement can only be obtained if these errors are eliminated. A computerized measurement technique which has been set up in the University laboratory to give an automatic on-line characterization of any two-port microwave circuit was used to calibrate out the errors in the network analyzer. In the case stripline circuits an additional error is introduced by the parasitics of the coaxial-to-stripline transition. A technique is given in Chapter 2 by which this additional error can be characterized.

The prediction of any circuit response, coupled by the use of measurement data to adjust the circuit parameters can be very effective in an effort to

achieve a final design which meets the desired performance. This is made possible by the availability of an analysis program which besides being rapid, also allows for the precise determination of the network functions. Chapter 3 describes the analysis program used in the project. The program uses the ABCD matrix approach and can handle four basic types of circuit elements.

Chapter 4 deals with the characterization of the p.i.n. diode. This diode is a variable resistance device. Its resistance is controlled by the amount of bias applied to it. Under forward bias, this resistance varies appreciably with change in the bias level, but under reverse bias, changes in the bias signal does not produce significant change in the resistance value. This characteristic makes the diode an ideal control device for most microwave applications. Its range of applications is limited only by the designers ingenuity rather than the operating characteristics of the device.

The chapter also describes the physics of the p.i.n. diode behaviour from which an equivalent circuit used throughout the project was derived. The component of this equivalent circuit was later obtained using an insertion loss technique. The measurement procedure and the design of all the associated bias circuitry are given in the chapter.

Chapter 5 reviews the switching characteristics of the p.i.n. diode which played a significant part in the multiplexer design. In particular, the effects of synchronous and stagger tuning techniques are presented.

In Chapter 6, an experimental investigation of the properties of a meanderline is described taking into account only the coupling between adjacent conductors. A procedure is given for computing the amplitude frequency characteristic and the susceptance loading parameters of the meanderline. The chapter also describes a compensation technique which was used to reduce the effects of the susceptance loading parameters of the meanderline.

Chapter 7 describes the design steps of the two-state multiplexer. The basic circuit is a meanderline circuit loaded with p.i.n. diode terminated stubs inside the meander-loops. A technique is given for matching the magnitude of the reflection coefficient of the diode circuit in its two bias states. The chapter also shows how to match the common junction of the designed multiplexer.

The thesis ends with a final conclusion which reviews the achievements and shortfalls of the project. Suggestions are given for further works resulting from the outcome of this project. Two papers have been published by the author on the results of this

work and these, together with all the appendices, are attached at the end of the thesis report.

work and these, together with all the appendices, are attached at the end of the thesis report.

CHAPTER 2

MICROWAVE CIRCUIT DESIGN

2.1 INTRODUCTION

The starting point of any microwave circuit design rests with the choice of the transmission line and dielectric material to be used in the fabrication of the circuits. At microwave frequencies, many factors influence the decision leading to the correct choice of the transmission line and dielectric material. The most important of these is that the structure should be 'planar' in configuration. A planar configuration implies that the characteristics of the structure can be determined by its dimensions in a single plane. Thus the width of a line on a dielectric substrate can be adjusted to control its characteristic impedance. This makes the circuit fabrication easier to be carried out by the techniques of photolitography.

There are several transmission line structures that satisfy the requirement of being planar. The most common of these are striplines, slotlines and coplanar waveguides. Out of these, striplines are the most frequently used. This is mainly due to the fact that its mode of propagation allows an easy analysis and yields wide band circuits. Also simple transitions to coaxial circuits are feasible.

There are two types of striplines currently in use. These are the balanced triplate and microstrip lines. Microstrip differs from triplate in that it is open at the top. This open configuration makes the microstrip very convenient for use in microwave integrated circuits. Also adjustments or tuning can be carried out easily after the circuits have been fabricated. However, along with these advantages, the open nature of the microstrip brings in some complications in the analysis and design. This is due to the fact that the presence of the dielectric-air-interface modifies the mode of propagation in microstrip to a non-transverse electromagnetic hybrid mode as compared to the pure TEM mode in the balanced triplate.

2.2 EVALUATION OF LINE PARAMETERS

2.2.1 Characteristic impedance: The essential parameters of striplines are the characteristic impedance and the attenuation of the line. A lot of work has been done on the techniques of evaluating stripline parameters and most of these works have given rise to numerical expression which can be used for such evaluation[1,2]. The evaluation of the parameters of the transmission lines used here was based on the expressions due to Wheeler[2] but modified to include the attenuation of

the line. This attenuation was computed from the incremental inductance rule approach. In this approach the conductor loss was derived in terms of the series resistance which is attributed to skin effect.

Two programs were written for the evaluation of the linc parameters. The programs input the dielectric constant of the material, the height of the dielectric and the conductor thickness. It then outputs the characteristic impedance of the line for various line widths. Fig. 2.1 defines the line parameters used in the programs. The programs are given in Appendix A.

2.2.2 Dielectric material: Choice of the right dielectric material is equally essential if accurate results are to be obtained. The factors considered here were not the same as those for choosing the substrate of a standard printed circuit board. Here the substrate is an integral part of the circuit and its characteristics affect the circuit performance. A lossy dielectric substrate will appreciable increase the insertion loss of the circuit. For these reasons, only those materials having a low loss tangent, suitable copper cladding and good environmental characteristics were considered.

Despite the large selection available, there is no universally accepted substrate which is best all round. Each material has advantages which make it

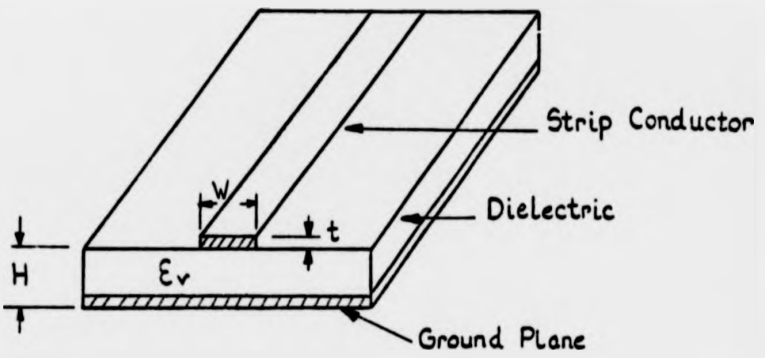

(a) Microstrip

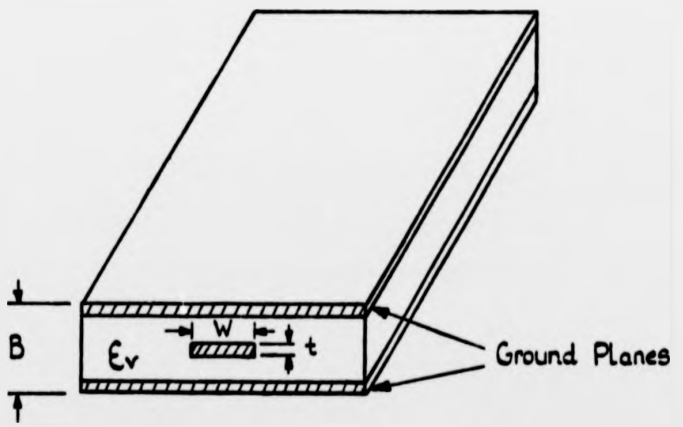

(b) Triplate

Fig.2.1 Planar Transmission lines used in MIC

desirable for some specific applications and disadvantages which limit its usefulness in other applications. Following an investigation into various copper clad materials, polyguide and duroid were selected for the project. The materials were chosen because of their high degree of compatibility with the production process.

Their dielectric loss was computed using the expression:

$$\alpha_d = \frac{27.3\sqrt{\varepsilon_r}}{\lambda_o} \cdot \tan\delta \quad \text{dB/unit length} \qquad 2.1$$

where α_d is the dielectric loss and tan δ is the loss tangent.

This loss unlike the conductor loss, do not vary with the transmission line configuration and is strictly a function of the dielectric material and the operating frequency.

2.3 PROCESSING TECHNIQUES

2.3.1 Masking and photolithograph: After computing the dimensions of the striplines making up the circuits, these are then fabricated as described below. First the desired artwork was drawn on 'cut-N-strip' film using a coradograph machine. The 'cut-N-strip' is a two-layered plastic film whose red film is opaque to

ultra violet light. When cut by the coradograph machine, this red part can be stripped away, thus exposing a white part which represents the required conductor pattern. The coradograph machine has vernier scales which permit the accurate positioning of the cutting blades to within ±0.01mm. The drawings were made ten or twenty times the actual size required so that any cutting or stripping irregularities would be significantly reduced during the photographic process.

The photo reduction was carried out in the laboratory. First, the approximate size reduction was obtained using a graph attached near the camera. By using a hand scale, the accurate size was obtained by adjusting the camera on a dummy photo plate and measuring the image. The same image was also examined through a travelling microscope to ensure sharp focussing. The focussing and aperture control were carried out by adjustments within the lens. The exposure time was automatically controlled to suit the reduction size and the high Kodak resolution plates used.

The development time was rigidly controlled and carried out according to table 2.1.

Throughout the process, the plates were gently agitated to ensure even distribution of the solution.

Table 2.1: Processing of Kodak Slides after exposure

Process	Solution	Time
Pre-wash	De-ionized water	2 mins
Developer	The developer used is Kodak HRP. This is mixed with de-ionized water in the ratio of 1:3	2 mins
Stopper	5% aquerous acetic acid	30 secs
Fixer	Kodafix and de-ionized water in ratio of 1:3	4 mins
Final wash	De-ionized water	15 mins

2.3.2 Circuit fabrication: The method adopted uses ready metallized substrates. Utmost care and cleanliness were observed at all steps. The substrate was first cleaned with acetone using an ultrasonic cleaner. It was then blow dried with filtered air. The application of the photo-resist is the most critical step in the process. Here the substrate was vacuum held on a rotating spinner. A thin layer of resist was evenly applied to the substrate and then spun at 2000 rpm for 20 seconds. This speed and time gave the substrate a 2-micron coat. Positive photo resist AZ 111 was used.

The substrate was then pre-baked for five

minutes at a temperature of $85^{o} \pm 5^{o}C$ using infra red light. It was then exposed on the mask-liner for 30 seconds and then developed for the same period. The developer is a solution of AZ 351 and de-ionized water. After development, the substrate was washed and post-baked for 20 minutes. Since it was essential to retain the copper ground plane, this area was coated again with photo-resist and once more baked for eight minutes.

Finally the unwanted copper was removed using standard etching techniques. The etchant is a solution of 50 grams of ammonium persulphate in 350 mils of water. The substrate was then washed in a cold stream of water and then blow dried using filtered air. To ensure mechanical stability, the substrate was glued to ¼ inch thick aluminium, using conductive epoxy. Apart from providing the mechanical support, the aluminium also provides a place for the coaxial connectors.

2.4 MEASUREMENT TECHNIQUES

2.4.1 Measurement techniques: Microwave circuit measurements are always made difficult by the fact that these measurements are not often made at the plane of the circuit element. Instead the measurements are made at or referred to some reference plane physically

removed from the circuit. In triplate and microstrip medium, this problem is made worse by the fact that these transmission lines are not often used for system interconnection. Therefore in all such cases, it is always necessary to transform from coaxial line into the stripline assembly. Unfortunately, the use of these coaxial transitions introduce some measurement errors which degrade the circuit performance. Moreover, the network analyzer equipment which was used throughout this work introduces its own errors which are inherent in the equipment.

For accurate measurements, it is necessary that all these errors are either eliminated or accounted for in the results. Two stages of correction were used here. First computer correction was used to calibrate out the network analyzer errors up to and including the APC-7 connector. Secondly, the errors arising from the coaxial transitions were separately characterized and the parasitic elements representing the transition were evaluated and embodied in all the designs.

Details of the set up of the on-line computer corrected network analyzer are given in the literature[3]. The basic principles of operation is that error arising internally in the network analyzer due to the variations of coupler directivity or amplifier gain are evaluated and stored by the computer via a series of preliminary calibration runs using standard terminations such as

matched or sliding loads. During each of these runs, either the reflection or the transmission coefficient of the standard termination is measured by the network analyzer. The results are then recorded and stored by the computer. Since the true reflection or transmission coefficients of these standard terminations are known, the overall effects of the errors at each frequency can be computed. Subsequent runs using the device under test are carried out for the same frequency range. The previously computed error data is then subtracted from the measured data to give the corrected results over the required bandwidth.

2.4.2 Coaxial-to-strip transition: The other significant source of measurement error comes from the transition between the launcher and the stripline assembly. The main problem at this transition is the discontinuity caused by the launcher tab. Since this tab lies on top of the stripline conductor, it increases its thickness and consequently reduces its characteristic impedance. This causes mismatch and degradation of the circuit performance. With the utilization of the computer correction described above, it was only possible to apply correction for the network analyzer errors up to and including the APC-7 SMA connector. Hence the error caused by the coaxial transitions had to be characterized separately.

The early technique proposed by Wight[4] for such characterization consists of using the launcher to make input measurements on various lengths of open circuited 50 ohm line. The excess phase characteristics generated by this open circuited line was then used to find the equivalent circuit of the parasitic reactances representing the transition. This followed from the knowledge that the excess phase angle at a line length of half wavelength was due entirely to the launcher shunt capacitance whilst at quarter wavelength it was due entirely to the launcher series inductance.

By superimposing the data for the electrical length on a transmission line chart, the numerical values for the inductance and capacitance can be evaluated. The disadvantage of this procedure is that the numerical evaluation of these reactive parasitics for large range of frequency steps is tedious. Moreover, the graphical solution of any problem is always an approximation since its accuracy depends on the person reading the graph.

Here the parasitic elements associated with the transition were evaluated by first assuming an approximate model for the discontinuity effects. The performance corresponding to the initial element values for the model was computed and compared with the required performance. The corresponding disparity or error function was then minimized until the model

performance falls within a specified range. The required performance was determined by measuring the input impedance of the circuit jig using the on-line computer corrected network analyzer.

Fig. 2.2 (a) shows the jig used in the characterization. It consists of a launcher feeding a 50 ohm open circuited line; MM^1 is the measurement plane, TT^1 is the transition region and RR^1 is the reference plane located along the line. The model chosen is shown in Fig. 2.2 (b). It comprises of a length of line, l_o, representing the physical length of the launcher between the junction with the end of the stripline and the coaxial interface at the other end. The transition region was represented by an equivalent T-network. It was assumed that this T-network was situated at the physical transition between the launcher and the end of the strip conductor. The length of the 50 ohm load is represented by l_1. There is also an additional length of line, Δl, due to the open circuited end effect of the line[5].

At any frequency, the input impedance of the transition region is given by:

$$Z_m = \frac{Z_{11}Z_L + Z_{11}Z_{22} - Z_{12}^2}{Z_L + Z_{22}} \qquad 2.2$$

where Z_L is the load impedance of the open circuited

line given by

$$Z_L = Z_o \text{Coth } Y(l_1 + \Delta l) \qquad 2.3$$

The input impedance Z_m of the transition region is related to the measured input impedance Z_{in} via the transmission line equation

$$Z_m = Z_o \left\{ \frac{Z_{in} - jZ_o \tan \beta l}{Z_o - jZ_{in} \tan \beta l} \right\} \qquad 2.4$$

2.4.3 Test and calibration results: To obtain the values of the T-network, six open circuited lines corresponding to different terminating impedances were made on two substrates. The coaxial launcher used was Selectro SMA connector type 50-645. The launcher was held in contact with the strip conductor by pressure on the tab. The measuring jig is shown in fig. 2.2. The input impedance of the test fixture was then measured as a function of frequency using the automatic network analyzer. The results are shown in fig. 2.3 From the results obtained and using equations 2.2 - 2.4, the explicit values of the parasitic reactances representing the transition were found as shown in fig. 2.2 (c).

To test the accuracy of these values, two 50 ohms calibration pieces were made using the same dielectric material and coaxial connectors. These were then measured using the network analyzer. The

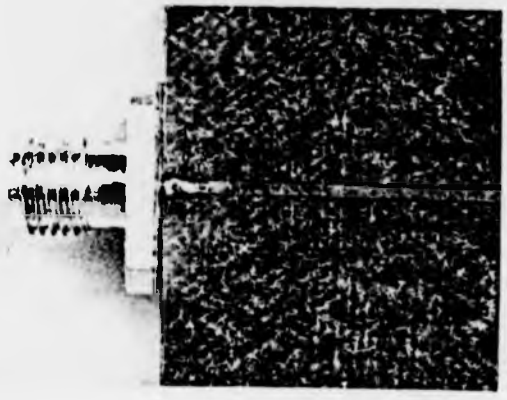

Fig. 2.2 (a) Jig for measuring coaxial-to-strip transition

results were then compared with the results computed using the equivalent circuit of fig. 2.4 which incorporates the previously obtained values of the transition parasitics. The measured and computed results are shown in fig. 2.5. Examination of these results shows a close agreement between the measured and the computed results.

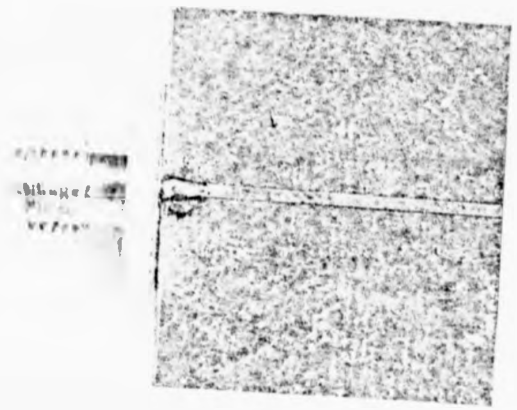

Fig. 2.2 (a) Jig for measuring coaxial-to-strip transition

results were then compared with the results computed using the equivalent circuit of fig. 2.4 which incorporates the previously obtained values of the transition parasitics. The measured and computed results are shown in fig. 2.5. Examination of these results shows a close agreement between the measured and the computed results.

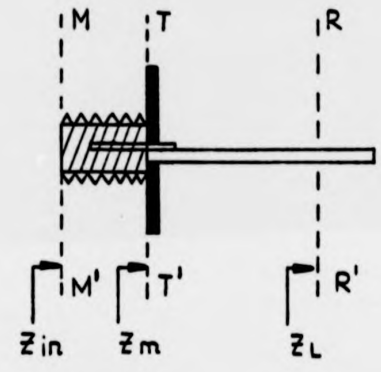

(b) Launcher feeding 50 Ω line

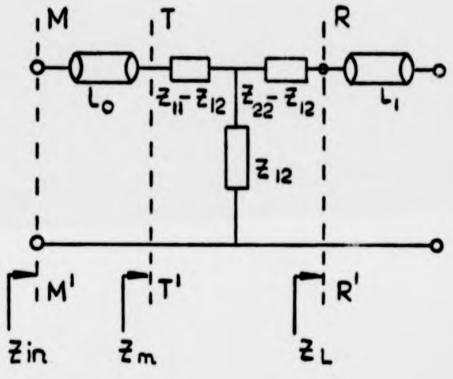

Model for transition

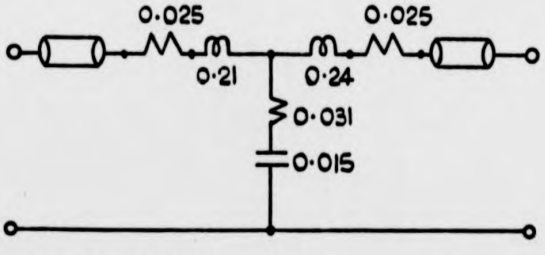

(c) Transition parasitics

Fig.2.2 Coaxial - to - stripline transition.

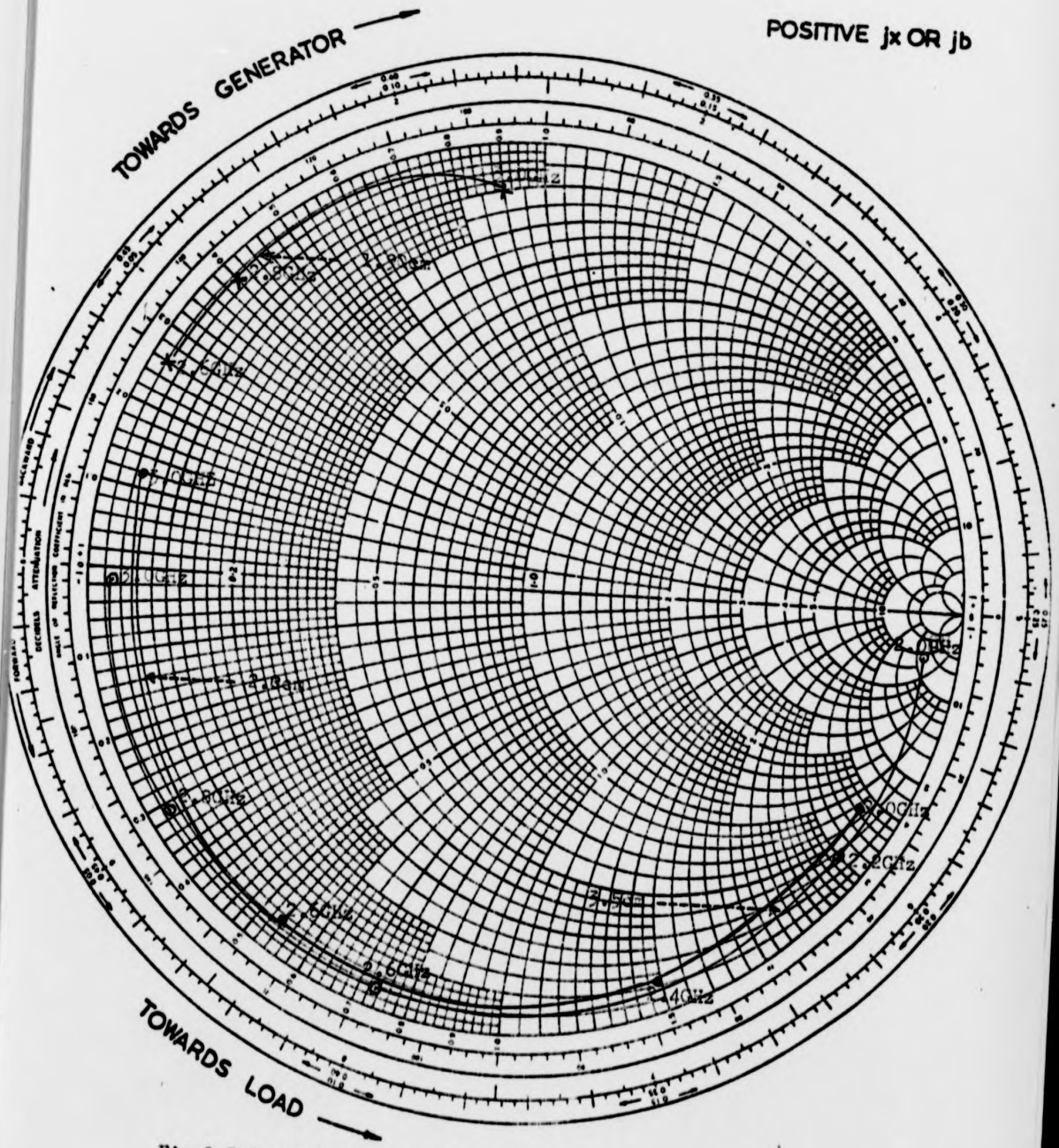

Fig.2.3 Input impedance of coaxial transition.

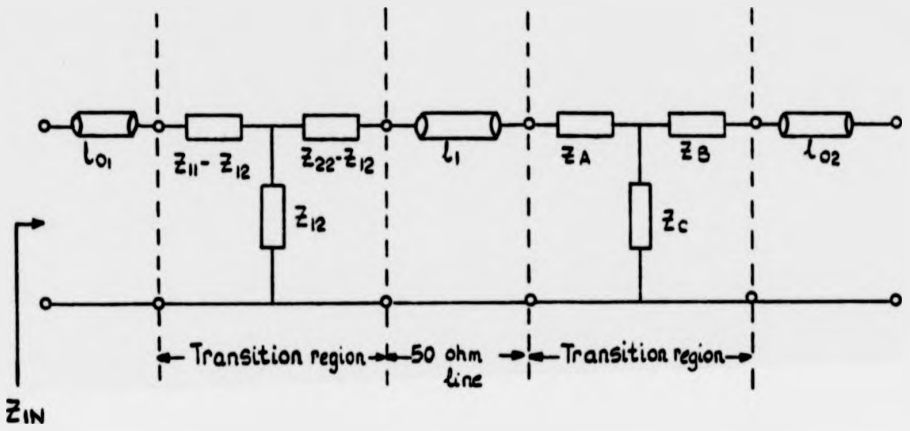

Fig.2.4 Test fixture for measuring through calibration line.

2.5 CHARACTERIZATION OF STRIPLINE DISCONTINUITIES

2.5.1 T-junction discontinuity: A complete understanding and design of microwave circuits require the characterization of various discontinuities included in the circuit. Apart from the discontinuity at the coaxial transition, the three other important discontinuities encountered in this work are:-

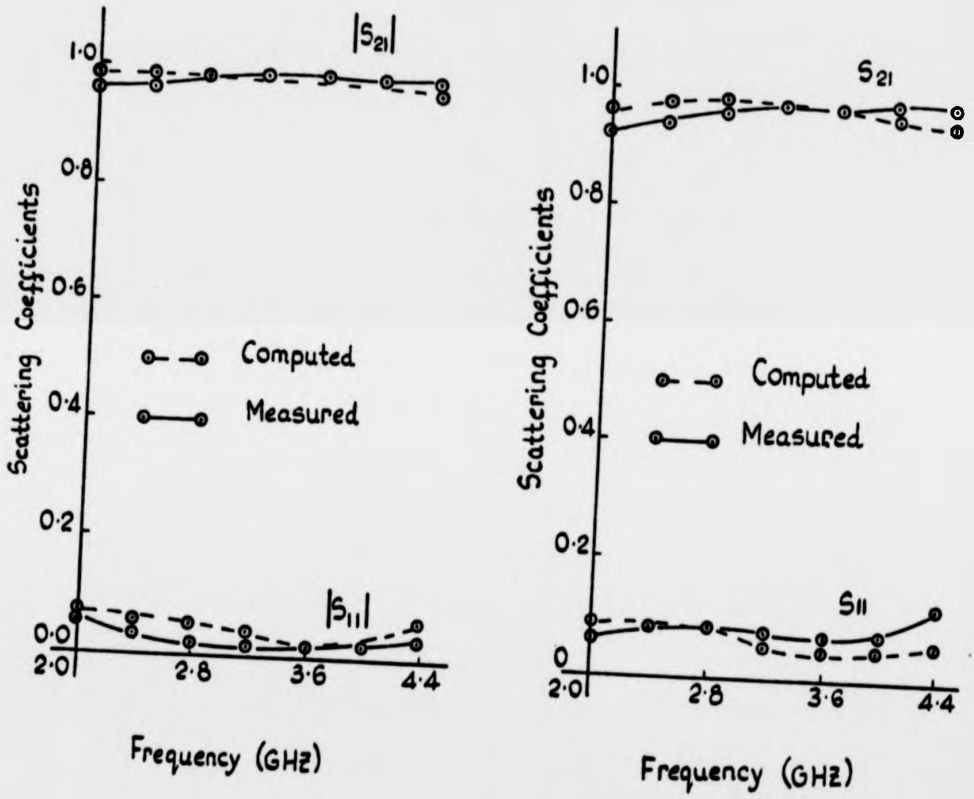

Fig.2.5 Variations of scattering coefficients with frequency for calibration pieces.

T-junction, step and right-angled bend. The first two are characterized in this section.

The structure and reference planes associated with the T-junction are shown in fig. 2.6. There are two main problems associated with this junction. These are the effects of the parasitic reactances associated with the discontinuity and the shift in the designed centre frequency resulting from it. The majority of reported procedures for determining these effects have resulted in many approximate formulae which can be used to evaluate the parasitic elements associated with the junction. However, because of the difficulties encountered in the use of these formulae, it was decided to opt for the compensation rather than the evaluation of these parasitics.

A compensation technique which has worked well for frequencies up to 15GHZ has been described by Dydyk[6]. The approach was to modify the line dimensions in the vicinity of the junction. Though this technique eliminates the shift in the reference plane, it does not account for the parasitic reactances associated with the discontinuity. To the best of the present author's knowledge, there are no known techniques for compensating for this reactance. A technique tried here involves introducing a slit across the width of the main stub line opposite the branch arms.

A narrow slit cut transversely into the microstrip line yields a predominantly series inductance effect[7]. Thus, if the exact value of the discontinuity capacitance is known, it is possible to neutralize its effect with a narrow slit. The first step then was to determine the relationship between the inductance introduced by the slit and the slits dimensions. Knowledge of this and the discontinuity capacitance enable an appropriate compensated network to be designed.

A narrow transverse slit and the equivalent circuit adopted by the author is shown in fig. 2.7. To find the value of the slit inductance, six 50 ohms lines were made on a 0.031 inch duroid substrates. Each line has a transverse slit of specific dimensions. The response of each line was then measured as a function of frequency using the on-line computer corrected network analyzer. By comparing the results with that of an unloaded 50 ohm line, the value of each slit reactance was found for various frequency steps. Using these values, a plot of slit inductance against slit width and depth was constructed as shown in fig. 2.8

Fig. B.1 shows the fully compensated T-junction. The dimensions of the line were obtained as explained in Appendix B. The response of this network was

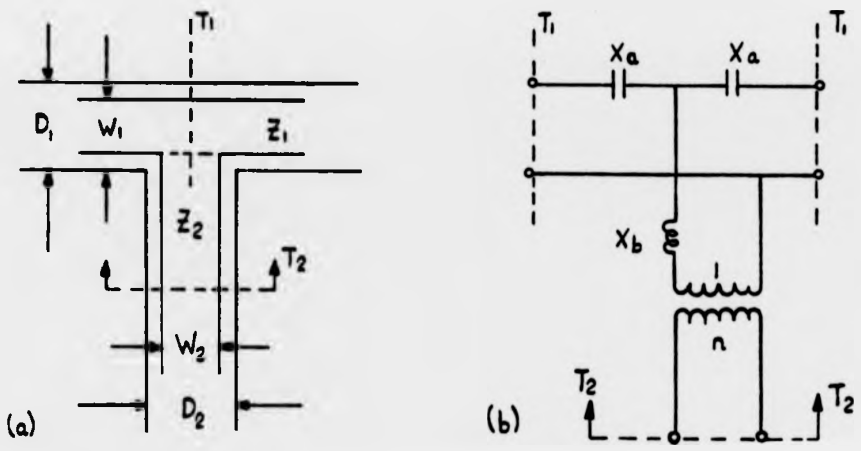

Fig.2.6 Structure and reference planes associated with T-junction.

measured and compared with the uncompensated junction. The result is shown in fig. 2.9.

2.5.2 *Step discontinuity:* This type of discontinuity was encountered here in the design of the biasing and matching circuits used in the later chapters. Unlike the T-junctions, there is no satisfactory way of compensating for the parasitic reactances associated with this discontinuity. Tapering the lines as suggested by Edwards[8] will in the opinion

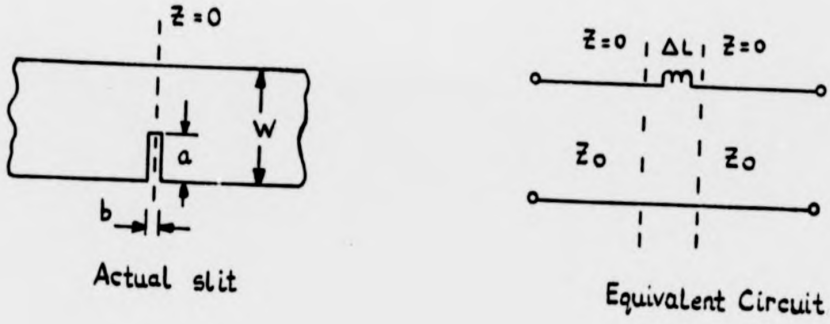

Fig. 2.7 The narrow transverse slit.

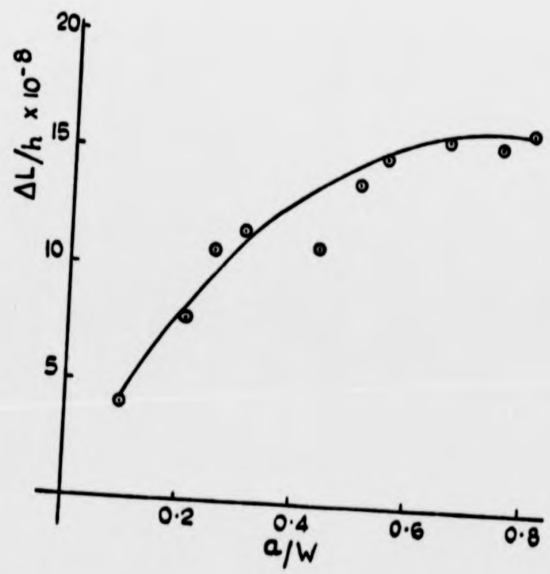

Fig.2.8 Variations of the slit inductance.

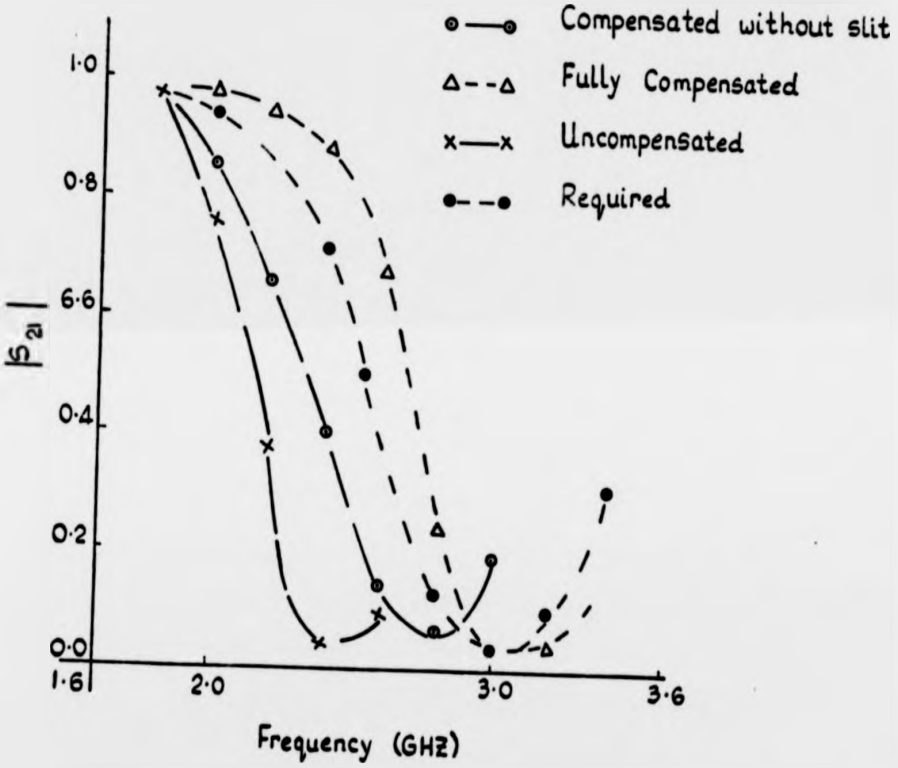

Fig.2.9 Response of T-junction.

of the author limit the useful properties obtained with circuits having this type of junction. Hence it was decided to fully characterize the discontinuity and evaluate the parasitic elements representing it. These elements are then embodied in all designs involving the use of this type of junction.

The characterization is similar to that used for the coaxial transitions where the discontinuity is represented by a three element equivalent circuit. Initial values for this equivalent circuit were then obtained by making input impedance measurements using the automatic network analyzer. The test fixture and the equivalent used in the characterization is shown in fig. 2.10. The first T-network represents the parasitic elements of the launcher, the second T-network represents the discontinuity effects of the two lines having widths W_1 and W_2. There is also an end effect due to the open circuited line. This is represented by an additional line length Δl.

To simplify the analysis, the equivalent circuit was partitioned into five planes as shown. From transmission line theory, the impedance at plane WW^1 is given by

$$Z_w = \frac{Z'_{11}Z_L + Z'_{11}Z'_{22} - Z'^2_{12}}{Z_L + Z'_{22}} \qquad 2.5$$

where Z_L is the load impedance of an open circuited line

given by:- $Z_L = Z_2 \text{ Coth } \gamma(l_2 + \Delta l)$

and Δl is the length due to the end effect.

The impedance at plane VV^1 is given by

$$Z_v = Z_1 \left[\frac{Z_\omega - jZ_1 \tanh(\gamma l_1)}{Z_1 - Z_\omega \tanh(\gamma l_1)}\right] \qquad 2.6$$

At plane UU

$$Z_u = \frac{Z_{11} Z_v + Z_{11}Z_{22} - Z_{12}}{Z_v + Z_{22}} \qquad 2.7$$

This is related to the measured input impedance Z_{in} via the transmission line equation:

$$Z_u = Z_o \left[\frac{Z_{in} - jZ_o \tan \beta l_o}{Z_o - jZ_{in} \tan \beta l_o}\right] \qquad 2.8$$

To find the values of the T-network representing the step-discontinuity, three step-impedance transformers with different width ratios were made on polyguide substrate. The input impedance of the open-circuited transformers were then measured using the automatic network analyzer over the frequency ranges 2.0 - 6.0 GHz in steps of 200 MHz. The results are shown in fig. 2.11 . By incorporating the values of the coaxial transitions which were evaluated earlier, it was possible to evaluate the values of the T-network as shown in fig. 2.12 . For the series

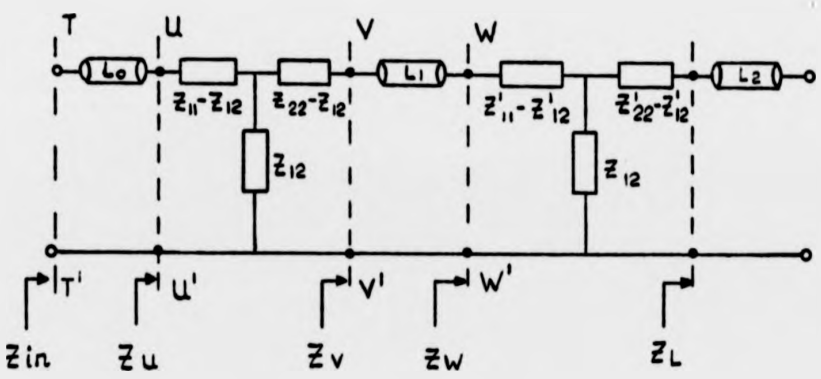

Fig.2.10 Test fixture and equivalent circuit of step

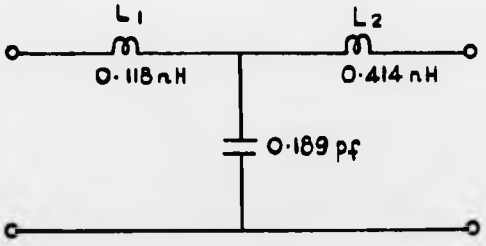

Fig.2.12 Values of T - networt.

inductance arms, these values are within five percent of that obtained using the methods of Gupta[9], however the value of the shunt arm is more than 14 percent of that obtained using the same method.

To find the effects of the width ratio using the above values, two port transformers were made and measured over the same frequency range. The results are shown in fig. 2.13. The effects of neglecting

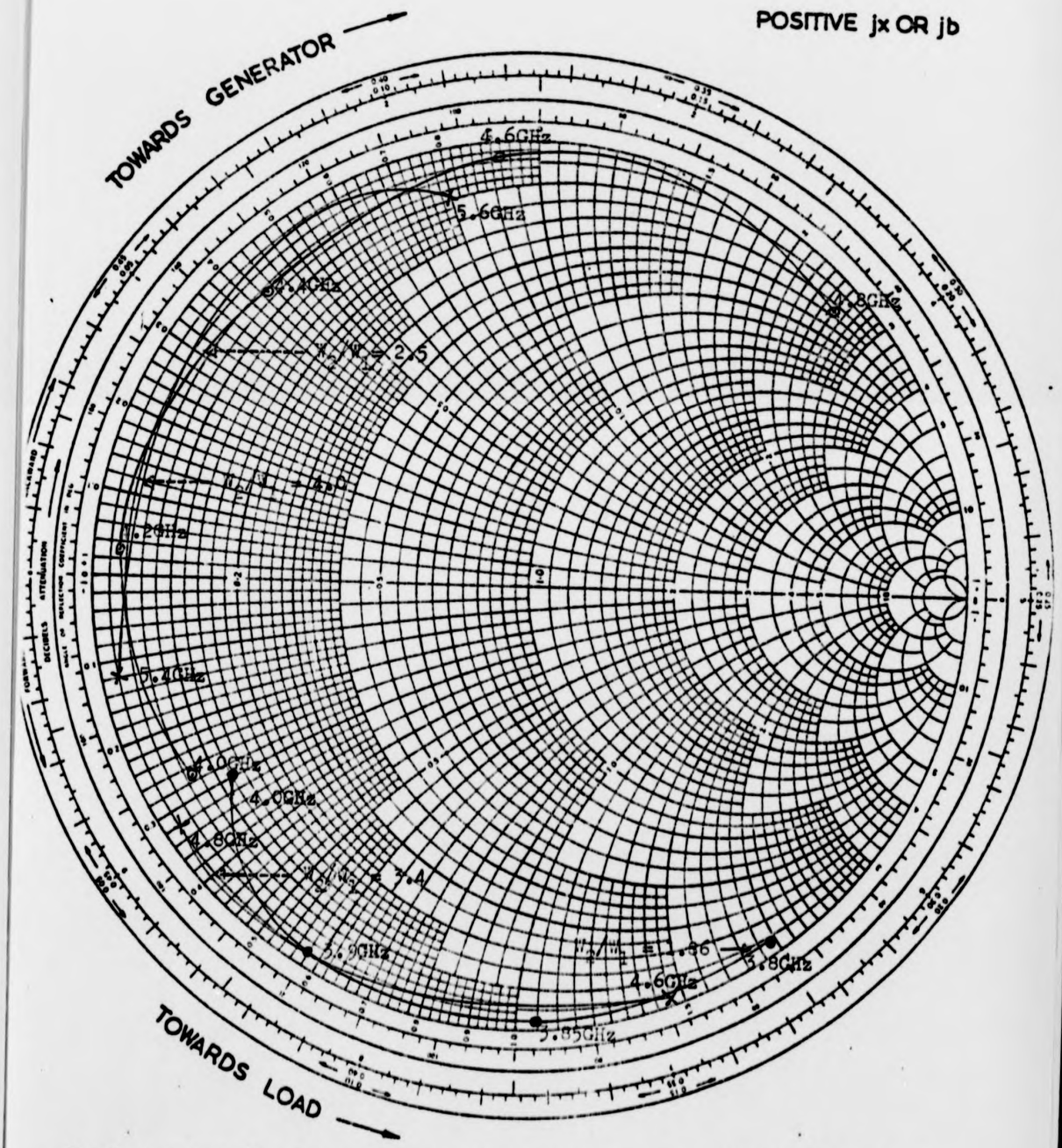

Fig.2.11 Input impedance of open circuited transformers. NEGATIVE jx OR jb

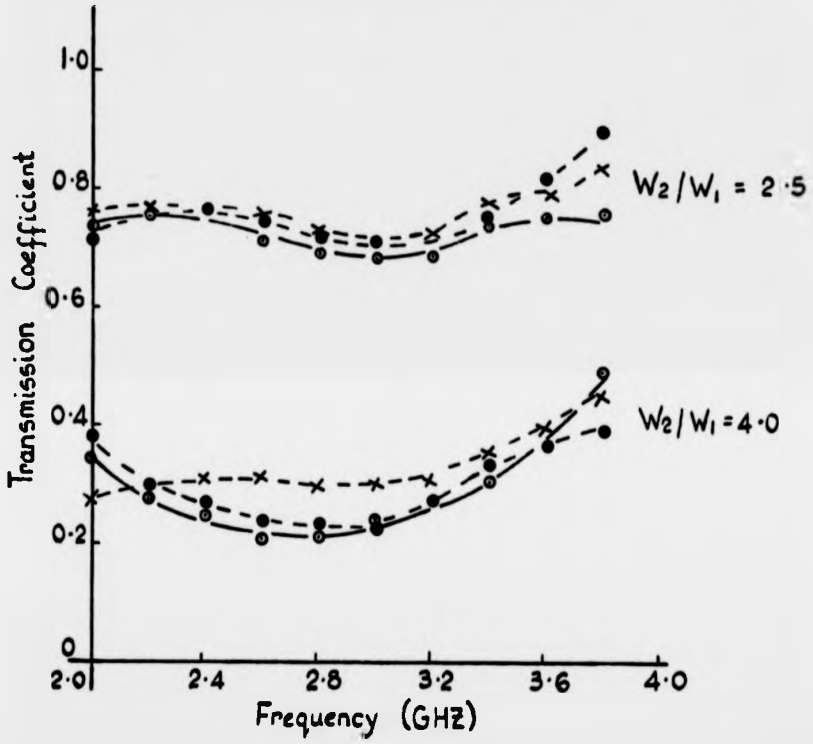

Fig.2.13 Comparison of the measured and computed transmission coefficient of the transformers.

x - - x Computed (without step)

● - - ● Computed (with step)

o——o Measured.

these elements are clearly demonstrated in the figure. The results also show that if the width ratio lies within the range $1.0 \leq W_2/W_1 \leq 3.0$, the effects of this discontinuity can be neglected.

REFERENCES

1. POH, S. Y., CHEW, W. C., and KONG, J. A., "Approximate formulas for the line capacitance and characteristic impedance of microstrip lines", IEEE Trans. Vol. MTT-29, 1981 Feb. pp.135-142.

2. WHEELER, H. A., "Transmission line propertiesof a strip on a dielectric sheet on a plane", IEEE Trans. Vol. MTT-25, 1977, pp. 631-647.

3. SHERMER, H. V., "A flexible microwave automatic network analyzer system", The Radio and Electronic Engineer, Vol. 51, No. 6, June 1981, pp.287-298.

4. WIGHT, J. S., "Equivalent circuit of microstrip impedance discontinuity and launcher", IEEE Trans. Vol. MTT-22, No. 1, 1974, pp. 48-52.

5. GARG, R. and BAHL, I. J., "Microstrip discontinuities", Int. Journal of Electronics, Vol. 45, July 1978, pp.81-87.

6. DYDYK, M, "Master the T-junction and sharpen your MIC designs", Microwaves, May 1977, pp. 184-186.

7. HOEFER, W. J. R., "Equivalent series inductivity of a narrow transverse slit in microstrip", IEEE Trans. MTT-25, No. 10, Oct. 1977, pp.822-824.

8. EDWARDS, T. C., Foundations for microstrip circuit design, Wiley 1981.

9. GUPTA, K. C., GARG, R. and BAHL, I. J., Microstriplines and Slotlines, Artech House 1979.

CHAPTER 3

COMPUTER AIDED DESIGN

3.1 INTRODUCTION

Early microwave circuit development was mainly centred around the 'empirical design' criteria[1] which uses approximate formulas to represent microwave circuit elements. While this method is certainly not without its virtues, it has limited applicability in many modern circuit designs. A more realistic design approach which is growing in use involves the use of a general purpose computer-aided design program (CAD), which is written in such a manner that the designer can iteratively analyze a circuit and change critical parameters until specific requirements are met. Such a program also provides an accurate and rapid means of solving numerous circuit problems which are far too complex to be handled by means of the Smith chart or slide rule.

The use of such computer-aided design programs for lumped and distributed element circuits are well documented[2,3,4]. This chapter describes the computer design program used throughout this work. Since only strip transmission line was used in this project, the program is limited to triplate and microstrip lines. However, it can easily be adapted for such other

transmission lines like coaxial lines and coplanar waveguides. The program uses the ABCD matrix described below.

3.2 THE ABCD MATRIX

3.2.1 Matrix concept: The mathematical concept of matrices is well known and since they can be handled very conveniently by a computer, the characterization of network elements in such forms enables calculations to be rapidly executed. At microwave frequencies, analysis are more easily made using the ABCD matrices[5]. This is because the lumped and distributed elements of a network are related to the matrix elements quite simply. Moreover, the elements are easily cascaded by multiplying their matrices. Thus the output of one network element is the input to the following element and so on.

The ABCD matrix definition is shown in fig. 3.1. From the figure

$$V_1 = AV_2 + BI_2$$

$$I_1 = CV_2 + DI_2 \qquad 3.1$$

where $A = (V_1/V_2)\big|_{I_2=0}$; $B = (V_1/I_2)\big|_{V_2=0}$

$$C = (I_1/V_2)\big|_{I_2=0} \text{ and } D = (I_1/I_2)\big|_{V_2=0} \qquad 3.2$$

The driving point impedance at the input port is given by

$$Z_{in} = (AZ_o + B)/(CZ_o + D) \qquad 3.3$$

The output impedance $Z_{out} = (DZ_o + B)/(CZ_o + A)$ 3.4

The voltage reflection coefficient at the input port

$$\Gamma_{in} = (Z_{in} - Z_o)/(Z_{in} + Z_o) \qquad 3.5$$

Voltage transfer coefficient is given by:-

$$|(V_o/V_2)|^2 = 1/4 \; |A + B/Z_o + CZ_o + D|^2 \qquad 3.6$$

3.2.2 Matrix of elements: The ABCD matrices representing the series and shunt elements used here are given by:

$$[ABCD]_Z = \begin{bmatrix} 1 & Z \\ 0 & 1 \end{bmatrix} \qquad 3.7$$

Shunt element with an admittance Y:

$$[ABCD]_Y = \begin{bmatrix} 1 & 0 \\ Y & 1 \end{bmatrix} \qquad 3.8$$

For a transmission line of length $l_{(m)}$ and characteristic impedance Z_o (ohms), the voltages and currents at each reference plane are related by

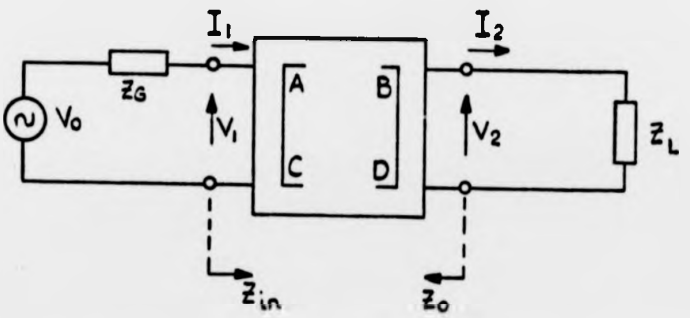

Fig. 3·1 (a) ABCD Matrix Definition

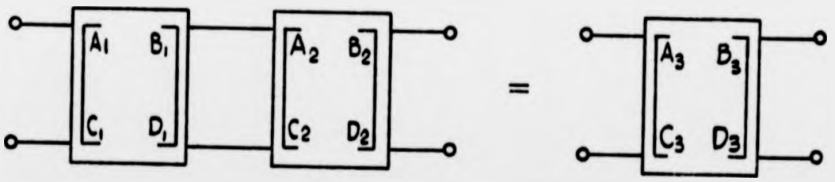

$$\begin{bmatrix} A_3 & B_3 \\ C_3 & D_3 \end{bmatrix} = \begin{bmatrix} A_1 & B_1 \\ C_1 & D_1 \end{bmatrix} \cdot \begin{bmatrix} A_2 & B_2 \\ C_2 & D_2 \end{bmatrix} = \begin{bmatrix} (A_1A_2+B_1C_2) & (A_1B_2+B_1D_2) \\ (C_1A_2+D_1C_2) & (C_1B_2+D_1D_2) \end{bmatrix}$$

Fig 3·1 (b) Cascade Combination

the equations:

$$V_1 = V_2 \text{Cosh}\ (\gamma l) + I_2 Z_o\ \text{Sinh}\ (\gamma l)$$

$$I_1 = V_2/Z_o\ \text{Sinh}\ (\gamma l) + I_2 \text{Cosh}\ (\gamma l) \qquad 3.9$$

where $\gamma = \alpha + j\beta$

with α = loss/unit length (i.e. nepers/m);

$\beta = \omega/V_p$ = phase constant

In matrix notation, a series connected distributed transmission line is given by

$$[ABCD]_l = \begin{bmatrix} \text{Cosh}(\gamma l) & Z_o \text{Sinh}(\gamma l) \\ Y_o \text{Sinh}(\gamma l) & \text{Cosh}(\gamma l) \end{bmatrix} \qquad 3.10$$

One of the interesting and powerful features of the use of ABCD matrix other than the speed of computation, is the ability to store the matrix representation of the individual network elements in computer memory. Individual element types and the related data were specified as integral parts of an overall network topology. Each type was coded, enabling the program to call upon the necessary algorithm to compute the ABCD matrix for that element and then cascading the elements in their correct sequence and computing their matrix product. Once a given element matrix is stored, there is no need

to recompute unless new values were specified either by the user or by an automatic search or iteration routine.

3.3 PROGRAM DESCRIPTION

3.3.1 Input subroutine: The flow chart for the program is shown in fig. 3.2. The major steps were divided into subroutines. This approach permits the complete program to be written in easier to visualize steps. The program is detailed in appendix C. The first subroutine (subroutine ELMNT) translates the element list into an array of data intelligible to the computer. The types of elements recognized by this program include transmission lines, open and short circuited stubs and series or parallel combinations of resistors, inductors or capacitors. All these elements are described by a three letter code word followed by three or more appropriate parameters.

Fig. 3.3 shows the schematic circuits and the parameter specifications for the elements used in the program. It was decided not to code single lumped elements like a single series or shunt resistor or inductor. This is because any of these elements can be obtained from the series or parallel combinations by simply removing the unwanted elements. Equally, a lossless transmission line was not entered as this

can be obtained from the lossy line by specifying zero attenuation constant when entering the parameters.

The code words used were made by abbreviating the requisite words such as 'SLC' for a series arrangement of an inductor, capacitor and resistor, while 'PLC' stands for a parallel arrangement of the same elements. Choice of the parameter values permits the removal of any of the unwanted L, C and R element parts of the arrangement. Other code words used here are descriptive such as 'STB' for a stub and 'LIN' for a transmission line.

The length of the transmission line or stub is referenced to the centre frequency for which the analysis is to be made. The electrical length and loss are recalculated for each analysis frequency. The subroutine has a string data list containing the code word of the element types. After being read, the list is stored in a string array which lists the element types in the sequence in which they appear. To avoid making a mistake in the spelling of the code word, a statement was included in the subroutine to compare the name entered with those on the data list. If any unrecognised name was entered, an error message would be printed out and the name is demanded again.

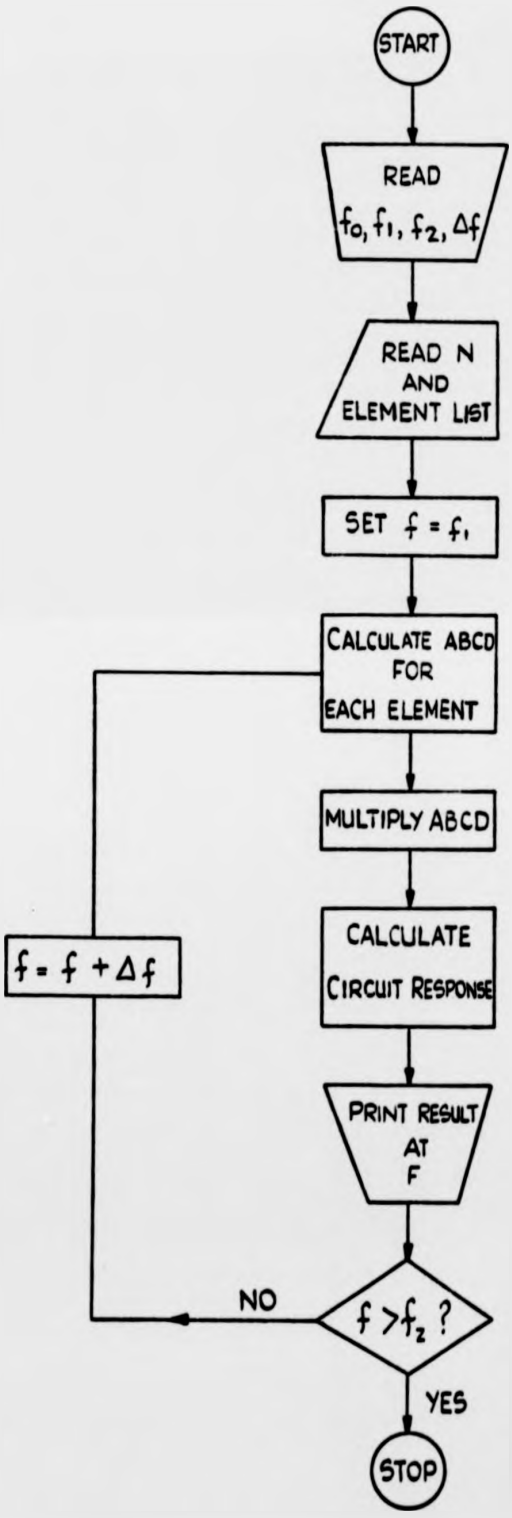

Fig.3.2 Flow chart for the network analysis program.

Element	Code Name	Parameters			
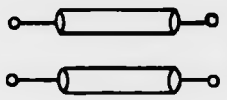	LIN	Z_0 (Ω)	Θ at f_0	α dB/λ at f_0	
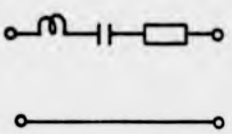	S LC	L nH	C pf	R Ω	
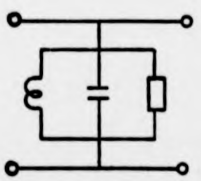	PLC	L nH	C pf	R Ω	
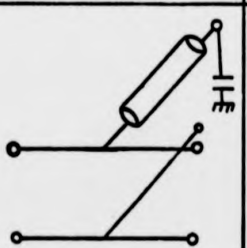	STB	Z_0 Ω	Θ at f_0	α dB/λ at f_0	C pf

Fig.3.3 Element kinds and description code for the analysis program.

3.3.2 Response computation: Having converted the elements into subscripted data which can be interpreted by the program, the next step was to assign the proper ABCD matrix description to them. This assignment was peformed using the subroutine ABCD. The subroutine first identifies the types of the element in the network. It then cycles through this identification and assigns the proper matrix specification for each of the N-elements in the network. The specific calculations of the ABCD parameters for each of the elements follow the requirements given in equations 3.7-3.10. Since all the elements used here are symmetric with respect to the input and output ports, it follows that A = D in the transmission matrix.

It was mentioned earlier that to obtain a single lumped element, the unwanted parts of the L, C and R elements had to be removed by inputing zero values for them. The matrix evaluation steps for the series or parallel combination of these LCR elements contain special provisions for those cases when the input of a zero value for a parameter would produce trivial results (or cause computer overflow) for the analysis. With the series 'SLC' combination, this situation occurs when the capacitance value is zero. This results in an infinite reactance which totally disconnects the input and output ports of the network.

To get over this problem, a statement was used

to replace any capacitance value which is less than 0.001 pico-farads with a capacitance of one farad. Thus this assignment of a very large capacitance value was interpreted as an indicative that the series LCR circuit consists of only an L and R combination. Since no difficulty arises with zero values of L and R elements, this provision was not required for them. For the parallel PLC elements, zero valued inductances and resistances were converted to large magnitudes. This effectively open circuits them and removes them from the circuit.

After the determination of the individual ABCD matrix element forming the network, they were multiplied together to form the resultant or total matrix which represents the terminal characteristics of the complete N-elements in the cascade. This procedure was done using the subroutine TOTAL. The procedure consists of equating the total ABCD to the last (N^{th}) element of the cascade. If N = 2, as in the case when the circuit under analysis has only one element then no multiplication is necessary. For N > 1, the next but last (N - 1) element matrix was set equal to a dummy matrix called NEXT, which in turn was used to multiply the total matrix. The result of the multiplication was used to overwrite the total ABCD. This procedure was then repeated through the N - 1 multiplications using a DO loop.

After the evaluation of the overall ABCD matrix of the network, the circuit response was calculated using the subroutine CALC. This subroutine calculates the input impedance Z_{in}, the input reflection coefficient, the transmission loss and the phase using equations 3.3 - 3.6. The subroutine accepts a complex ABCD matrix array along with complex generator and load impedances.

3.3.3 Program execution: The program execution is controlled by a main program which calls for a matrix computation for each set of element data from a set of subroutines. Once the overall ABCD matrix was found for each frequency, its components were stored and used to compute the desired output parameter in a separate subroutine. Changes in the parameters of the elements making up the network were readily accomplished in the editing mode of operation. Here lines of data were examined, deleted or added. Individual characters can be quickly replaced depending on need. The computed results for such modifications can then be typed out immediately by switching back to the run mode.

REFERENCES

1. MATTHAEI, G.L. et al; "Microwave filters, impedance matching networks and coupling structures," Artech House (Dedham Mass) 1981.

2. FIDLER, J.K. and NIGHTINGALE, C.;"Computer-aided circuit design," Nelson 1979.

3. CALAHAN, D.A.; "Computer-aided network design," McGraw Hill 1972.

4. CHADHA, R. and GUPTA, K.C.; "Computer-aided analysis of stripline circuits including discontinuity reactance effects," Inst. of Electronics and telecoms. Engr. Journal. Vol.26 No. 6 1980 pp.290-292.

5. WHITE, J.F.; "Semiconductor control." Artech House (Dedham Mass) 1976.

CHAPTER 4

DEVICE CHARACTERIZATION

4.1 INTRODUCTION

The use of a semiconductor device in any application requires an accurate knowledge of the behaviour of the device. At microwave frequencies, the behaviour of semiconductor devices is most readily predicted if the devices are represented by lumped element networks. However, it must be said that at the higher end of the microwave region, the use of such lumped-element representation is limited in accuracy. This is because at these frequencies, the physical components of the device exhibit distributed characteristics.

Below 15 GHz, the use of these lumped elements can be very good for circuits confined to electrically small regions. Since a diode is ordinarily small compared to the wavelength of the applied field, lumped-element representation was used throughout this work. The exact nature of the lumped elements representing a p.i.n. diode circuit is derived in this chapter. Though there has been some works on the derivation of p.i.n. diode equivalent circuits, most of these works have given rise to complex networks which are too difficult to incorporate in an analysis

program[1,2]. For most analysis, a simplified equivalent circuit can be constructed without serious loss of accuracy. The equivalent circuit used here was derived by considering the diode behaviour in each bias state and taking into account only those diode parasitic elements which are significant in each state.

The values of the elements were then found by a careful measurement of the diode and its embedding network, and deducing the required lumped constants from the results obtained. For a more predictable performance, the diode was measured under the same conditions in which it will be eventually used. The chapter describes the measurement techniques used. The design of the biasing, blocking and driving networks are also given. The diodes used for the project were supplied by AEI Semiconductor - types DC 2518G and DC 2418A.

4.2 DERIVATION OF THE EQUIVALENT CIRCUIT

4.2.1 I-layer: The p.i.n. diode consists of a semiconductor wafer which is mounted on a package as shown in fig. 4.1a. Each of the flat surfaces is heavily doped with boron and phosphorus to form the p- and n-layers respectively. These are separated by a weakly doped layer of high resistivity intrinsic material. Electrical contacts are made to the two heavily doped

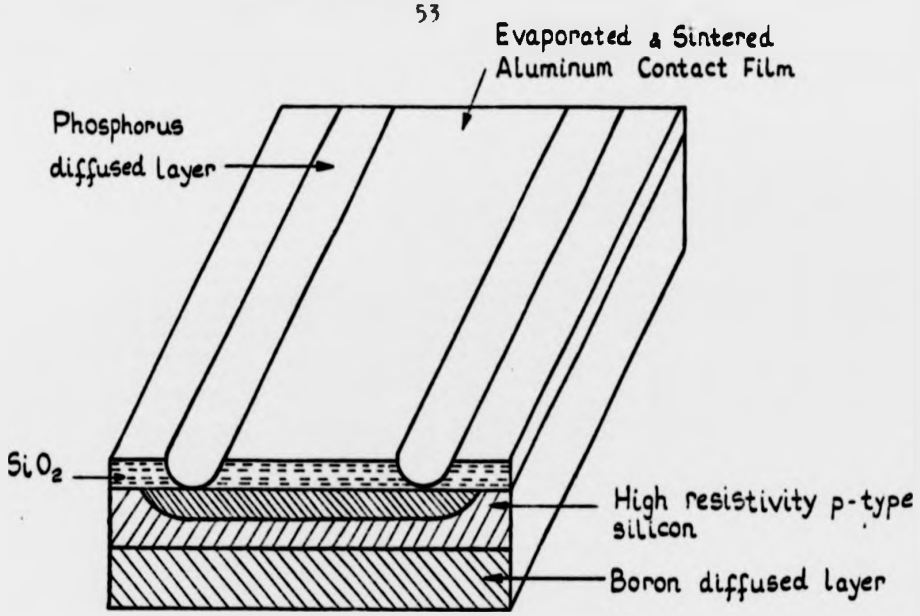

Fig. 4·1 (a) Microwave p.i.n wafer

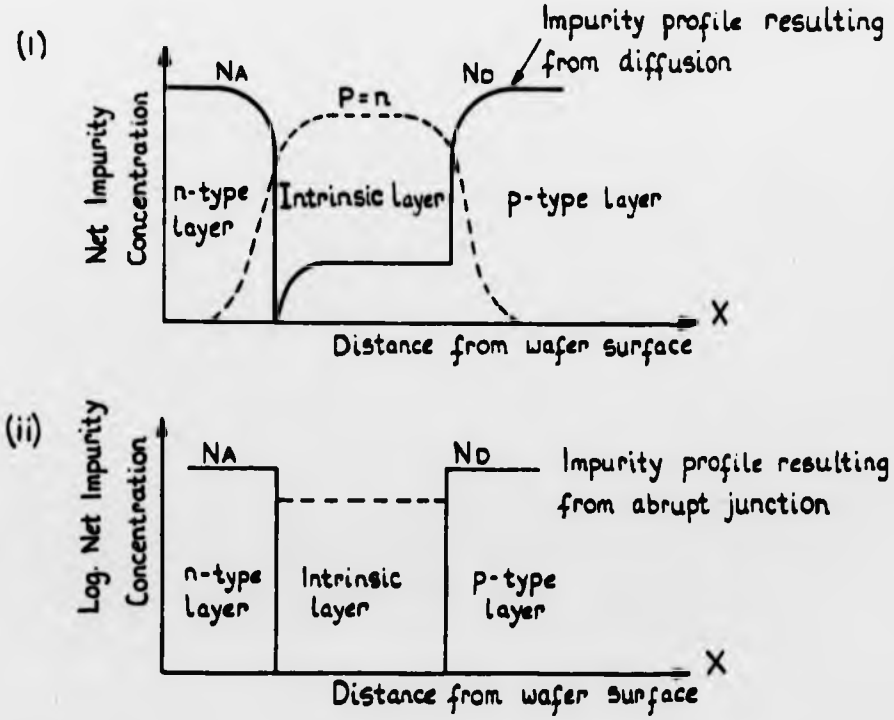

Fig. 4·1(b) Doping profile (solid line) and distribution of stored charge (dashed line) of a real (i) and an idealised (ii) p.i.n diode.

layers. The doping profile of the device is shown in fig. 4.1 (b).

In practice, a truly intirinsic layer does not exist in a p.i.n. diode. This is because it has not been technologically feasible to maintain intrinsic resistivity in the layer through the processing of a diode. In effect, the lightly doped high resistivity region is a π or v layer depending on whether the conductivity is a p- or n- respectively. The difference between an ideal p.i.n. diode which has an intrinsic layer and a practical p.i.n. diode in which the layer is actually a π, can be compared by considering what happens to the space charge density and the electric field distribution of both as a reverse bias is applied to them.

At zero bias, the diffusion of holes and electrons across the junction causes space-charge regions to form in the p- and n- layers adjacent to the i-layer. For the ideal diode, with an i-layer that has no impurities, the layer is completely depleted of mobile carriers. Thus we have a region of fixed negative charge in the p-layer and a region of fixed positive charge in the n-layer with no charge in the i-layer as shown in fig. 4.2(a). As reverse bias bias is applied to the diode, a uniform electric field appears in the i-layer and this drops linearly to zero through the depletion regions in the p- and n- layers as

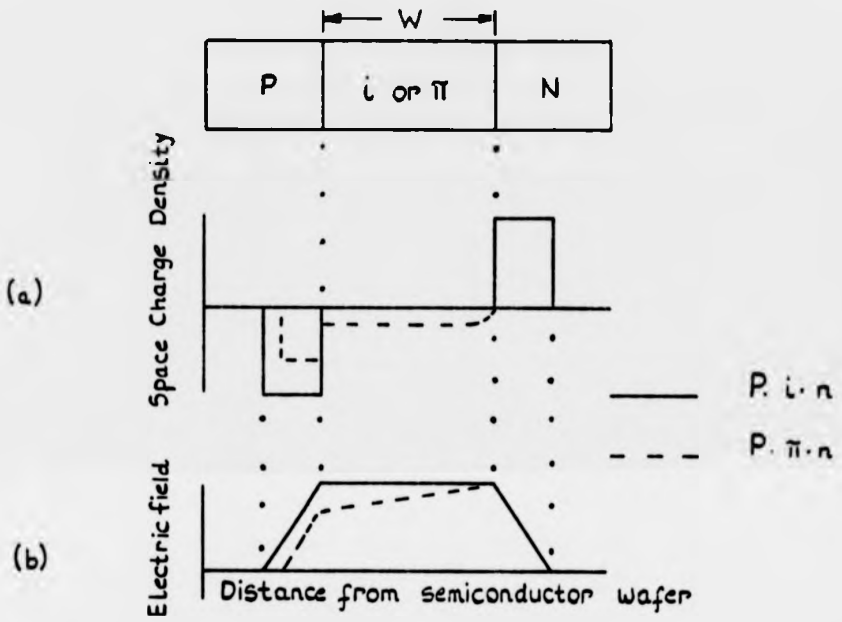

Fig.4.2 Charge and field distribution in p.i.n. p.π.n. junction.

illustrated in fig. 4.2(b).

If the high resistivity region is a π-layer, then with no applied bias, the diffusion of holes and electrons across the n-π junction will produce a very thin depletion region in the n-layer and a thicker depletion region in the π-layer. As reverse bias is applied, the depletion regions become thicker until the entire π-layer is swept free of mobile carriers. Increasing this bias does not produce significant changes in the regions.

The conclusion drawn from the above comparisons is that the i-layer of an ideal diode is completely swept at zero or any reverse bias whereas in a practical diode, a small bias must be used to sweep out the i-layer. This point was noted as it means that measurements made under zero bias condition does not accurately represent the reverse bias behaviour of the diode.

4.2.2 Reverse bias parameters: As explained above, when zero bias is applied to a p.i.n. diode, a depletion is formed at the junction of the n- and i- interface. The extent of this depletion layer is a function of the resistivity of the i-layer. As a reverse bias voltage is applied to the diode, a large current begins to flow immediately, this current being limited only by the impedance of the voltage source.

The i-region will be completely depleted of mobile carriers. When this happens, the conductivity of the diode decreases and the total impedance of the diode becomes essentially a constant capacitance in series with a very high resistance. This condition is represented by the capacitance C_d and the reverse resistance R_r in fig. 4.3 (c). This capacitance is independent of the applied bias. This is because any further increase in the applied voltage does not increase the thickness of the depletion region.

4.2.3 Forward bias parameters: When forward bias is applied to the diode, the i-layer becomes flooded with injected carriers. Electrons are injected into the region from the n-layer and holes from the p-layer. As the carriers diffuse into this intrinsic region their concentration diminishes with the depth of the region. When this happens, the diode exhibits very low resistance and appears as a virtual short circuit across the transmission line. This condition is represented by the forward resistance R_f and the series inductance L_s in fig. 4.3 (c). Unlike the reverse bias capacitance, the value of this forward resistance is a function of the applied bias. As will be demonstrated later, a certain amount of bias is required before the lowest value of forward resistance can be attained.

The diode is mounted on a package so that it may be conveniently handled as illustrated in figs 4.3. This package contributes its own parasitic reactances represented by L_p and C_p. The values of these components are determined in section 4.4. The biasing networks used in the measurements are dosigned in the next section.

DC 24 18 A

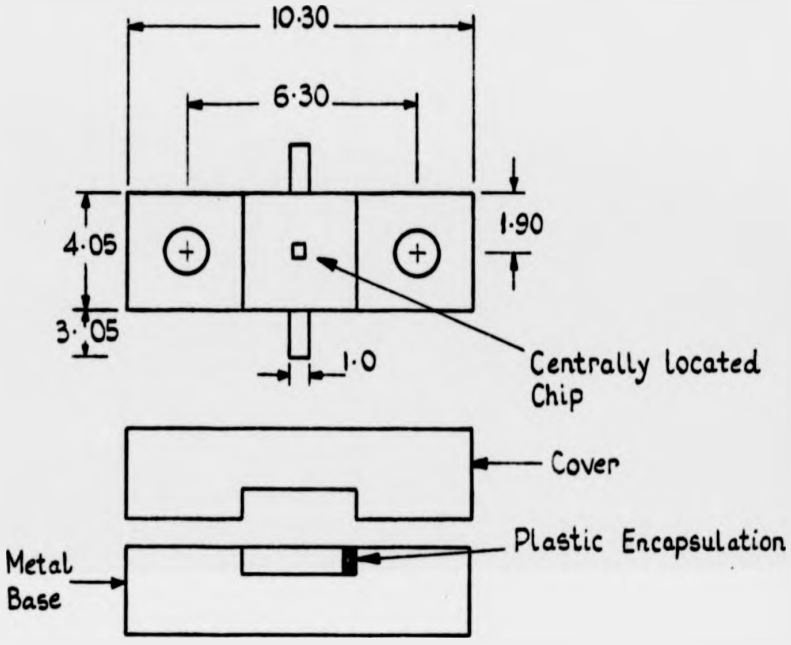

Fig. 4·3 (a)

DC 25 18 G

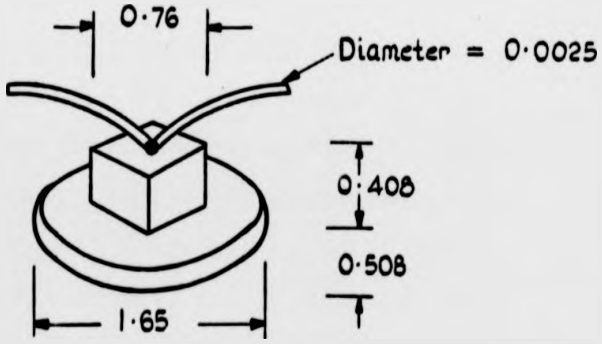

Fig.4.3 Packaged p.i.n. diode.

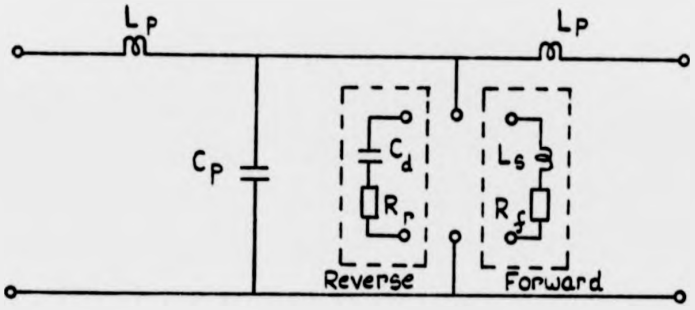

Fig.4.3c P.i.n. diode equivalent circuit.

4.3 BIASING CIRCUITS

One of the main problems associated with the design of p.i.n. diode circuits is how to separate the d.c. or low frequency bias signal from the r.f. signal. In all cases, some frequency selective networks are added to separate these two signals. These networks are termed the biasing circuits. The three major components of these circuits are the bias filter which introduces the bias signal to the r.f. line, the d.c. block which prevents the bias signal from impinging on the rest of the r.f. circuits and the circuit driver which serves as a buffer stage between the power supply and the p.i.n. diode device.

The design of the networks used to perform these functions is given in the following paragraphs. In

all cases the primary design consideration is that the networks should have a minimum insertion loss in the operating band. This is because in the later chapters, the effects of these circuits on the p.i.n. diode performance were neglected. Hence it is very essential that their insertion loss is below the accepted maximum.

4.3.1 Bias elements: The main function of the bias filter is to block the passage of the r.f. signals into the bias line and at the same time allow the d.c. signal from the bias port to reach the device. In achieving these objectives, the bias filter should contribute a minimum delay to the signal and it should have a flat response to the bias. The most common filter used is a low-pass filter.

The design of the low-pass filter used here was based on the fact that at microwave frequencies, short sections of strip transmission lines can be made to approximate to quas -lumped reactive elements. Short lengths of relatively high impedance line will behave predominantly as a series inductance. Also a very short length of relatively low impedance line will act as a shunt capacitance. Thus a ladder network of lumped elements can be realized by cascading alternate sections of high and low impedance lines.

A computer program was written to calculate the required lengths of line which will yield the desired characteristics. Since the parameters of the various lengths of line are interrelated, initial calculations were first made and then corrected progressively via an iterative procedure. One point must be mentioned regarding the choice of the characteristic impedances of the inductive and capacitive line. It must be emphasized that optimum results are obtained if the ratio of the impedances is greater than five. The reasons for this were explained in chapter two. However the value of the high impedance line should not be made too large as the author has found that impedances greater than 150 ohms are very difficult to realize as a narrow line.

Three-and five-elements filters were designed. The stripline patterns of the three-elements filter are shown in fig. 4.4. The filters were designed for a cut-off requency of 3.0 GHz with a 0.1dB ripple in the operating band. The equivalent circuit of the filter is given in fig. 4.4 (b). By incorporating the values of the coaxial transitions and step-discontinuities determined in chapter two, it was possible to compute the response of the filter. Slight adjustments were made on the actual computed dimensions of the filter so that a good agreement of the desired performance was obtained. The

dimensions of the filters are given in table 4.1.

The measured and computed response of the filter is shown in fig. 4.5. For the three-element filter, a minimum of 20dB isolation was maintained throughout the operating band, while the five-element filter gave 35 dB isolation. It should be pointed out that despite the close agreement obtained between the measured and the computed results, this design technique works well only when the ratio of the two impedances is greater than five.

A distributed d.c. block was designed for a centre frequency of 3GHz. The design uses the parallel coupled transmission line approach[3]. By proper choice of the coupling coefficients, the appropriate dimensions of the network were found. The response of the network is shown in fig. 4.6. As seen this type of network has a narrow bandwidth compared to the lumped-element block. However at higher frequencies it has a lower insertion loss and lower reflection coefficient than the lumped capacitor.

Table 4.1 Dimensions of Bias Filter (mm)

Filter Degree	d_1	d_2	d_3	d_4	d_5	d_6	d_7
3	7.13	12.94	7.13				
5	4.85	6.07	11.33	6.07	4.85		
7	3.92	5.86	6.97	9.08	6.97	5.86	3.92

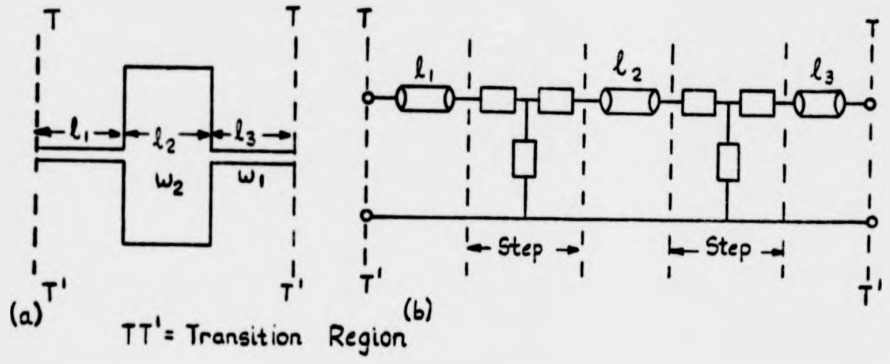

Fig.4.4 Low - pass filter.

4.3.3 Circuit driver: Effective biasing and hence effective control of the diode conductance depends very much on the design of the driver that biases the diode. Also the switching time between the two states of the diode depends on the speed with which the driver is able to provide adequate bias current or voltage. Despite these essential functions, published literatures on p.i.n. diode drivers are scarce[4,5].

To design a good circuit driver requires an accurate knowledge of the diode specifications. For the forward conducting state, the diode requires a

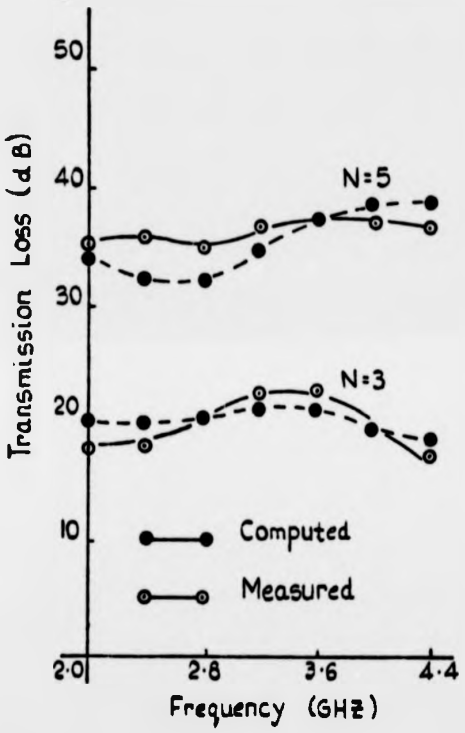

Fig.4.5 Bias filter

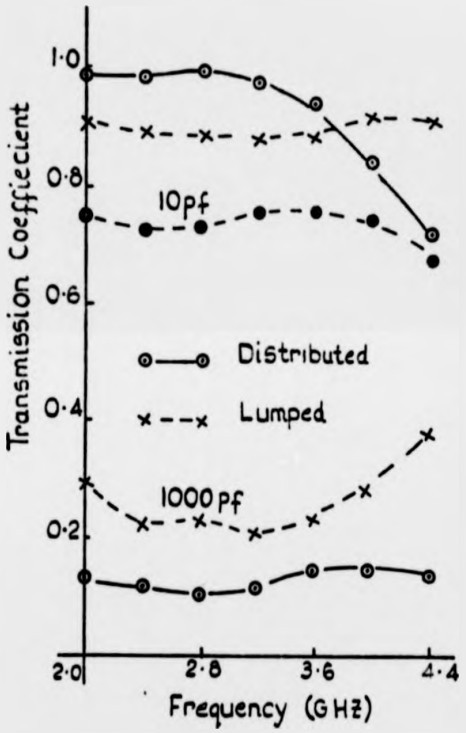

Fig. DC Block

Figs.4.5 & 4.7 Response of bias elements.

relatively low forward voltage and a high forward current. Conversely for the reverse bias state, the diode requires a high reverse voltage and low reverse current. A combination of these specifications plus the additional requirement of rapid switching times between the two states introduce complexities in the driver design.

Fig. 4.8 shows the circuit diagram of the designed driver. It uses a simple pre-amplifier stage and can switch the p.i.n. diode between a fixed reverse bias voltage and a foward bias current whose magnitude can be adjusted by the resistor R_3. The operation of this driver is such that a logic '1' applied to its input terminals turns transistor Q_2 "on" and the p.i.n. diode will be connected to the reverse bias voltage through R_5. During this state transistor Q_1 is non conducting. The value of R_2 chosen is such that there will not be enough voltage to turn Q_1 on. A logic '0' applied at the input terminals switches on transistor Q_1, thereby creating a path from the voltage supply to the diode through R_5.

To ensure that Q_2 is turned off during the forward biased state, a diode D_1 was inserted in the circuit and its polarity is such that it achieves this objective in this bias state only. Transistor Q_2 also serves to amplify the current through R_4, thus providing a more rapid removal of the i-region charge in the p.i.n. diode.

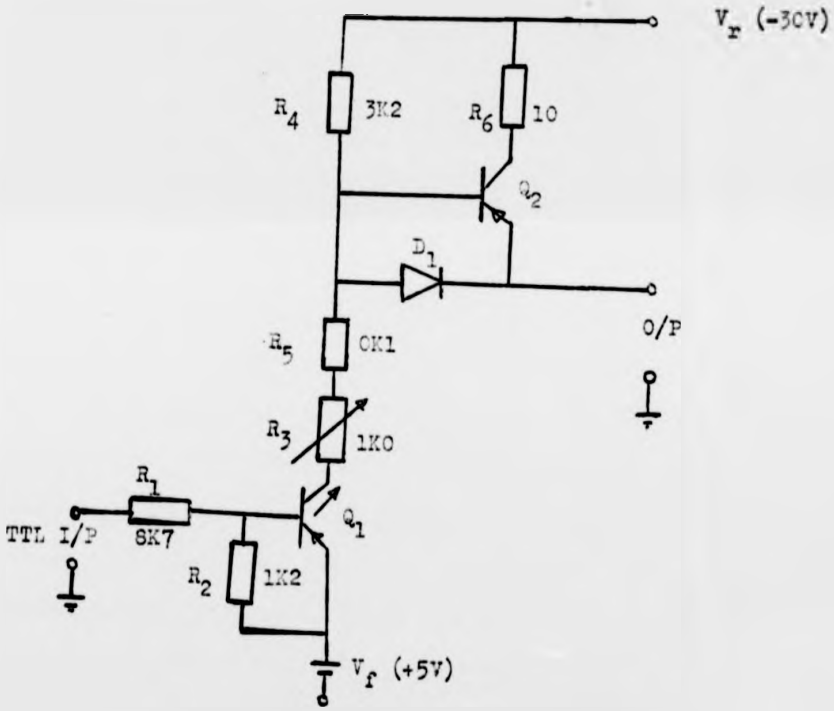

Fig.4.8 Circuit driver.

The transistors used are type QDG-BFY51. Important consideration made in the selection of these transistors include the maximum permissible bias voltage. The transistor should have a breakdown voltage of more than twice the maximum bias voltage. In high reliability applications, the use of toroidal coil in place of the output transistor is recommended. This should serve as an energy storing and discharging device for the p.i.n. diode. Apart from reducing cost, this also increases reliability.

4.4 DIODE MEASUREMENT

4.4.1 Measurement technique: Early methods of measuring p.i.n. diode parameters have been reported, the simplest of which is a low frequency bridge measurement where the package parameters are ignored. For most microwave applications, the package reactance of the diode influences the diode performance and hence can not be ignored particularly if the operating frequency is more than 2.0 GHz. Refinement in diode measurements began with the work of Getsinger[6] which uses resonant technique in calculating the equivalent circuit parameters of the device. This method is claimed to give accuracies better than three percent. With the advent of the computer corrected network analyzer, faster methods of diode measurements have been developed[7,8].

The procedure used here involves characterizing the embedding network first in order to account for all parasitic elements arising from the mounting arrangement. Then the equivalent circuit elements of the diode were determined by measuring the loss produced by the test fixture and the diode and deducing the values of the elements using graphical techniques. The same equivalent circuit was used for the two diodes.

A measurement jig was built to house the device. The substrates were fabricated from 0.159cm thick polyguide dielectric material (e_r = 2.32) with a one ounce copper cladding. The input and output ports have 50 ohms characteristic impedance lines. To ensure adequate grounding of the planes, conductive epoxy was used to glue aluminium planes to the unetched copper face of the dielectric material. The jig is shown in fig. 4.9.

The scattering parameters of the jig without the diode in position were then measured over the frequency range 0.4-4.0 GHz in steps of 100 MHz using the computer corrected network analyzer. The results are shown in fig. 4.10. The results show that the jig has a minimum transmission coefficient $|S_{21}|_m$ of 0.985 and a maximum reflection coefficient $|S_{11}|_m$ of only 0.02 throughout the operating band. These are equivalent to an insertion loss of only 0.13dB and a VSWR of 1.04.

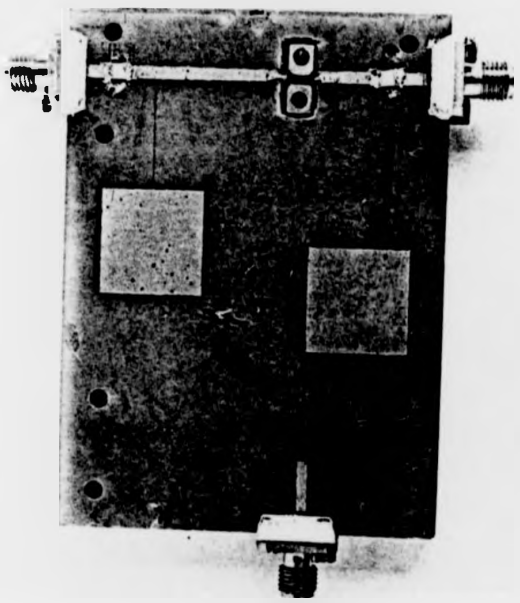

Fig. 4.9 Jig used for diode characterization.

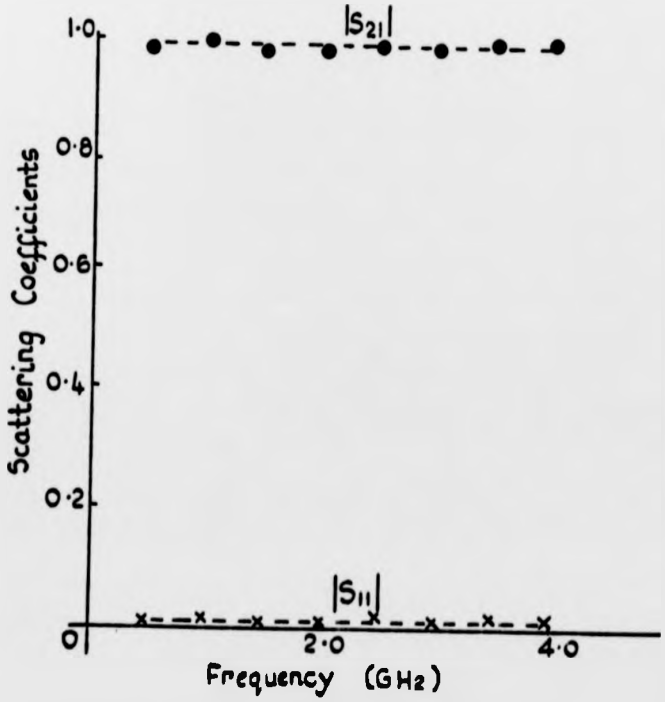

Fig.4.10 Response of embedding network.

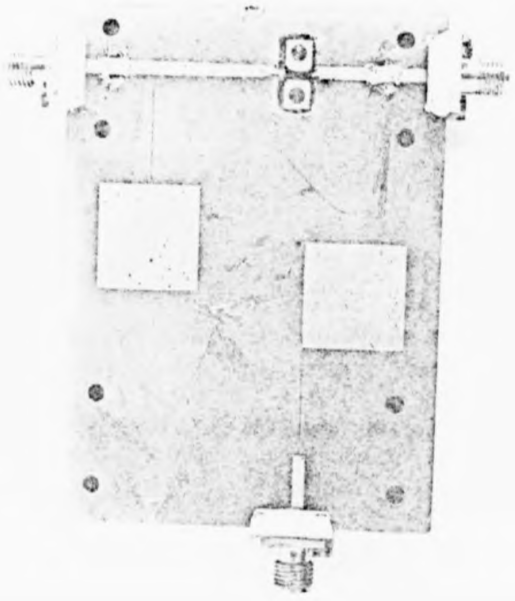

Fig. 4.9 MIC used for Mode characterization.

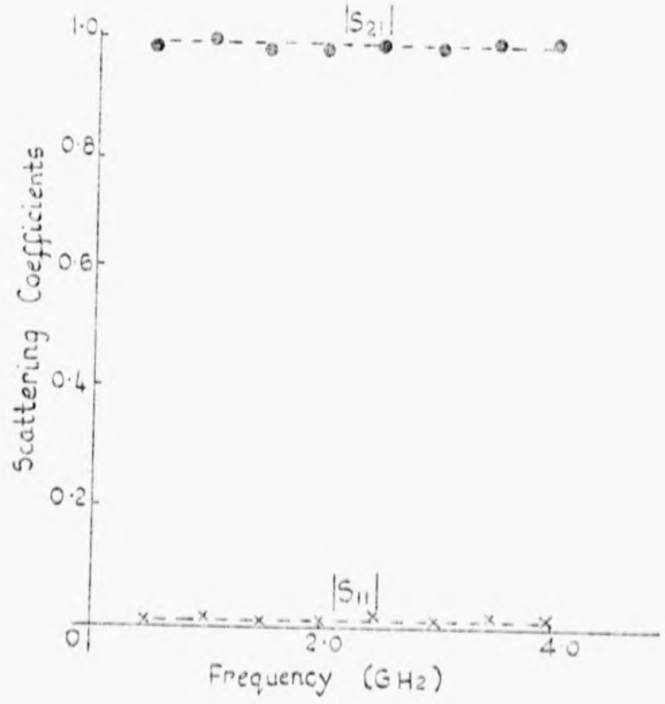

Fig.4.10 Response of embedding network.

This loss is due to effects of coaxial transitions, dielectric and conductor losses.

The diode was then placed in a slot which was milled in the centre conductor to a depth to allow the diode to make contact with aluminium plate while at the same time ensuring that the diode leads rest flat on the conductor pattern. The overall test fixture was then remeasured over the same frequency band using various bias currents and voltages. The results are shown in figs. 4.11 to 4.16.

4.4.2 Determination of forward elements: When the diode was forward biased, the resulting loss is given by[9]

$$\alpha = 20 \log |1 + Z_o/2Z_d| \text{ dB} \qquad 4.1$$

where Z_d is the diode impedance and Z_o is the characteristic impedance of the line.
From fig. 4.3 (c) the diode impedance under forward bias is

$$Z_f = \left[\frac{R_f}{(1-\omega^2 L_s C_p)^2 + (\omega C_p R_f)^2}\right] + j\left[\omega L_p + \frac{\omega L_s (1-\omega^2 L_s C_p) - \omega C_p R_f^2}{(1-\omega^2 L_s C_p)^2 + (\omega C_p R_f)^2}\right] \qquad 4.2$$

To simplify matters, it was assumed that

$$(\omega C_p R_f)^2 << (1 - \omega^2 L_s C_p)^2$$

and

$$C_p R^2_f << L(1 - \omega^2 L_s C_p) << 1$$

Hence $Z_f \simeq R_f + j\omega L_n$ 4.3

where $L_n = (L_p + L_s)$

Thus $\alpha = 20 \log |1 + Z_o/2(R_f + j\omega L_n)|$ dB

This was re-arranged in the form

$$1/(A - 1) = (\omega^2 L_n + R_f^2)/Z_o(R_f + Z_o/4) \quad 4.4$$

where $A = 10^{\alpha/10}$

Eqn. 4.4. is in the form of $y = mx + c$.

Using the values obtained for a bias current of 50 mA, a graph of $1/(A-1)$ against ω^2 was plotted as shown in figs. 4.11 and 4.12. By process of extrapolation, the values of L_n and R_f were obtained from the gradient and intercept respectively as
L_n = 2.75nH for DC 2418A and 2.93nH for DC 2518G;
R_f = 1.32 ohms and 1.06 ohms respectively.

Knowing L_n, the values of the package inductance L_p were found by relating the geometry of the diode

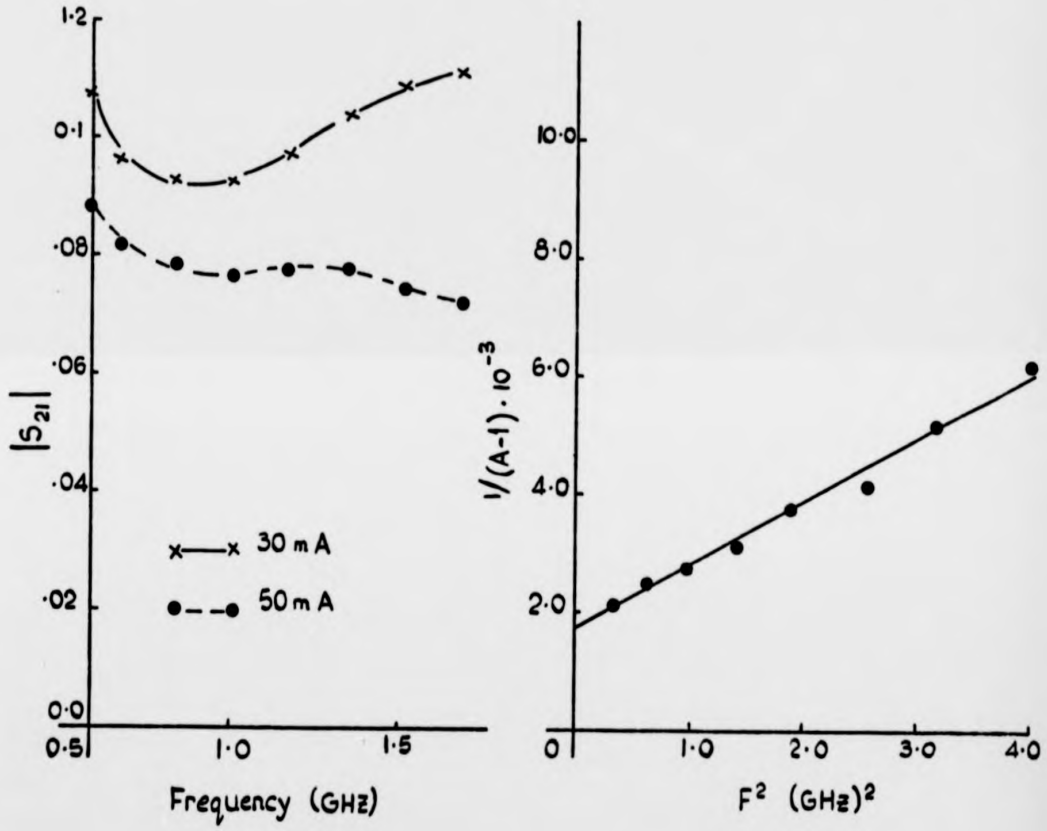

Fig.4.11 Forward bias measurement (DC 2418A)

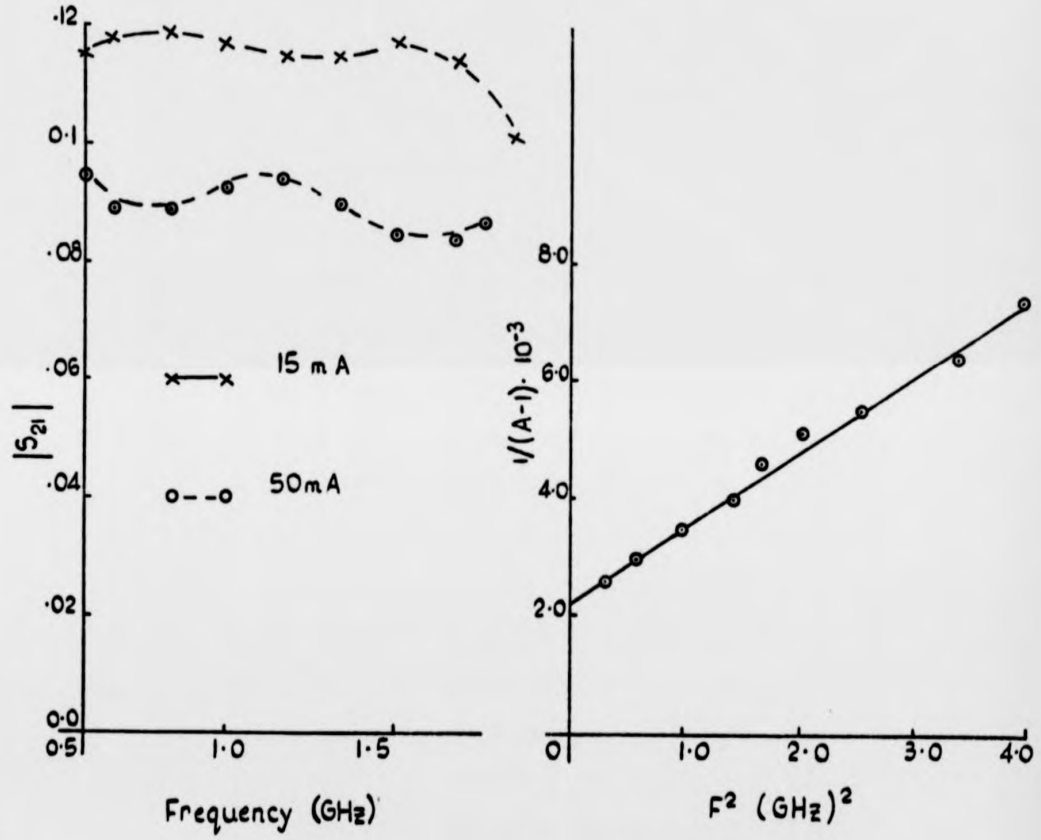

Fig.4.12 Forward bias measurement (DC 2518C).

leads to that of the strip transmission line. Although this is an approximation, it is the only known method of evaluating this element. The dimensions of the package leads are given in fig. 4.3. Basic transmission line theory gives this inductance as

$$L_p = Z_p S_{in}(2\pi l/\lambda g)/w \qquad 4.5$$

where l is the length of the diode and Z_p is the equivalent impedance of the line.

L_p was computed as 2.5nH and 3.11nH for the two diodes from which L_s = 0.249nH for DC 2418A and 0.18nH for DC 2518G.

These measurements were made at the lower microwave range where the effects of the package capacitances C_p were neglected. At frequencies above 2.0 GHz, these elements become significant. To find C_p, the frequency of minimum isolation was noted for the two cases. This corresponds to a parallel resonance of L_n and C_p. Since L_n is known in each case, C_p was found from the relation $C_p = 1/(2\pi f)^2 Lp$. The values are 0.91pF for type 2418A and 0.13pF for 2518G.

4.4.3 Determination of reverse elements: The principles used above were equally adopted to find the reverse bias elements. When the diode is reverse biased, the impedance from fig. 4.3 (c) becomes

$$Z_r = \left[\frac{R_r}{(1-\omega C_p[\ -1/\omega C_d])^2 + (\omega C_p R_r)^2} \right] +$$

$$j\left[\omega L_p + \frac{(-1/\omega C_p)(1-\omega C_p) - \omega C_p R}{(1-\omega C_p[\ -1/\omega C_d])^2 + (\omega C_p R_r)^2} \right] \quad 4.6$$

Using similar assumptions as before, this reduces to

$$Z_r = R_r + j\, X_r \quad 4.7$$

where $X_r = (\omega L_p - 1/\omega C_d)$

Using bias voltages of -30V, the frequency of maximum insertion loss was noted to be 7.09 and 9.6 GHz. This corresponds to a series resonance of L_n and C_d. Since the values of L_p are known, C_d was found in each case from the relation $C_d = 1/\omega^2 L_n$ to be 0.183pF for DC 2418A and 0.09 pF for type DC 2518G. This measurement also yields the value of R_r because the attenuation at this frequency is given by

$$\alpha = 20 \log |1 + Z_o/2R_r| \quad 4.8$$

R_r was found to be 1.56 k-ohms and 1.23 K ohms respectively. Fig. 4.17 shows an impedance sweep measurement for the two states of diode 2418A.

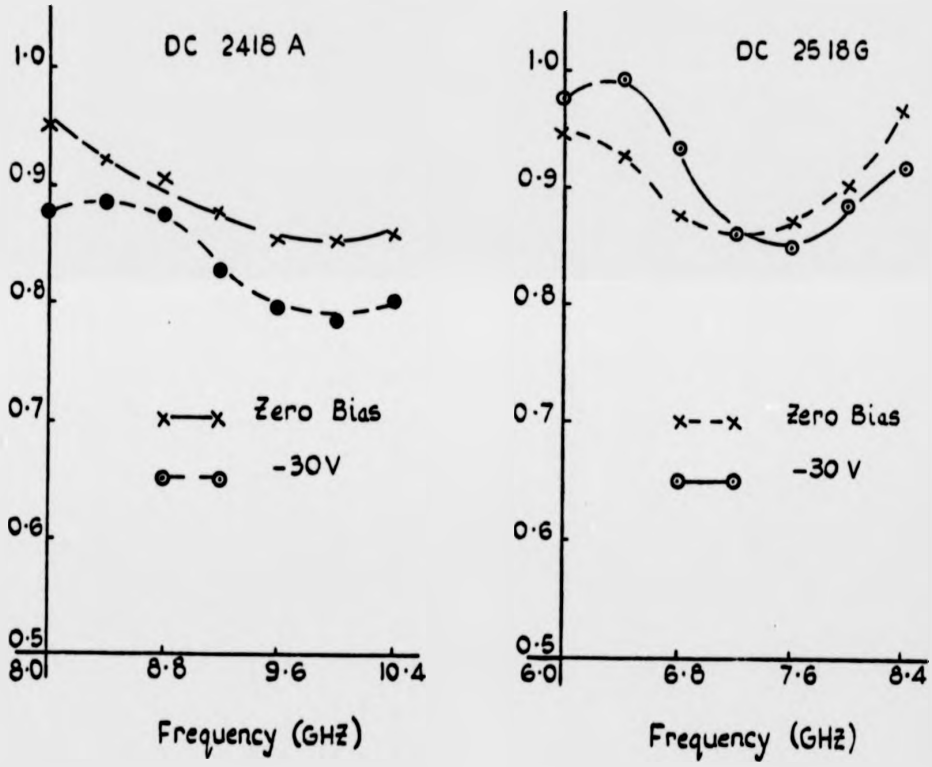

Fig.4.13 Reverse bias measurement

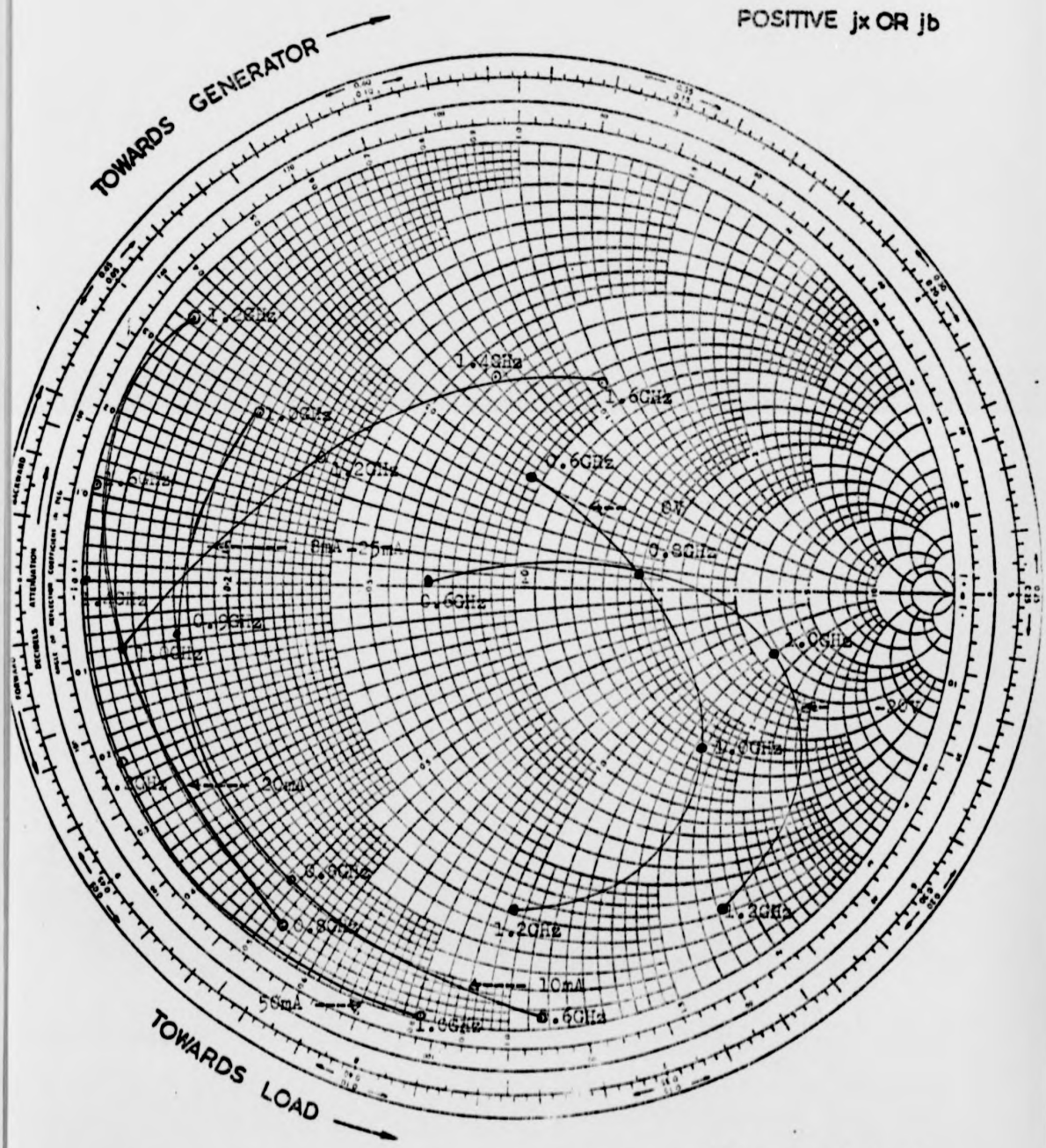

Fig.4.14 P.i.n. diode impedance (DC 2418A)

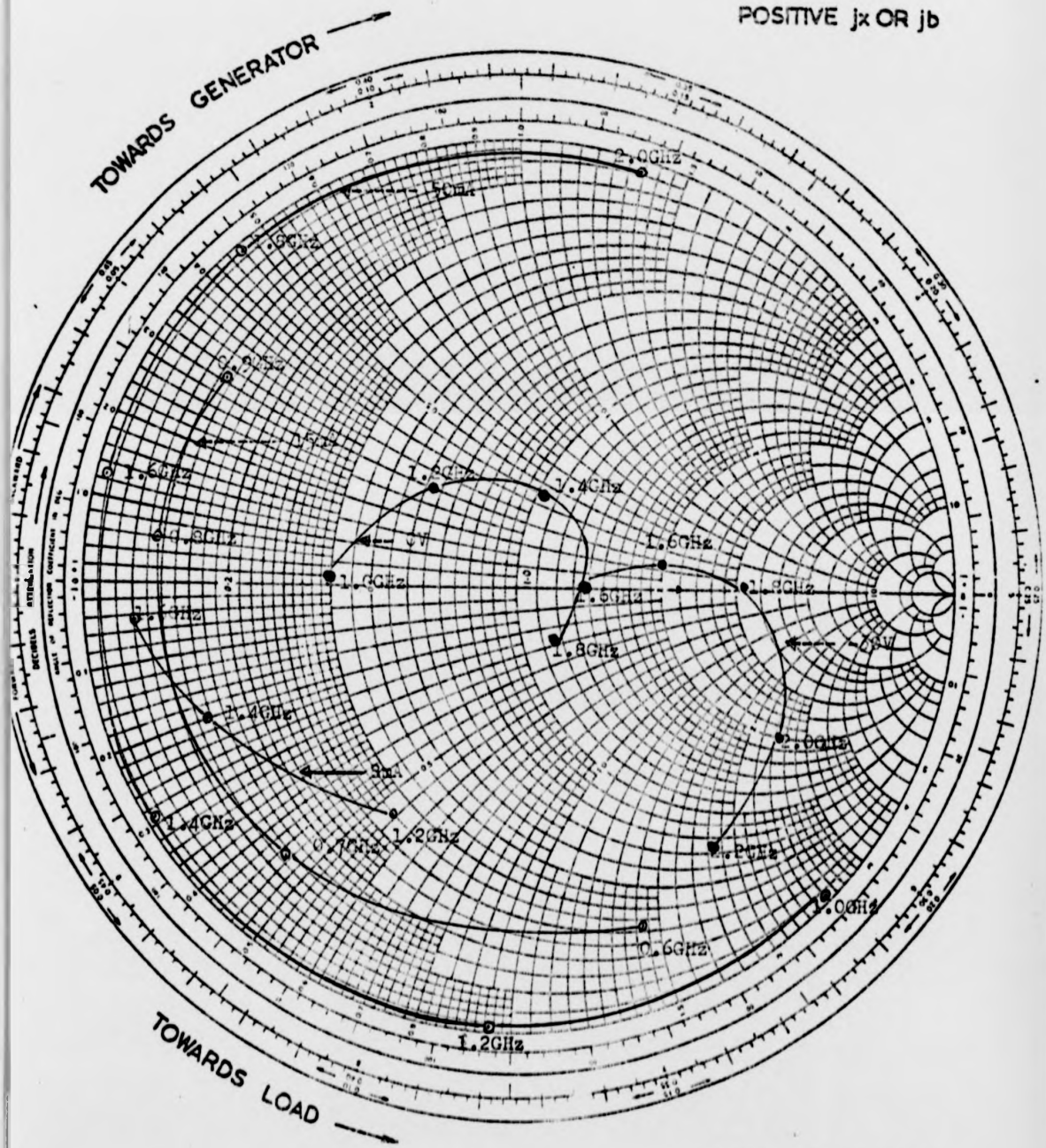

Fig.4.15 P.i.n. diode impedance (DC 2518C)

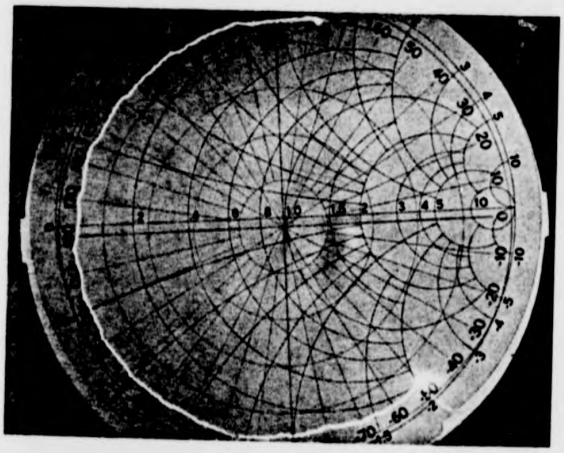

Forward Bias
(100mA)

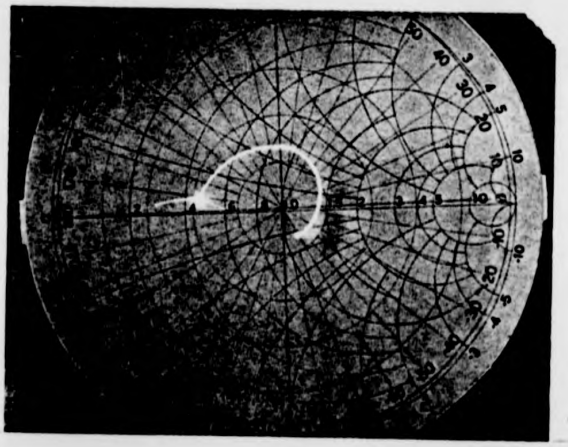

Zero Bias

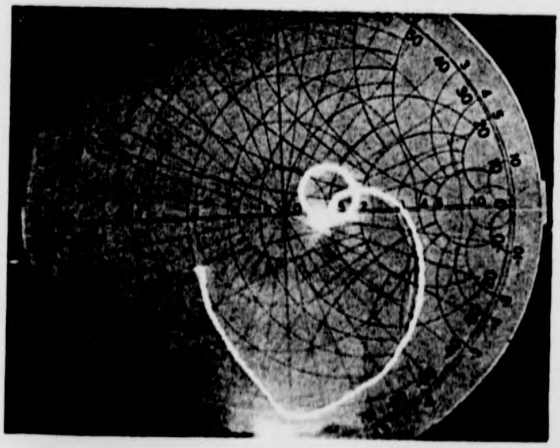

Reverse Bias
(-50V)

Fig. 4.16 Impedance sweep of P.i.n. diode

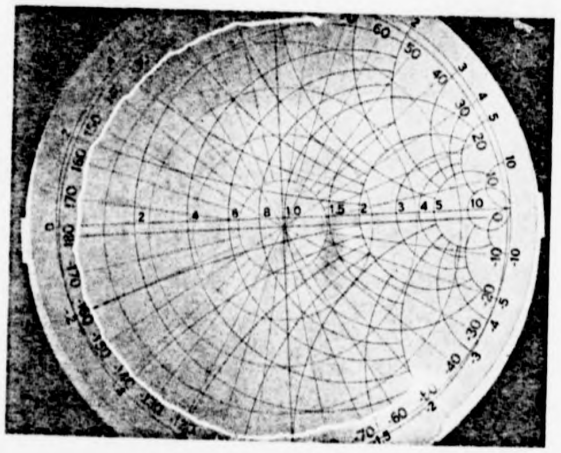

Forward Bias
(100mA)

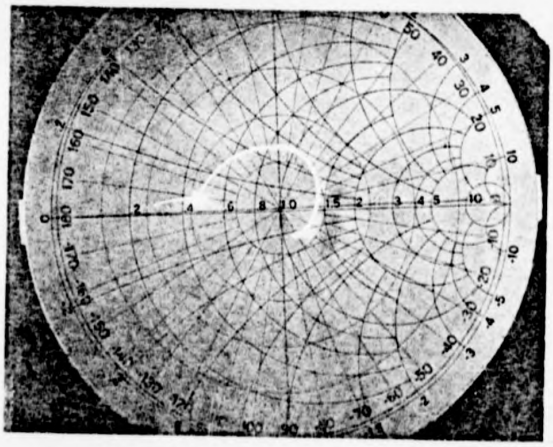

Zero Bias

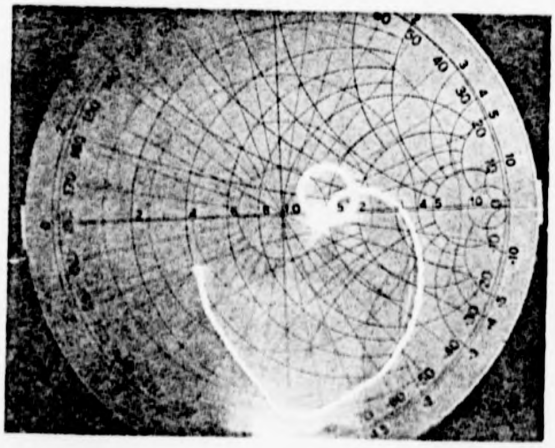

Reverse Bias
(-50V)

Fig. 4.16 Impedance sweep of P.i.n. diode

REFERENCES

1. CHAFFIN, R. J., Microwave semiconductor devices - fundamental and radiation effects, Wiley 1973.
2. WATSON, H. A., Microwave semiconductor devices and their circuit applications, McGraw-Hill 1969.
3. D'INZEO, G., et al, 'Design of circular planar networks for bias filter elements in microwave integrated circuits', Alta Frequenza, Vol. 48, No. 7, July 1979, pp.425-431.
4. DARKO, K., and VIDULA, B. S., 'Design equations for symmetric DC blocks', IEEE Trans. Vol. MTT-28 1980, pp.974-981.
5. GEORGOPOULOS, C. J., 'P.i.n diode driver saves time', Microwaves 1972, pp.50-55.
6. GETSINGER, W. J., 'The packaged and mounted diode as a microwave circuit', IEEE Trans. Vol. MTT-14 1966, pp.58-69.
7. HAMILTON, C, 'An insertion loss method to determine p.i.n diode parameters', NTZ, Vol. 28, part 8, 1975, pp.284-286.
8. WHITE, J. F., Microwave semiconductor control, Van Nostrand Reinhold (New York) 1981.
9. HAPGOOD, D. W., 'Determination of varactor by a modified DeLoach method', Microwave Journal, Nov. 1981, pp.83-90.

CHAPTER 5

SWITCHING CHARACTERISTICS OF P.I.N. DIODE

5.1 INTRODUCTION

The rectifying actions of a p-n junction diode becomes less and less effective as its frequency of operation rises. This effect is used in the production of semiconductor devices which presents a substantially linear impedance to microwave signals. The p.i.n. diode is one such device. This device acts as an ordinary diode at frequencies below 100 MHz. However above this frequency, it ceases to be a rectifier and acts as a variable resistance device whose value can be controlled by the application of a d.c. or low frequency bias signal.

It was shown in the last chapter that the microwave resistance of the device changes from a value of 1.32 ohms under forward bias to 1.56 K-ohms under reverse bias. Hence, if the device is mounted across any transmission line, the power flow will be unaffected under reverse bias, whereas under forward bias most of the power will be reflected and hardly any is transmitted.

The design of the two state multiplexer investigated in the later chapter makes use of this switching action of the p.i.n. This chapter explores

those switching characteristics of the diode which will be significant in the intended application. These characteristics include the isolation and insertion loss that can be obtained from a single and multiple diodes. The chapter looks at the various ways of increasing the isolation and reducing the insertion loss of the diode so that it can approximate more closely to an ideal switch. The use of synchronous and stagger tuning techniques are also investigated. Finally, the variations of the diode parameter with changes in the bias signal were fully investigated.

The work was restricted to single pole switches where only one port serves as the input. Throughout the analysis, the effects of the biasing networks were neglected as it was shown in the last section that they contributed negligible loss to the circuit. However, the effects of the coaxial transitions were accounted for in the design. This is because when the diode is reverse biased, these transitions contribute about 20% of the total losses.

5.2 SINGLE POLE SINGLE THROW SWITCH

5.2.1 Single diode switching: Two circuits were made on polyguide substrate which has a 1-oz sheet of copper bonded on one side and a 0.25 in thick aluminium plate bonded on the other side. The aluminium provides the

necessary mechanical stabilization for the polyguide and also serves as a mounting structure for the connectors and a heat sink for the diodes. The bias filter was situated at the output side of the diode so that power should be reflected from the port that is connected to the diode module. The d.c. block used is a 1000pF chip capacitor and two of these are located at the input and outputs respectively. The overall circuit is shown in fig. 5.1.

The matching sections of the circuit are 35 ohms quarter-wave transformers designed to match the load to the characteristic impedance of the line. The diode was located at a length 'θ' from the input port such that $60^{o} \leq \theta \leq 120^{o}$ throughout the operating band. The circuit response was then measured over the frequency band 2.0 - 4.0 GHz in steps of 200 MHz.

Fig. 5.2 shows the variations of the insertion loss of the diode with frequency when the diode is reverse biased. The response shows a minimum transmission coefficient $|S_{21}| = 0.94$ at 3.2GHz and a maximum reflection coefficient $|S_{11}| = 0.11$ for the zero bias condition. When the bias is increased to -30V, the transmission coefficient minimum increases to 0.96 which is equivalent to 0.36 dB insertion loss.

Fig. 5.3 shows the variation of the isolation of the diode when a forward bias is applied to it. With 50mA bias current, the minimum isolation obtained was

$|S_{21}|$ = 0.093 (20.6dB) for type DC 2418A and $|S_{21}|$ = 0.072 (22.8dB) for DC 2518G. When the bias was reduced to 15mA, this value reduces to $|S_{21}|$ = 0.12 (18.4dB) and 0.14(17.1dB) respectively. The difference between the measured and the computed response was greater for type DC 2518G.

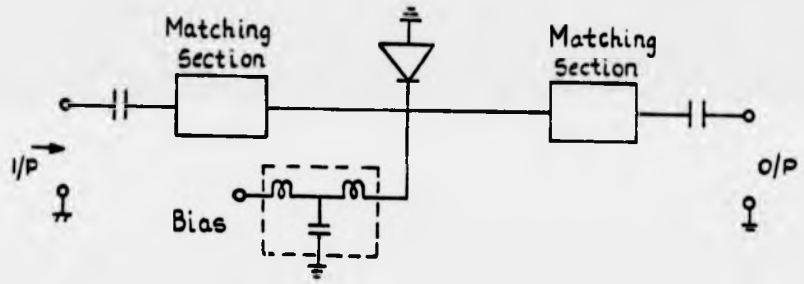

Fig.5.1 P.i.n. diode switch.

5.2.2 Effects of bias: As explained in chapter 4, the effect of biasing the diode is either to increase or reduce the carrier concentration in the i-layer. This affects the r.f. conductance of the diode in a manner given by the expression[1]:

$$G_{rf} = KQ_d \qquad 5.1$$

where G_{rf} = R.f conductance of the diode

Q_d = charge stored in the diode

K = constant

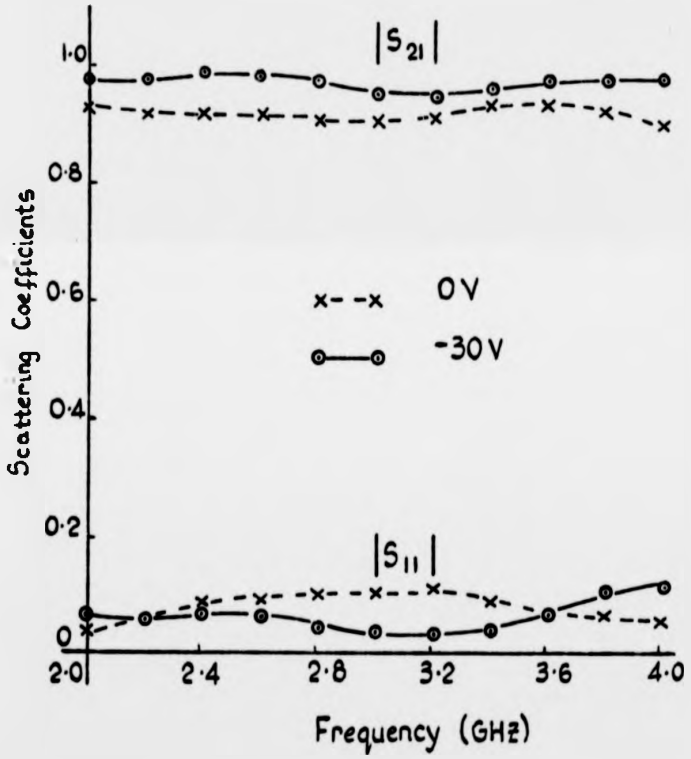

Fig.5.2 Variations of the transmission and reflection coefficients of a reverse bias diode.

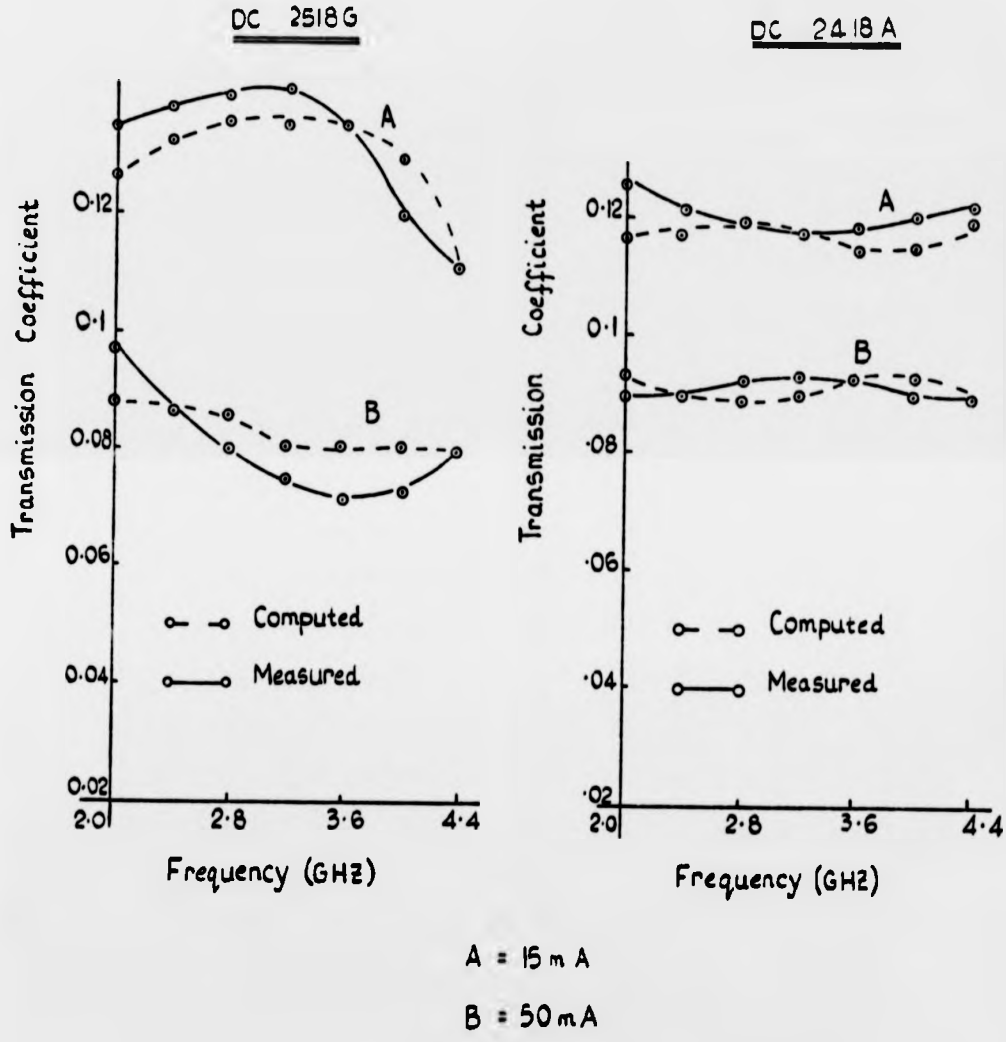

Fig.5.3 Variations of the magnitude of the transmission coefficient with frequency for a forward biased diode.

From eqn. 4.3, the isolation of the diode is given by

$$\alpha = 20 \log |(1 + G/2Y_o) + (B/2Y_o)| \qquad 5.2$$

where G + jB is the diode admittance.

To obtain maximum isolation, the forward bias conductance should be as large as possible. From eqn. 5.1, this implies that the forward bias current should completely saturate the intrinsic region with charge, thus producing the highest possible conductance level. To investigate the above phenomenon, various bias levels were used to bias the diode and the circuit was measured over the frequency range 2.0 - 10 GHz.

Fig. 5.4 shows the results obtained. As seen, the isolation increases proportionally as the current is increased from 0 - 10 mA. However above 10 mA, any increase in the bias current produces only a small increase in the value of the isolation. Above 30 mA, the isolation enters the saturation region. Here increase in current does not produce any increase in isolation. The graph also shows that for a given bias, the isolation varies with frequency. The isolation obtained at 2.0 GHz reached a maximum of 22.8dB compared to 18.8dB obtained for 10 GHz.

Using the results obtained at 2.0 GHz, the admittance of diode was calculated for the various bias levels. Using these calculated values, a graph of admittance against bias current was constructed as

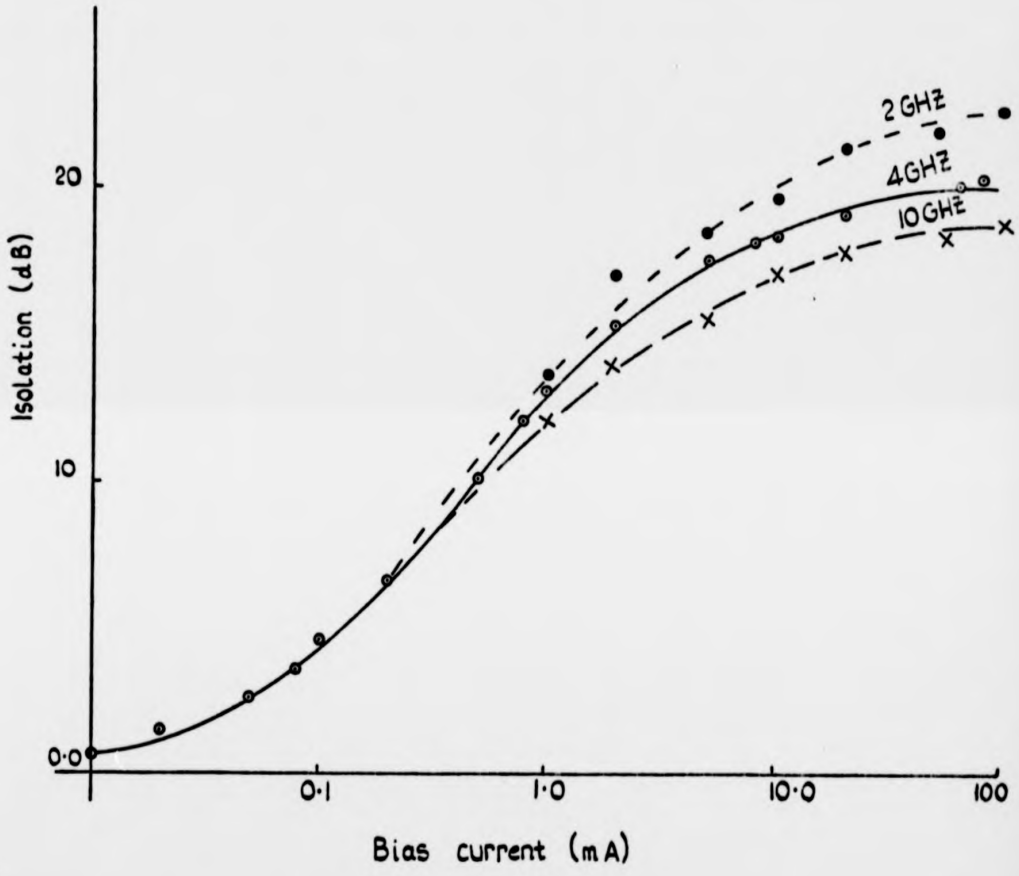

Fig.5.4 Variations of isolation with forward bias current with frequency as a parameter.

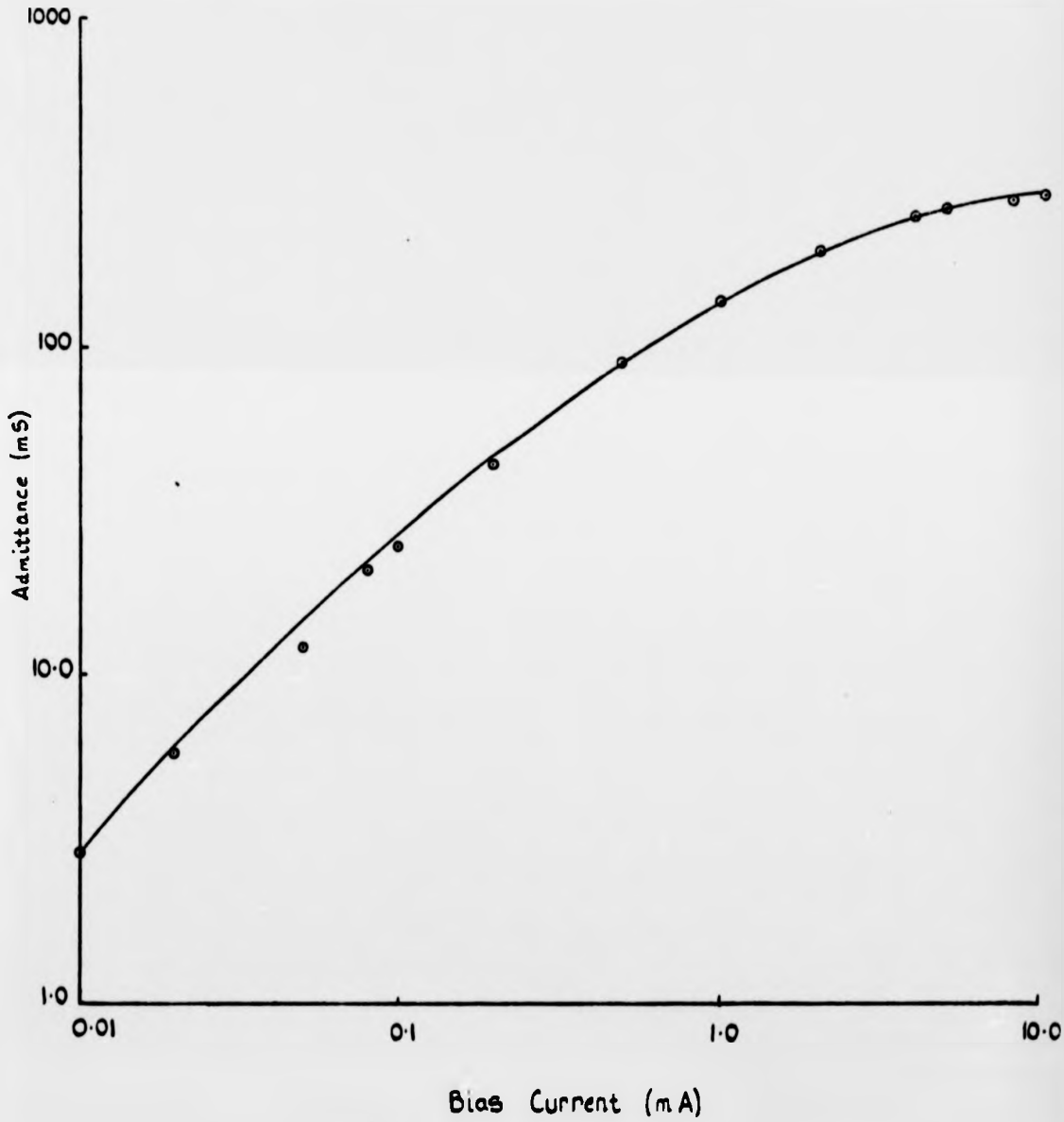

Fig.5.5 Variations of admittance with foward bias signal.

shown in fig. 5.5. This shows that the admittance of the diode varies from 2.8mS for a bias current of 0.01mA to 300mS when the bias is 10mA. To ensure that maximum admittance was always obtained, the circuit driver was adjusted so that the forward current is never below 20mA. In doing this it was ensured that the forward voltage drop does not exceed the maximum limit.

5.2.3 Multiple diode circuit: Since it is difficult to obtain more than 25dB of isolation from a single diode, it was decided to incorporate multiple diodes in the circuit. Two circuits were made for N = 2 and 3 diodes. The diodes were biased separately as shown in fig. 5.6. The length of the transmission line separating the diodes was made quarter-wavelength at 3.0GHz. The circuit was measured using bias currents of 30mA and 50mA, and a reverse voltage of -30V.

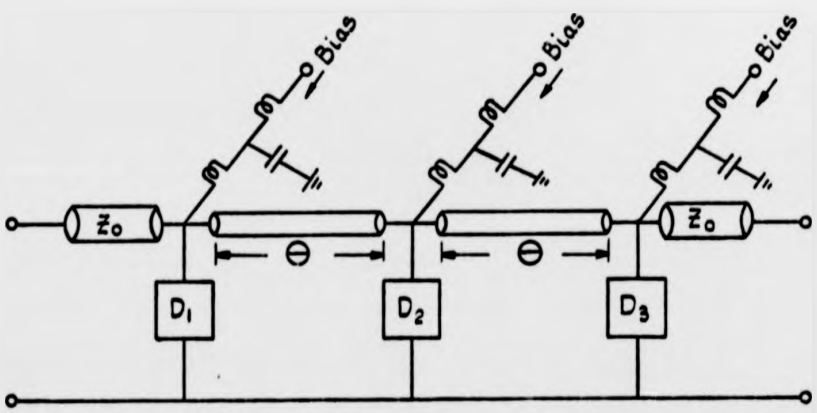

Fig. 5·6 Multiple diode switch

Fig 5.7 shows the response of the reverse biased diodes. For the case of N = 2, the transmission coefficient has a minimum of $|S_{21}| = 0.92$ (0.72 dB) compared to $|S_{21}| = 0.90$ for N = 3. The maximum reflection coefficient in each case was $|S_{11}| = 0.07$ and 0.09 respectively. The forward bias behaviour is shown in fig. 5.8. An isolation of 44 dB was obtained with two diodes over a 30 percent bandwidth compared to 53.9 dB for three diodes.

5.3 RESONANT MODE SWITCHING

5.3.1 Single diode tuning: To use this mode of switching a new diode model was constructed in place of the equivalent circuit of Fig. 4.3(c). In his model, shown in fig. 5.9, $X_n(n=1,2)$ represents the net reactance which includes the effects of the package capacitance C_p and other stray reactances. The value of X_n was found from fig. 5.3. Since this net reactance is predominantly positive, the resulting reactance was neutralised by inserting a capacitor to resonate with the inductance at 3.9 GHz.

The required capacitance to achieve this objective was computed to be 17.83 pF. The exact value of this capacitance could not be obtained hence it was decided to use a standard value of 22 pF. The measured response is shown in fig. 5.10.

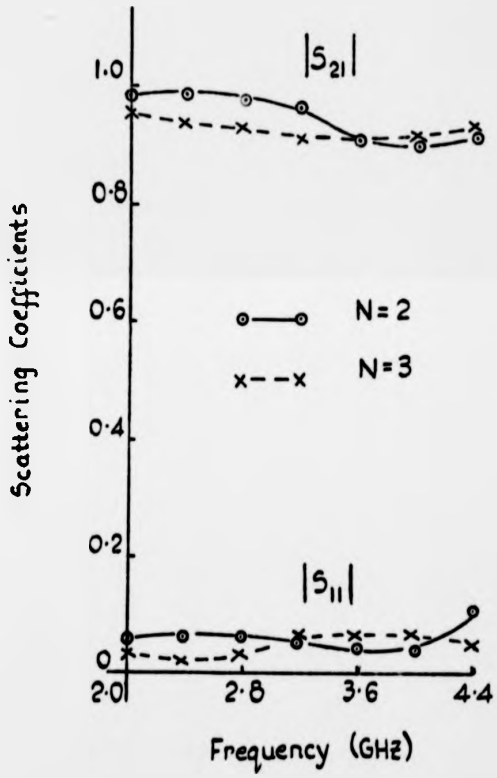

Fig.5.7 Reverse

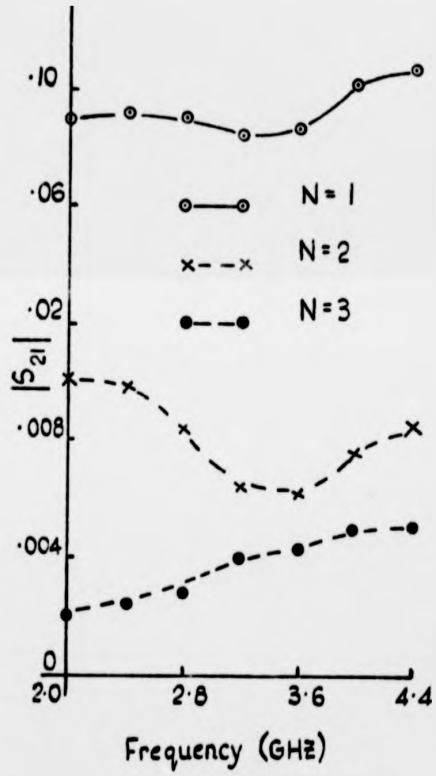

Fig.5.8 Forward

Figs.5.7 - 5.8 Response of multiple diodes.

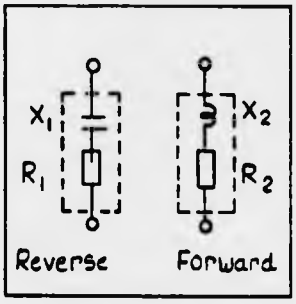

Fig.5.9a New diode model.

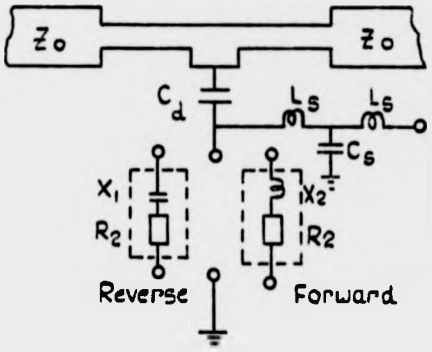

Fig.5.9b Resonant circuit switch.

5.3.2 Single stub tuning: This technique was equally investigated. Two single stub tuned diode circuits were made as shown in fig. 5.11. The stub length was chosen to be λg/4 at 3.0 GHz. The diode was located at the end of the stub line. The measured diode impedance in each state was used to calculate the stub admittance. Because of the discontinuity at the end of the stub, fig. 5.11 (b) was adjusted to compensate for the shift in the centre frequency introduced by

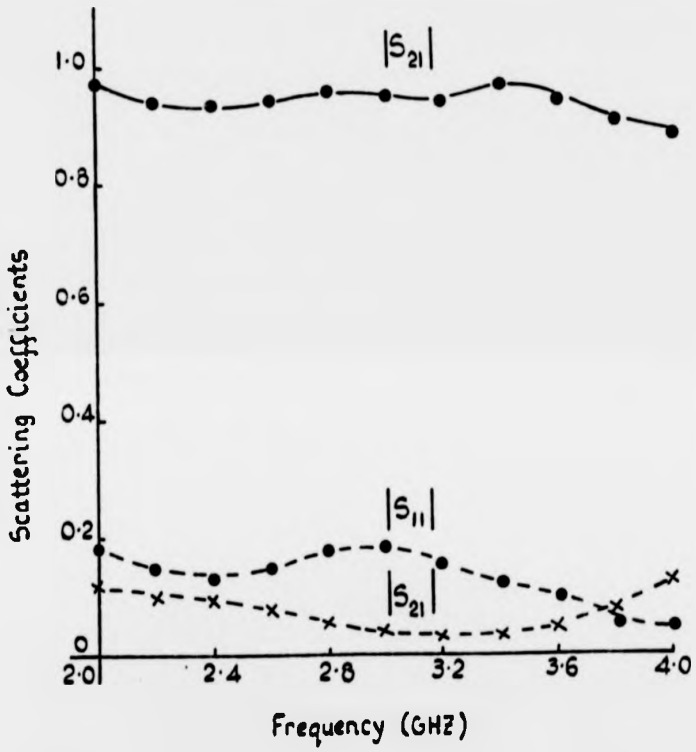

Fig.5.10 Transmission and reflection coefficients of a resonant diode switch.

o —— o Reverse bias
x - - x Forward bias

the junction discontinuity.

The circuit response was then measured using bias signals of 50 mA and -10V. The results are shown in fig. 5.12. The transmission coefficient of the matched circuit reached a maximum of only $|S_{21}| = 0.87$ compared to 0.95 obtained with the uncompensated circuit. However, the former has a bandwidth of 60 percent compared to 30 percent in the latter. Secondly the uncompensated circuit shifted from the design centre frequency of 3.0 GHz to 3.8 GHz. In the reverse biased state, the compensated circuit has $|S_{21}| = 0.21$ compared to 0.30 in the latter case.

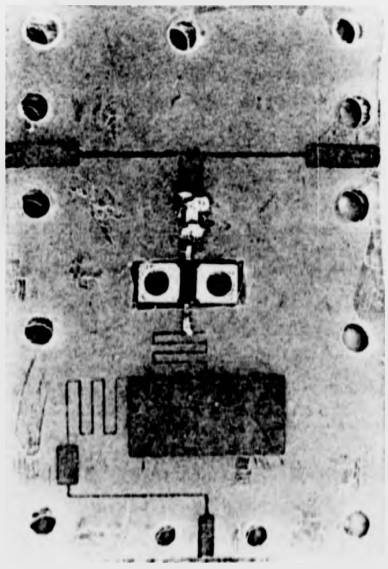

Fig.5.11b Single stub diode circuit.

the junction discontinuity.

The circuit response was then measured using bias signals of 30 mA and -10V. The results are shown in fig. 5.12. The transmission coefficient of the matched circuit reached a maximum of only $|S_{21}| = 0.87$ compared to 0.95 obtained with the uncompensated circuit. However, the former has a bandwidth of 60 percent compared to 30 percent in the latter. Secondly the uncompensated circuit shifted from the design centre frequency of 3.0 GHz to 3.8 GHz. In the reverse biased state, the compensated circuit has $|S_{21}| = 0.21$ compared to 0.30 in the latter case.

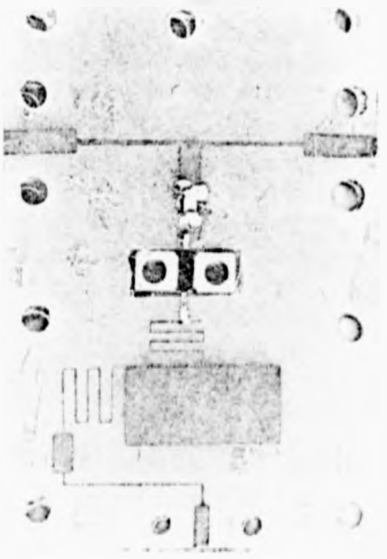

Fig. 5.12 Single stub diode circuit.

The reflection coefficient $|S_{11}|$ obtained in both bias states showed the improvement obtained with the compensated circuit. An important point noted with this type of technique is that the characteristic of the diode were reversed because of the stub transformation. This means that the high (low) impedance of the diode in the reverse (forward) bias state was transformed to a low (high) impedance at the diode stub line yielding a high isolation when the diode is reverse biased and a low insertion loss under forward bias.

5.3.3 Synchronous and stagger tuning: To investigate this technique, two double stub circuits were built on a 0.063 ins thick polyguide substrate. The circuits and the appropriate line dimensions are shown in fig. 5.13. In fig. 5.13 (b) the stubs were staggered to obtain greater bandwidth. The choice of the centre frequency of the individual stubs was made with the results obtained in fig. 5.12 (a). Knowing that the matched stub can maintain constant transmission coefficient over 15 percent on either side of the centre frequency, the lengths of the stagger tuned stubs were chosen such that the difference between their two lengths, $\Delta\theta$, always lies within the range $10^{o} \leq \Delta\theta \leq 30^{o}$.

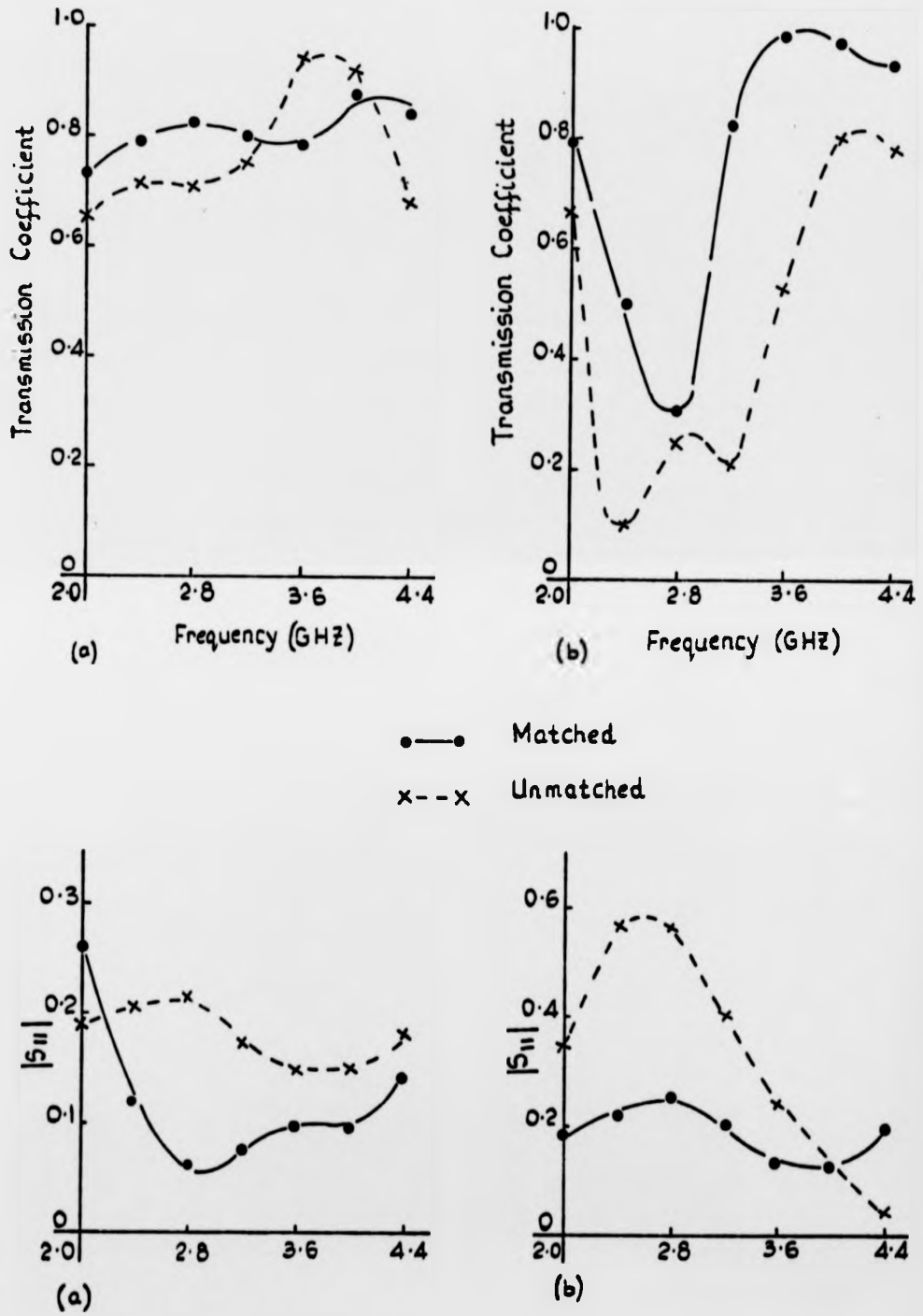

Fig.5.12 Response of stub tuned diode
(a) Forward bias
(b) Reverse bias

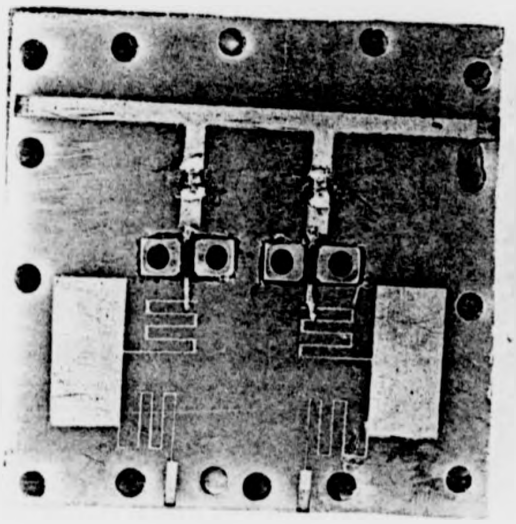

Fig. 5.13a Synchronous stub diode circuit.

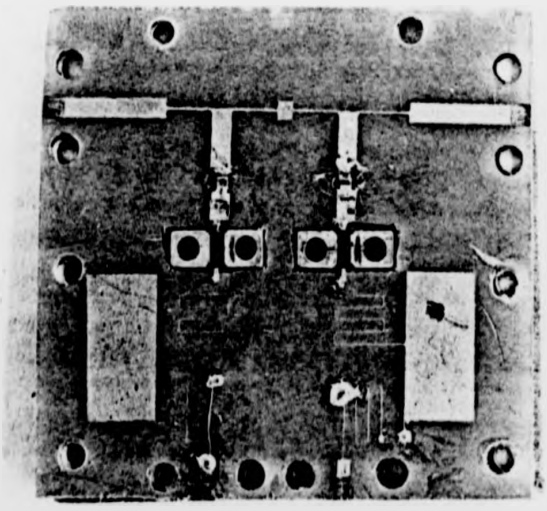

Fig. 5.13b Stagger stub diode circuit.

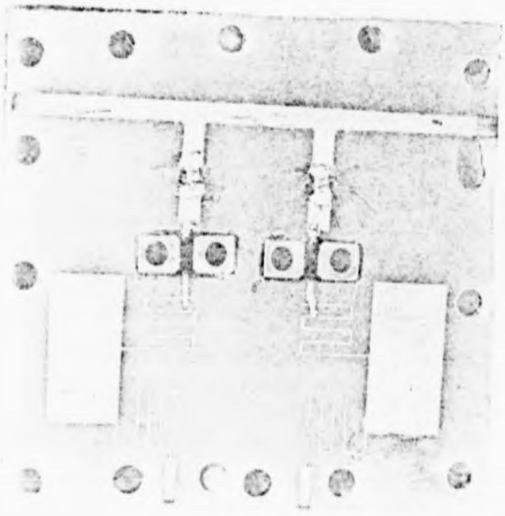

Fig. 5.12a Symchronous stub diode circuit.

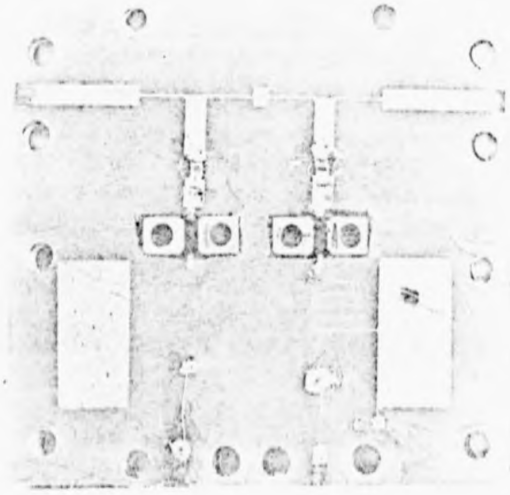

Fig. 5.12b Staggered stub diode circuit.

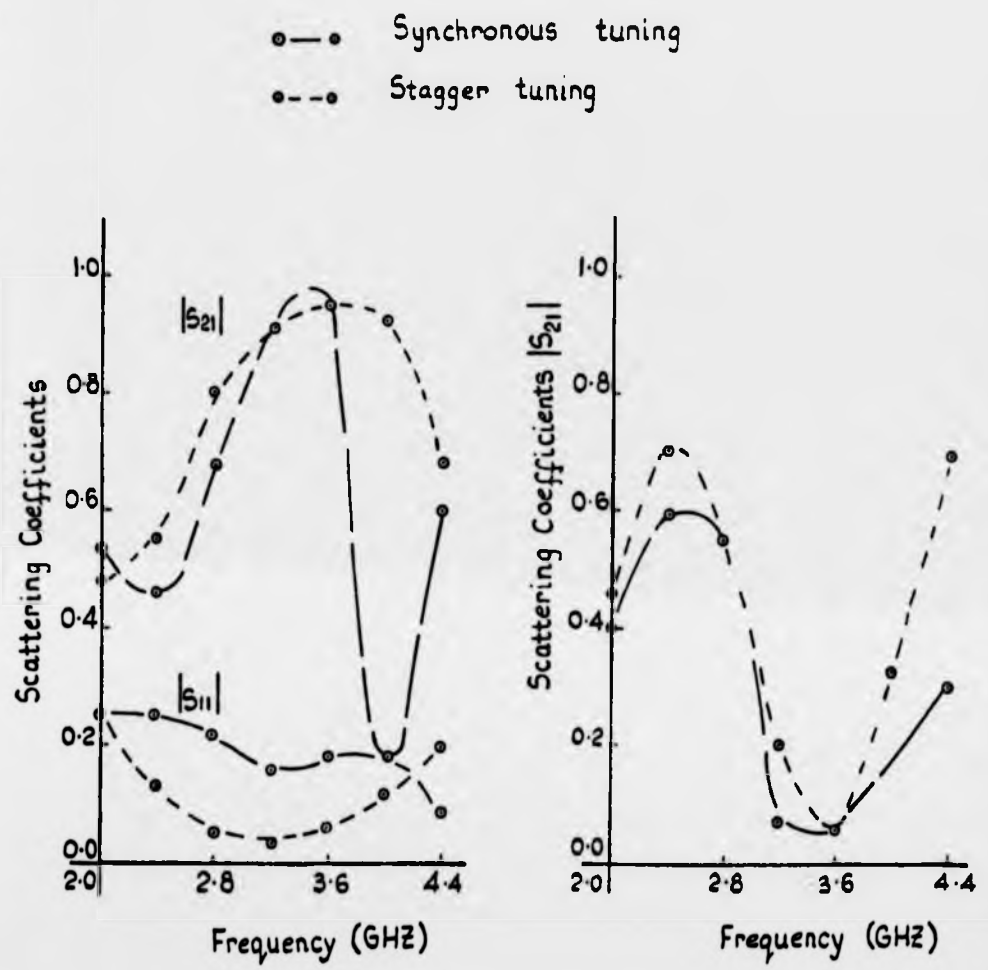

Fig.5.14 Response of synchronous and stagger tining.

The circuits were measured using bias signals of -10V and 50 mA. The results are shown in fig. 5.14. Though the synchronous circuit has a higher transmission coefficient $|S_{21}| = 0.98$. The staggered stub circuit gave a wider bandwidth and better reflection coefficient compared to the former.

5.4 DOUBLE THROW SWITCH

5.4.1 Double throw (SPDT) switch: A single pole double throw switch was designed as shown in fig. 5.15. The operation of the circuit is such that when diode D1 is reverse biased, energy at the input port will flow past the diode towards the output ports. Forward biasing this diode will isolate the output ports. The matching networks at the input and output ports were chosen to give the best broadband results over the operating range. The d.c. return situated at point A is quarter-wavelength at the centre frequency of 3.0 GHz.

The dimensions of the matching networks and the circuit response are shown in table 5.1 and figs. 5.16 - 5.17.

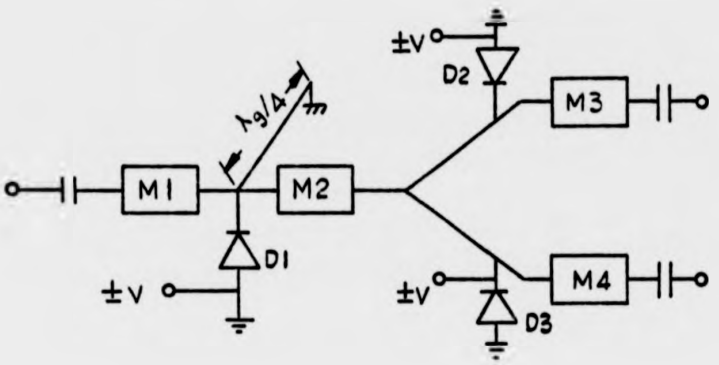

Fig.5.15 SPDT Switch.

Table 5.1

Matching Network	Impedance Z (ohms)	Electrical length (radians)
M1	36.25	0.24
M2	32.5	0.28
M3	37.5	0.50
M4	37.5	0.50

REFERENCE

1. FORGE, C; "Driving the p.i.n. diodes," Microwaves 1972 pp.30-37.

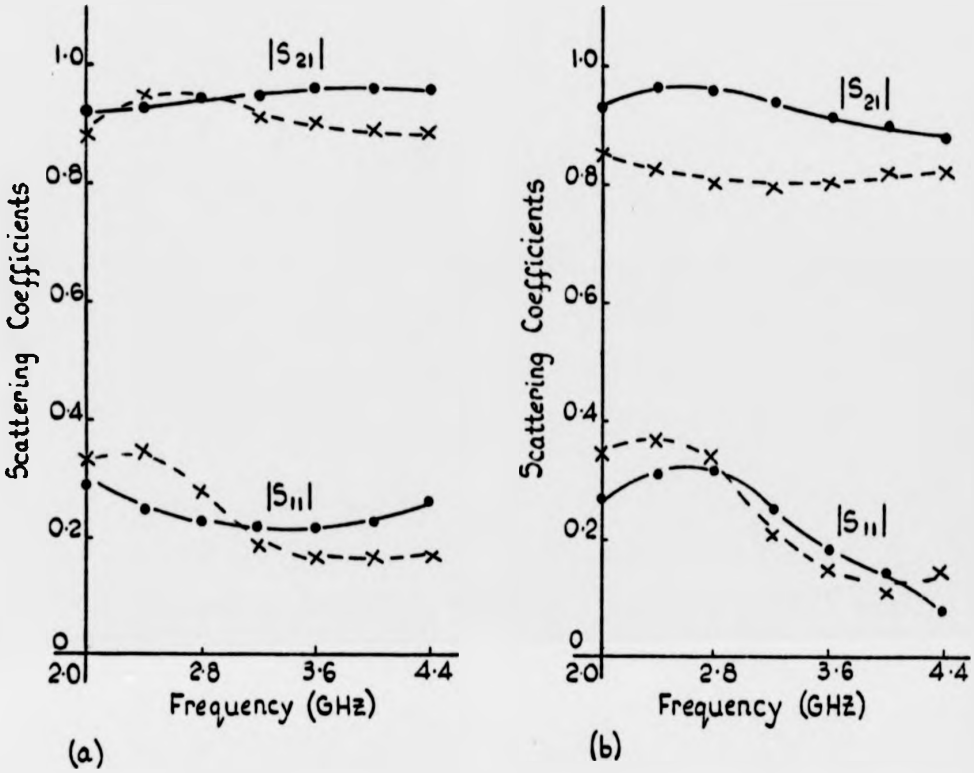

Fig. 5·16 Reverse biased SPDT switch

(a) Other port reverse biased

(b) Other port forward biased

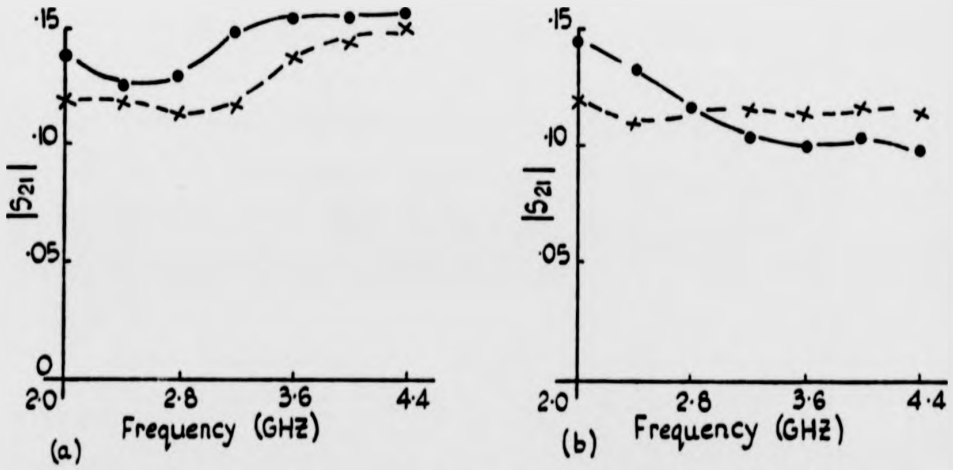

Fig. 5·17 Forward biased SPDT switch

CHAPTER 6

MEANDERLINE DESIGN

6.1 INTRODUCTION

A meanderline configuration consists of an array of parallel coupled transmission lines with an alternating end connections at the beginning and at the end of each line. Because of the coupling of electromagnetic fields, a meanderline like any pair of coupled lines, can support two different modes of propagation. These modes have different characteristic impedances. The velocity of propagation of these modes is equal when the lines are imbedded in a homogenous dielectric.

The growing interests in this structure resulted from the fact that recent works[1,2] have revealed that useful characteristics can be realized by suitably specifying the topology of its boundary elements. Because of these characteristics the structure is finding increasing use in microwave and millimetre wave applications. This growing use has created the need to formulate accurate design criteria for the structure.

Few analytical techniques have been proposed for the determination of the propagation characteristics of the meanderlines and to date, the explicit

expression for the network function has not yet been obtained. There are many reasons why this structure is difficult to analyze. While on one hand the structure can be regarded as a periodic structure loaded at regular intervals, on the other hand the coupled characteristics of the structure makes it more difficult to analyze the structure from its periodic behaviour.

Roome and Hair[3] first analyzed the meanderline using magnetic and electric walls as boundary planes. They partitioned one pair of coupled lines with an electric wall and the adjacent pair with a magnetic wall and then applied transmissionline theory. From the results they concluded that the even and odd mode impedances of a meanderline are identical since a change in excitation simply interchanges the boundary conditions.

The approach by Libbey[4] yielded different characteristic impedance and phase velocities for the even and odd mode propagation. The only draw back to that technique is that it cannot be used when the turns of the meanderlines are odd as the lines have to be partitioned in twos. The graph transformation technique of Iwakura[5] combated this drawback by considering the coupling variations of each line. This technique involves the use of graph equivalent in the network analysis. The technique is claimed to

yield accuracies less than three percent. However, like other graphical techniques, it suffers from the fact that it is difficult to incorporate in a design program.

In this chapter, a faster and easier method of analyzing the meanderline is given. The technique involves analyzing the meanderline in terms of its coupling and susceptance loading parameters. To evaluate the coupling parameters, the waves propagating along the coupled sections of the meanderline are expressed in terms of the even and odd mode characteristic impedances. The mode characteristic impedances were obtained by considering the effects of the self and mutual capacitances on the individual uncoupled lines. The method is quite applicable to both symmetric and assymmetric meanderlines. It has the advantage that it can be easily incorporated into any computer-aided design.

6.2 DESIGN TECHNIQUES

6.2.1 Design problems: Fig. 6.1(a) shows the schematic diagram of a single meanderline. The length of the line connecting adjacent elements is d, its width is δ and the element length is l. Because of the discontinuity susceptance at each turn, the meanderline can be represented by a transmission line periodically loaded with shunt discontinuities and coupled to its

next neighbour by its coupling parasitics. The equivalent circuit formulated by the present author for this structure is shown in fig. 6.1(b). In this equivalent circuit, the black box represents the coupling and the susceptance loading parameters of the meanderline.

The main design problems are thus concerned with the successful evaluation of these parameters. Since these parameters are not related by a common expression, it was decided to evaluate them separately and to incorporate the results into the analysis program. The evaluation of the susceptance parameters was limited to the case of uniform strip transmission lines only.

6.2.2 Evaluation of coupling parameters: Because of its coupled mode characteristics, the meanderline of fig. 6.1(a) can be described by its even and odd mode characteristic parameters as illustrated by the electric and magnetic field distribution of fig. 6.2(a). The even mode parameters are the parameters measured from one strip to ground when the strips carry currents in the same direction, while the odd mode parameters represent those measured when the strips carry currents in opposite directions.

These parameters may be obtained from the complete elliptic functions of a coupled line. However, the evaluation of these elliptic functions is both time

consuming and also involves some sacrifice in accuracy. Hence it was decided to evaluate the parameters using the quasi-static approach. To do this, the coupled parameters of the meanderlines were written in terms of its fringing capacitances. The values of these fringing capacitances were obtained using the function subprogram given in appendix D. The model used for computing these capacitances are given in fig. 6.2(b).

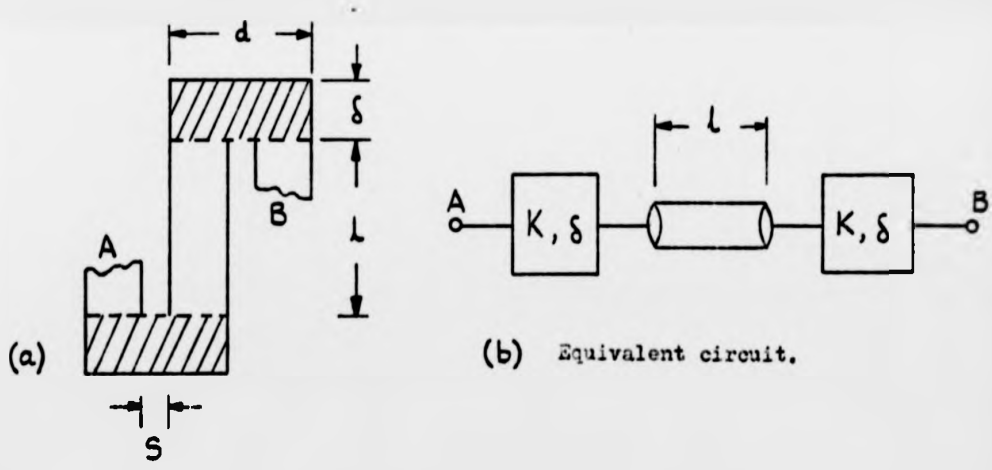

Fig.6.1 Meander-line and equivalent circuit.

The program can be used for either microstrip or triplate. The condition H1 = H2 defines the balance triplate. The program computes the total even mode and the odd mode capacitances to ground. This is

done by adding the appropriated components of the fringing capacitances to ground and the parallel plate component. It is noted that the coupling parameters of the outermost lines are not the same as that of the interior lines since for these lines either the magnetic or the electric wall is absent and one side of the line is unbounded. Hence the coupling parameters for these lines had to be appropriately modified. This was achieved by including the effects of the fringing capacitance which was evaluated from the capacitance of a single line geometry.

Only the coupling to the adjacent strips were considered. The coupling capacitances between strips which are separated by more than one strip were neglected. To obtain the voltage coupling between the meander-turns, the coupling between lines i and i + 1 was defined as

$$K_{i,i+1} = \frac{KM_{i,i+1}}{\left[(KG_i + KM_{i,i+1})(KG_{i+1} + KM_{i,i+1})\right]^{\frac{1}{2}}} \qquad 6.1$$

where KG_i is the total capacitance to ground per unit length for the ith conductor.

$KM_{i,i+2}$ is the mutual capacitance per unit length between the ith and the (ith + 1) conductor and is given by

$$KM_{i,i+1} = (KFO - KFE)_{i,i+1} \qquad 6.2$$

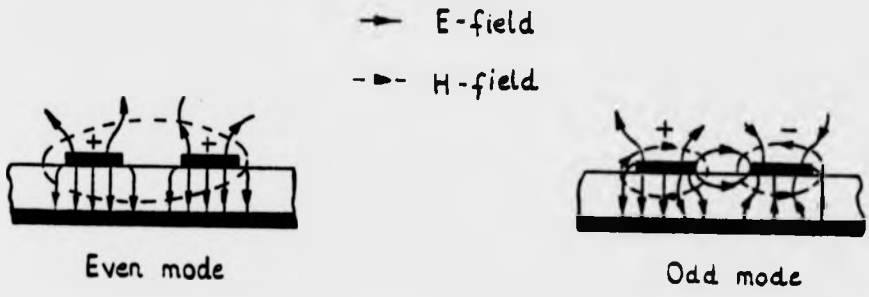

Fig. 6·2 (a) Field distribution of Even and Odd mode.

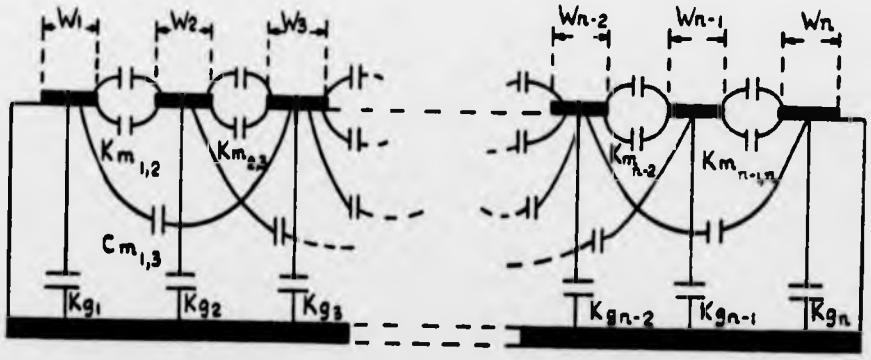

Fig.6.2b Model for computing coupling parameters.

KFO, KFE are the odd and even mode parameter evaluated as in appendix D.

Using equations 6.1 and 6.2, the even and odd mode impedances were then computed using the relations[6]

$$Z_{oe} = \left[\frac{1 + K_{i,i+1}}{1 - K_{i,i+1}}\right]^{\frac{1}{2}} \qquad 6.3$$

$$Z_{oo} = \left[\frac{1 - K_{i,i+1}}{1 + K_{i,i+1}}\right]^{\frac{1}{2}} \qquad 6.4$$

Having obtained the coupling parameters and the mode impedances, the next step in the design procedure was to characterize and compensate for the effects of the susceptance discontinuity at the bends.

6.3 SUSCEPTANCE DISCONTINUITY

6.3.1 Characterization of susceptance discontinuity:

The abrupt change in the geometry of any transmission line alters the electric and magnetic field distribution which results in discontinuity. The altered electric field gives rise to a change in the line capacitance whilst the changed magnetic field can be written in terms of an equivalent inductance. Thus the characterization of the susceptance discontinuity

of the meanderline simply involves the evaluation of these capacitances and inductances. This characterization can be based on the quasi-static considerations or it can be based on the more rigorous fullwave analysis using the planar waveguide model.

The technique used here involves making input impedances measurements on various lengths of a right angled bend. For an equivalent circuit description of the discontinuity region of the right angled bend, an approximate model similar to that previously used in section 2.4 was adopted. The choice of this model was based on its conceptual simplicity and ease of application. Fig. 6.3 shows the configuration and the measuring jig used in the characterization.

To find the values of the equivalent T-network representing the discontinuity reactances, two 50 ohms right-angled bends were made on polyguide substrate. The lengths l_1 and l_2 of the bend were chosen to be 90^{o} at 3.0 GHz and 3.5 GHz respectively. The input impedance of the individual network was then measured over the frequency range 2.0 - 5.0 GHz in steps of 200 MHz using the on-line computer corrected network analyzer.

From fig. 6.3 and using transmission line theory, the impedance at plane SS^{1} is related to the open circuit impedance via the relation:-

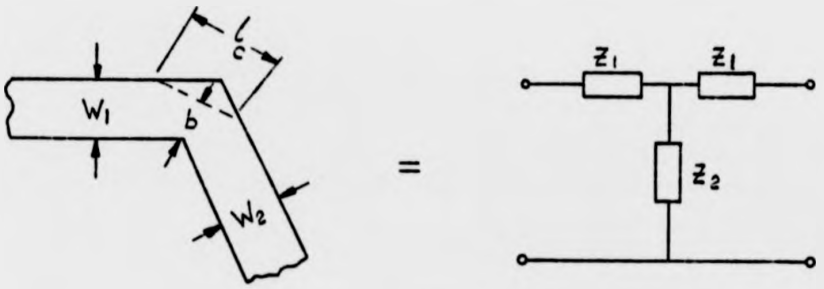

Fig. 6·3 (a) Right angle and equivalent circuit

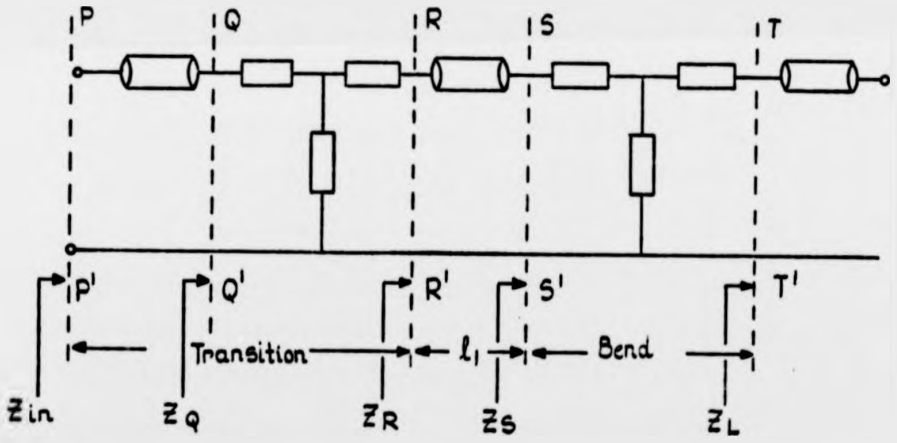

Fig.6.3b Measuring jig for right angle.

$$Z_S = \frac{Z_1^2 + 2Z_1Z_2 + Z_T(Z_1 + Z_2)}{Z_1 + Z_2 + Z_T} \qquad 6.5$$

Similarly the impedance at the other planes are related as explained in section 3.4. The measured input impedance is related to the impedance at plane QQ^1 via the transmission line equation:-

$$Z_Q = Z_o \left[\frac{Z_{in} - jZ_o \tan \beta l_o}{Z_o - jZ_{in} \tan \beta l_o}\right] \qquad 6.6$$

Since the expressions contain two unknowns, only two measurements were needed. By incorporating the values of the parasitic elements representing the coaxial transition, the susceptance reactances were found to be 0.023nH and 0.156pF respectively. The accuracy of these values were tested by measuring the transmission and reflection coefficients of a through right angled bend. The results are shown in fig. 6.4.

6.3.2 Compensation technique: The best known techniques for compensating for the discontinuity reactance of the right-angled bend are to use curved or chamfered transitions. Measurements by Easter[7] and by Anders et al[8] indicate that a chamfer length of 1.8 and 1.6 line width respectively give a VSWR of less than 1.12

up to 12 GHz. However, none of these authors gave an equivalent representation of the chamfered bend and there are no theoretical computation in other literatures showing how far such chamfering reduces the shunt susceptance of the bend.

In this section, the percentage reduction resulting from such compensation was evaluated using the results obtained for the right-angled bend. The evaluation was based on the assumption that the chamfering improves only the shunt capacitance. Hence any difference in the results was attributed to a decrease in that capacitance. Compensation using curved transition was also investigated and this was compared with the results obtained for the chamfered bends.

Six 50 ohms lines with varying degrees of bends were made on polyguide substrate 1.59mm thick. Samples of these are shown in fig. 6.5. The VSWR of these networks was measured over the same frequency range as the right angle.

To find the percentage reduction of the shunt capacitance the initial values obtained for the right angle were modified until there was a close agreement between the computed and the measured results. The results are shown in fig. 6.6. The results show that a VSWR of 1.05 was obtained with a chamfer length of 1.414 compared to 1.10 and 1.25

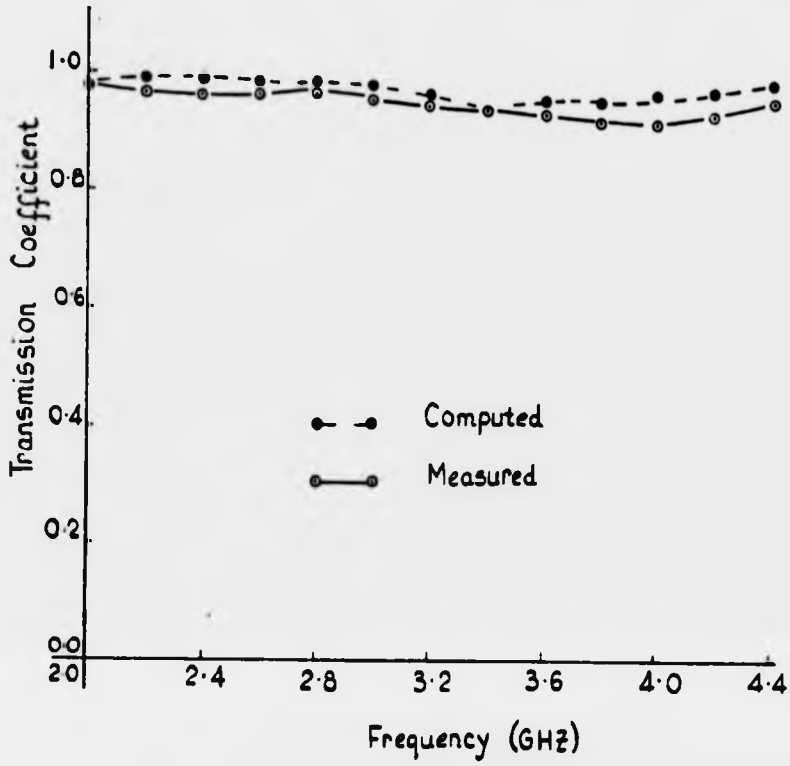

Fig.6.4 Variations of transmission coefficient with frequency for a right angled bend.

Fig.6.5 Samples of various bends.

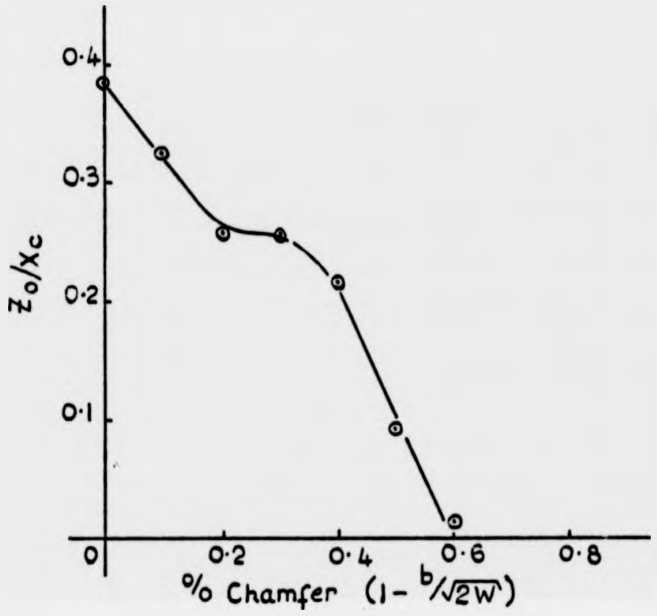

Fig.6.6c Variations of shunt capacitance as a function of percentage chamfer.

obtained for the curved and right angled corners. The effect of changing the chamfer length is shown in fig. 6.6(b). Using these results, a percentage reduction obtained with various chamfer lenghts was easily obtained. This is plotted in fig. 6.6(c)

6.4 DESIGN AND RESULTS OF MEANDERLINES

6.4.1 Design results: Using the procedures obtained in sections 6.2 and 6.3, fifteen meanderline circuits were designed with varying degrees of coupling and turns ratio. The computer program permits arbitrary choice of coupling between the turns including no

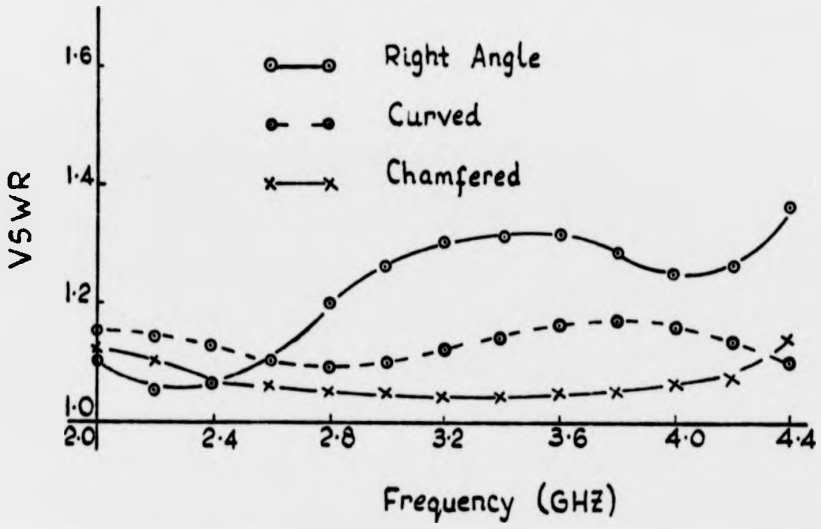

Fig. 6·6 (a) VSWR of various bends

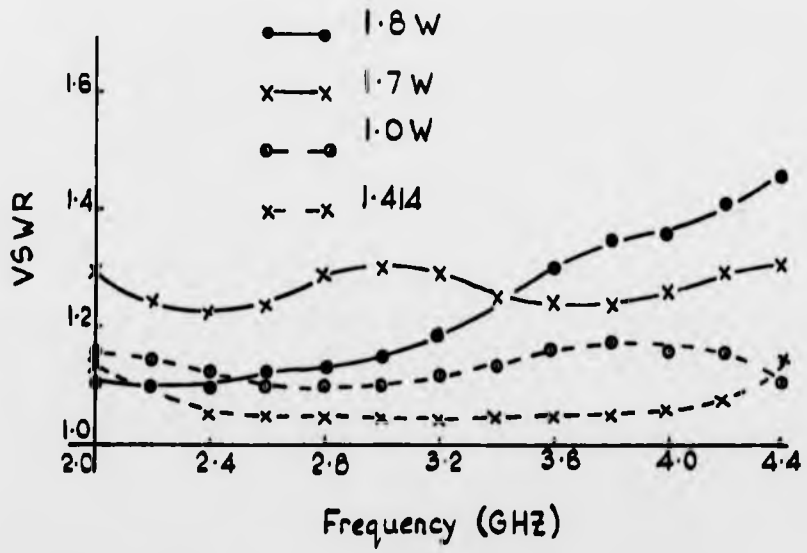

Fig.6.6b VSWR of various chamfers.

coupling between some of the turns as in the case of the hybrid and stub design. Fig. 6.7 shows the variations of the magnitude of the transmission coefficient and VSWR with frequency for an 11-turns meanderlines centred at 4.0 GHz.

The results clearly show the periodic stop-band characteristics of the structure. However, the measured response shifted from the designed value of 4.0 GHz to 3.8 GHz. The reason for this is probably due to the extra line-lengths introduced by the lines joining the adjacent strips. In the pass-band range, the transmission coefficient of the response reached a value of $|S_{21}| = 0.90$.

The effects of changing the spacing, S, and the electrical length, L, are shown in fig. 6.8. In the case of the former, decrease in the conductor spacing gives a lower transmission coefficient and hence higher attenuation in the stop band. However, the processing technique used here restricts the minimum spacing between the strips as values of $S < 0.07$mm could not be successfully procesed. This means that to obtain higher coupling ratio, wider conductor surfaces had to be used. This affects the attenuation characteristics in a manner shown in fig. 6.9.

The figure shows that the best stop-band attenuation is obtained if the coupling ratio is limited to between 0.10 and 0.22. Tighter or less coupling

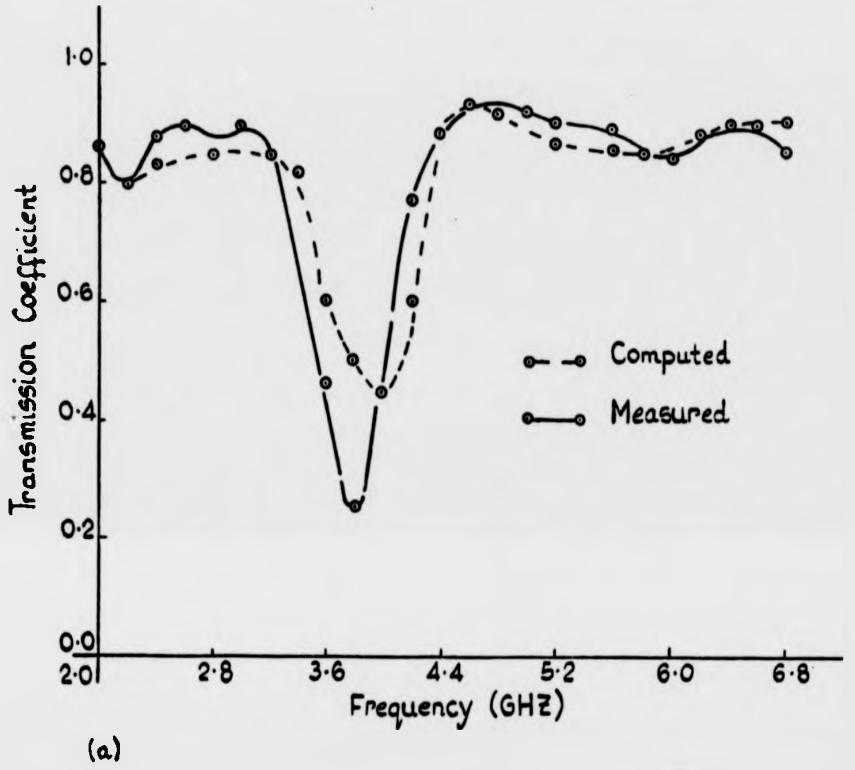

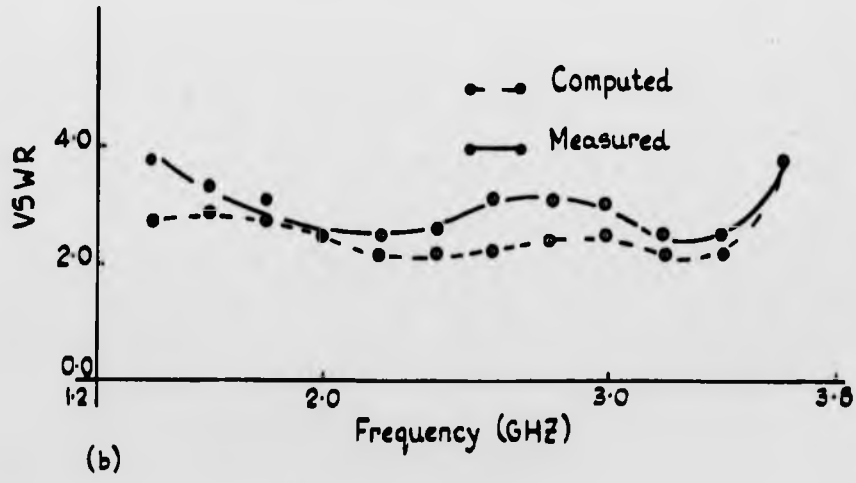

Fig.6.7 Variations of (a) transmission coefficient and (b) VSWR with frequency for a meanderline with N=11

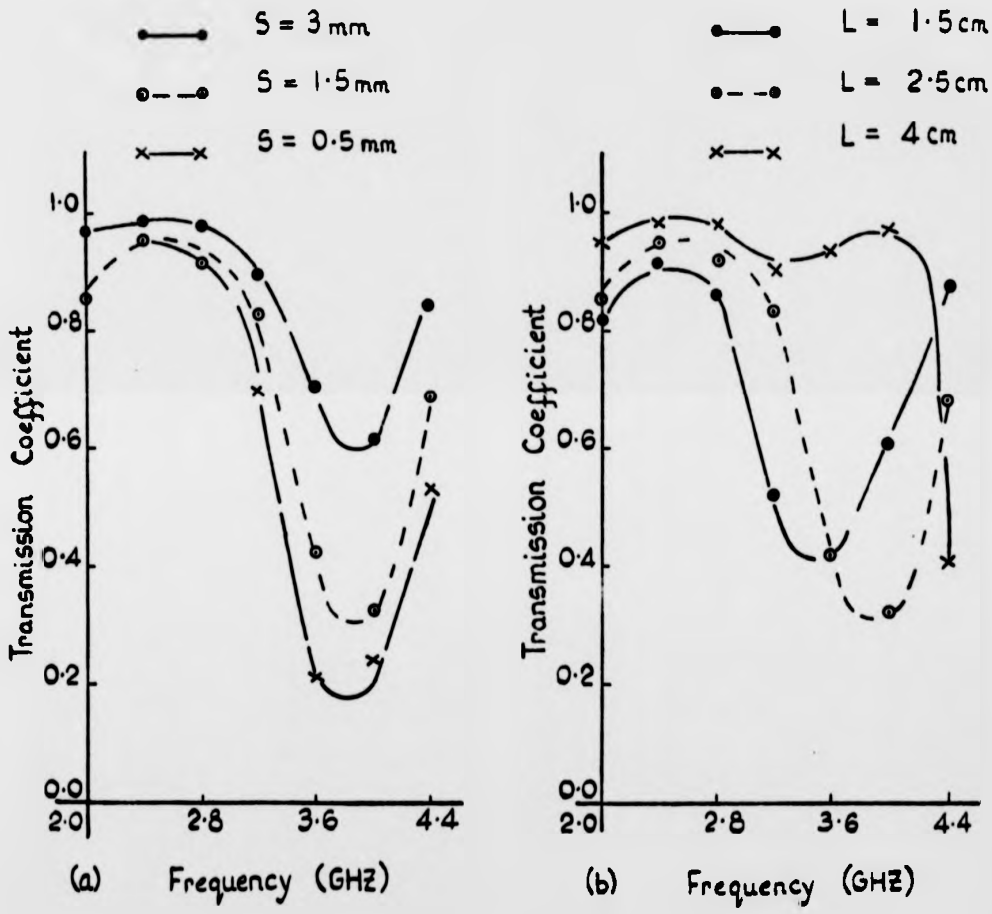

Fig.6.8 Effects of (a) spacing S, and (b) electrical length, L, on the transmission coefficient.

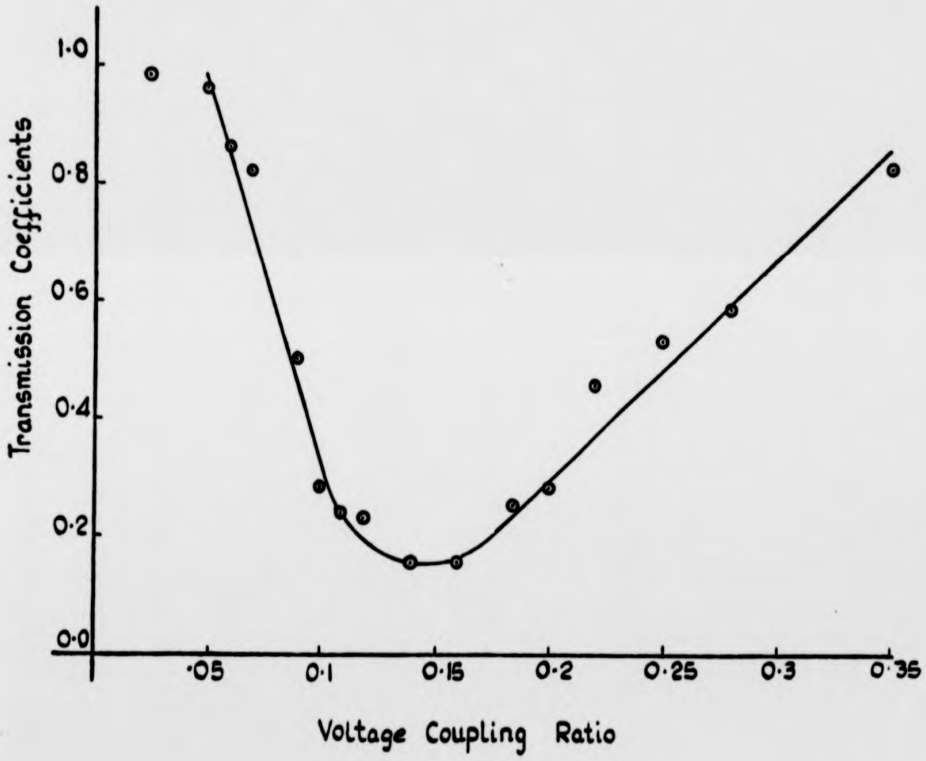

Fig. 6.9 Effects of voltage coupling ratio on transmission coefficients.

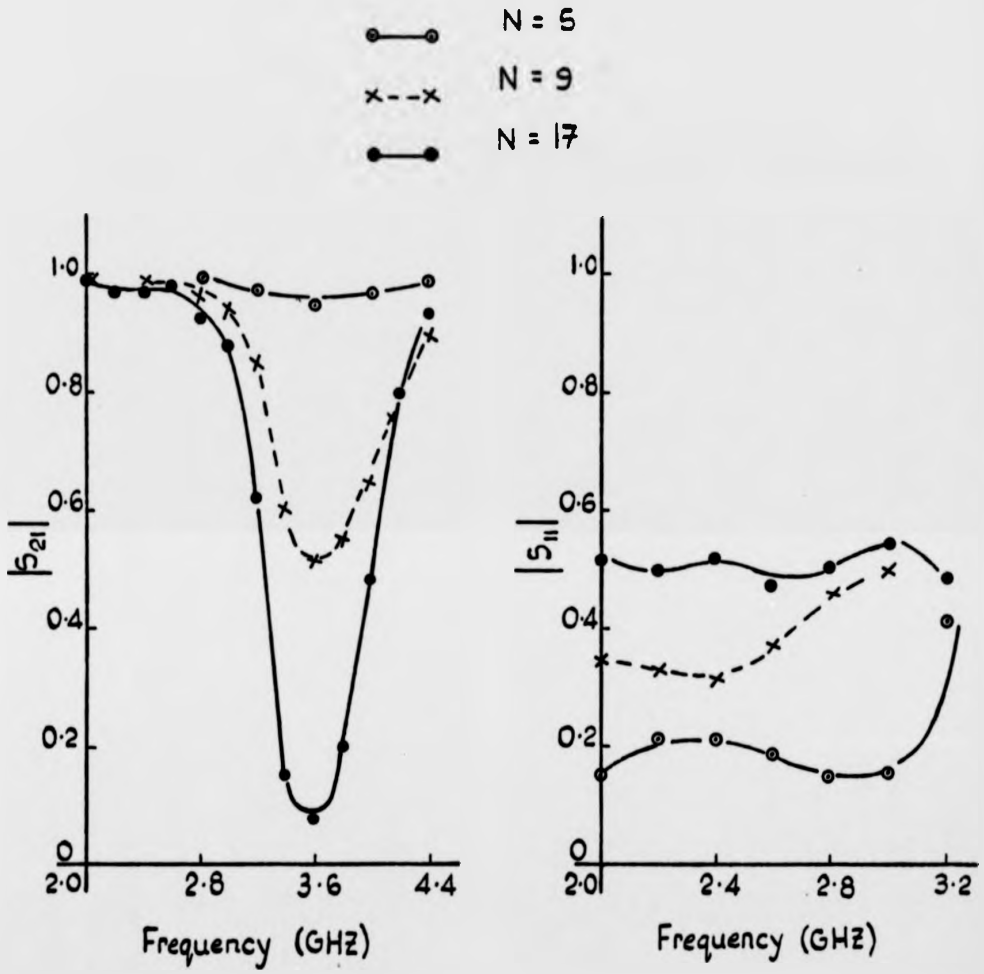

Fig. 6.10 Variations of transmission and reflection coefficients with frequency for meanderlines with various turns.

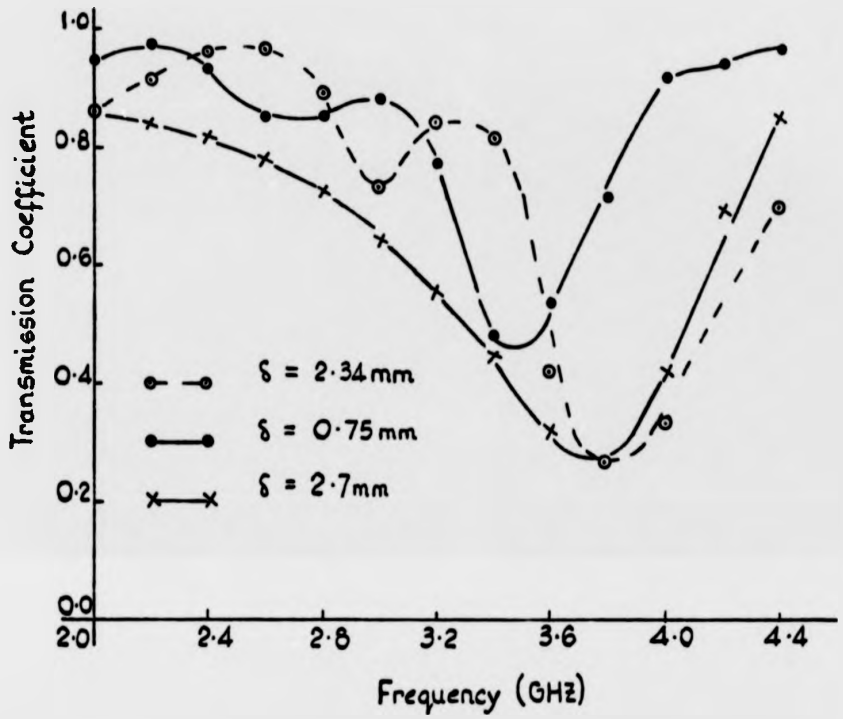

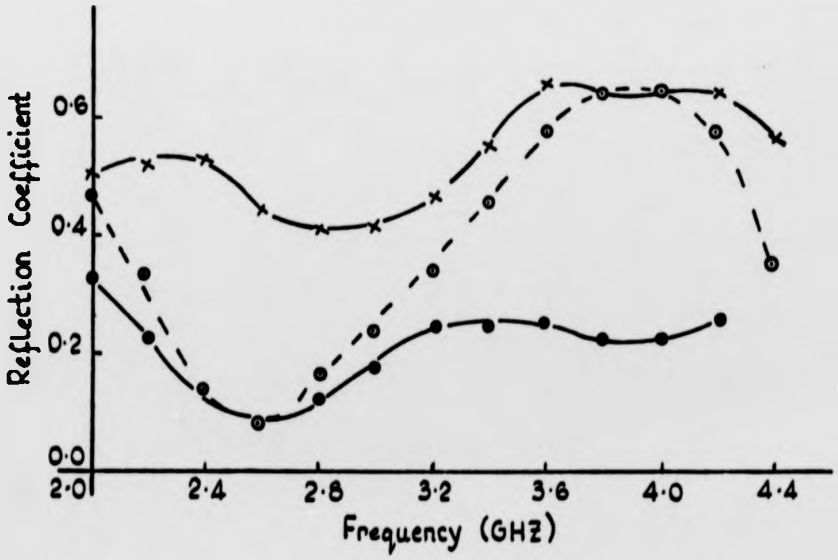

Fig.6.11 Effect of susceptance parameter on transmission and reflection coefficient.

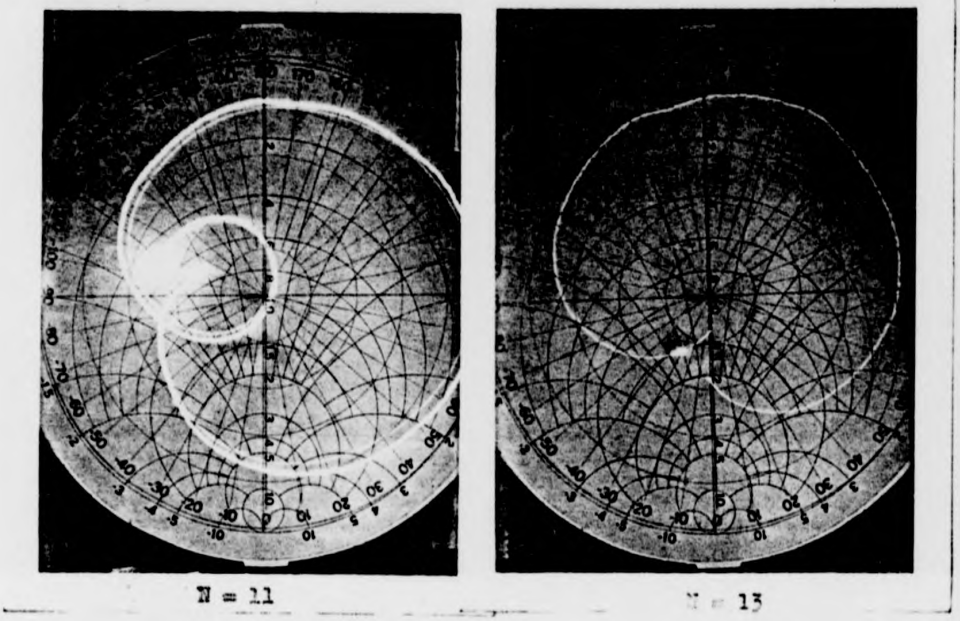

N = 11 N = 13

Fig.6.12 Impedance sweep (3.3 - 4.0GHz.) of meanderlines

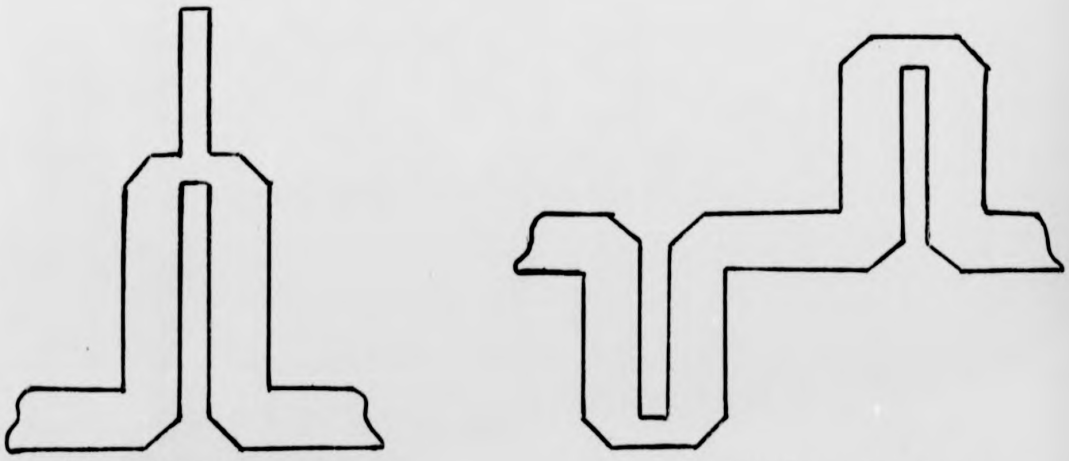

(a) Stub meanderline (b) Hybrid meanderline

Fig.6.13 Meanderlines with (a) stubs (b) hybrid configuration.

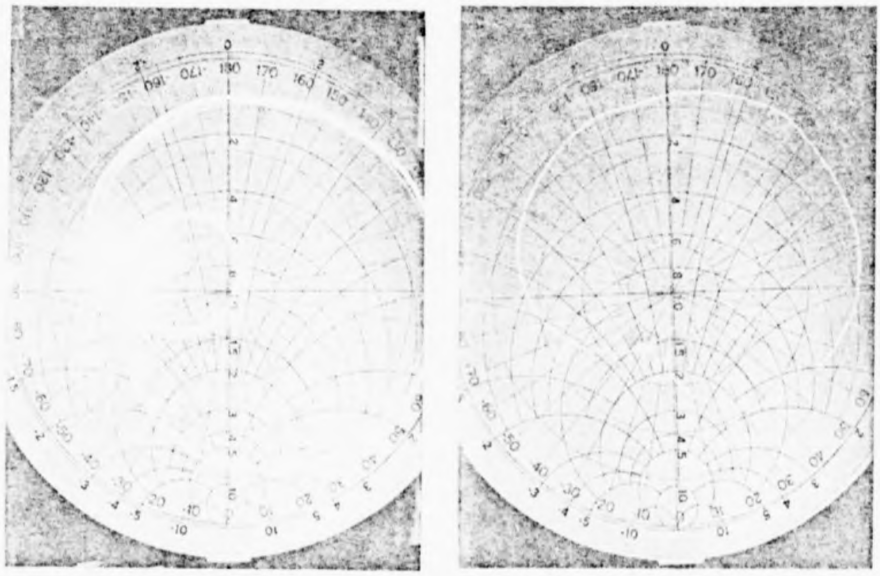

Fig.6.32 Impedance among (7.7 - 7.8GHz.) of resonators

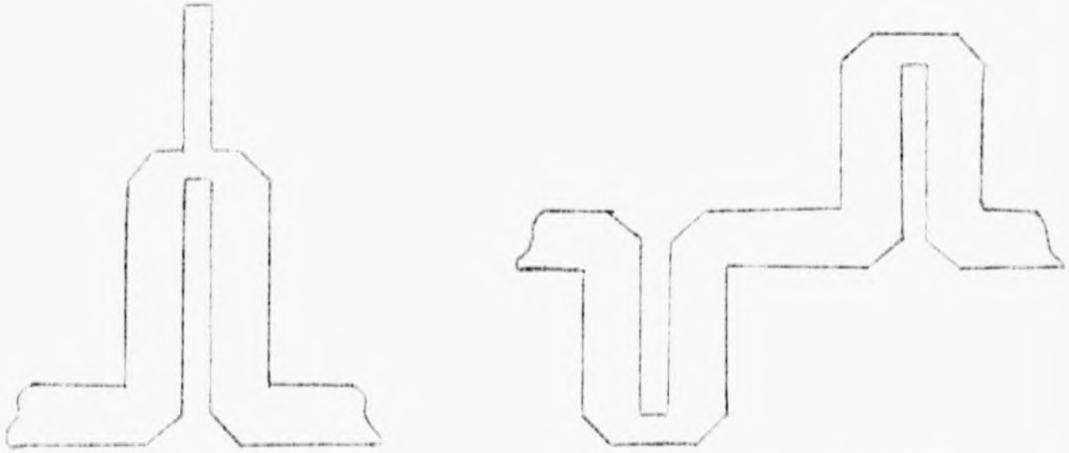

Fig.6.33 Coupled lines with (a) stubs (b) hybrid configuration.

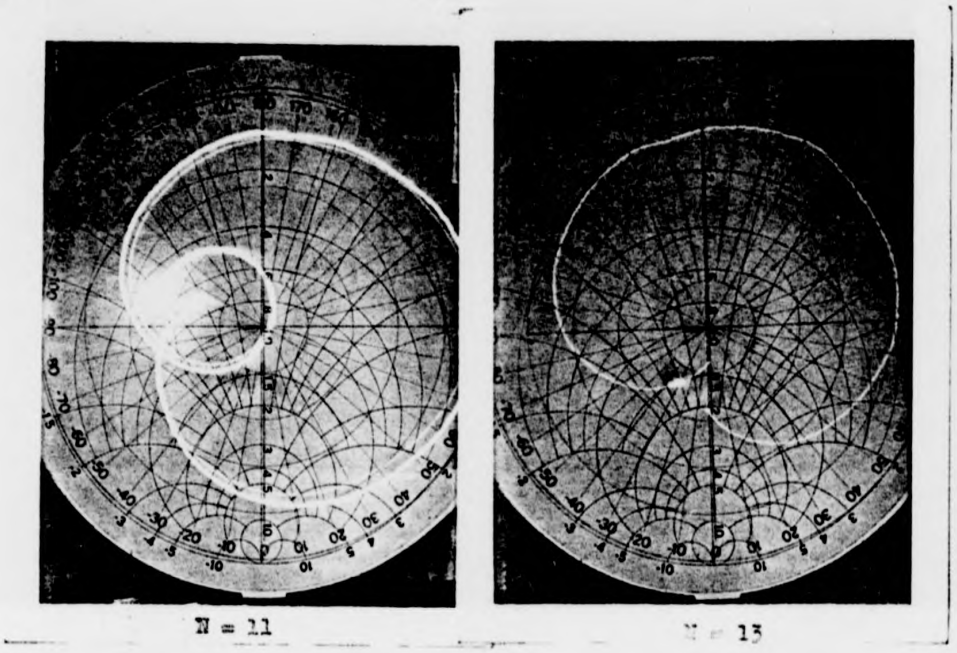

N = 11 N = 13

Fig.6.12 Impedance sweep (3.3 - 4.0GHz.) of meanderlines

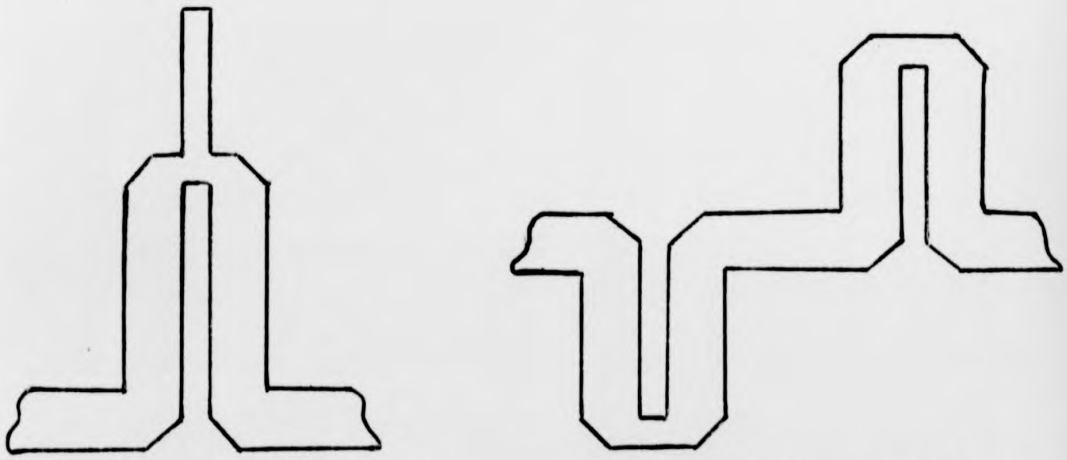

(a) Stub meanderline (b) Hybrid meanderline

Fig.6.13 Meanderlines with (a) stubs (b) hybrid configuration.

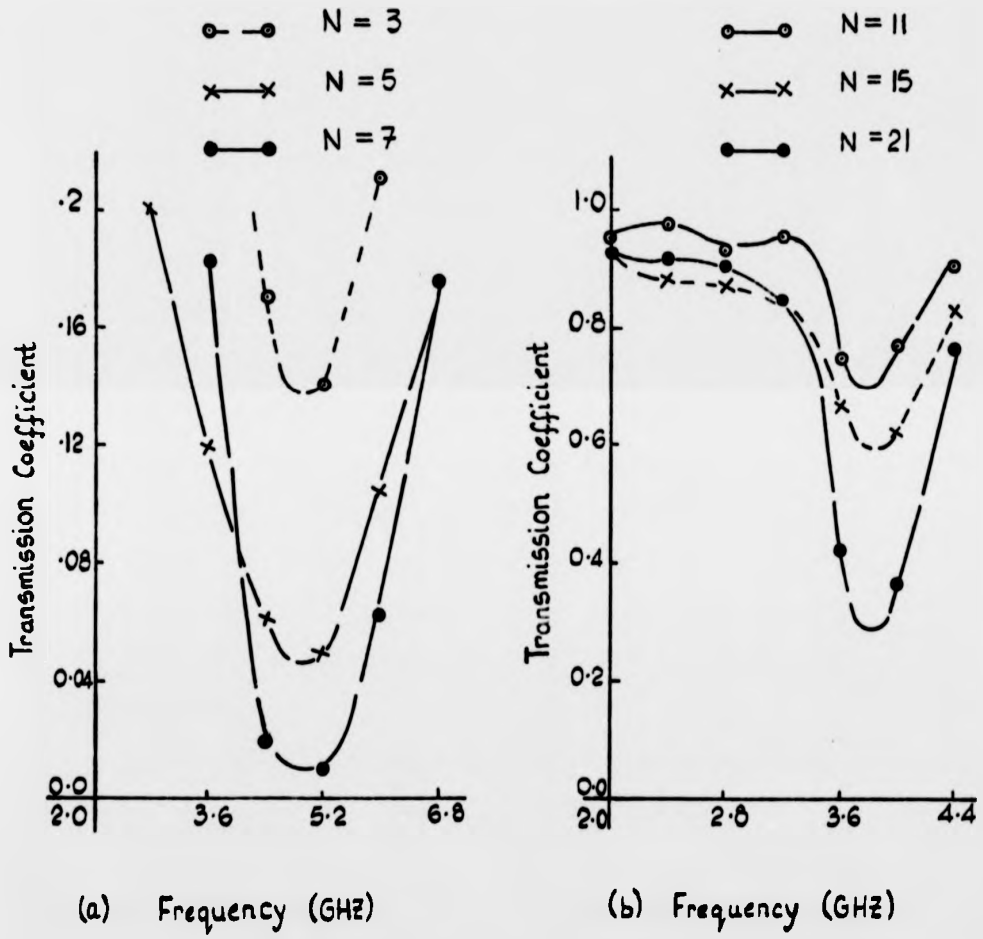

Fig.6.14 Variations of transmission coefficient with frequency for (a) meanderline with stubs and (b) hybrid meanderline.

decreases this attenuation. The reason for this is that the main coupling parameter from each conductor to its next neighbour, $KM_{i,i+1}$ has the largest influence on the attenuation characteristics of the meanderline. Since the variation of this parameter is not linear with conductor spacing, it follows that the meanderline which obtains its main coupling by large conductor surfaces attains a lesser attenuation value in the stop-band.

The effect of the susceptance discontinuity on the meanderline response is shown in fig. 6.11. As expected, better transmission and reflection coefficient were obtained by decreasing the width of the connecting line, δ. The effect of increasing the meander-turns is shown in fig. 6.10 while fig. 6.12 shows the impedance sweep of several meanderline structures.

Two other forms of meanderline were designed as shown in fig. 6.13. The hybrid configuration of fig. 6.13(b) allows flexibility in the design. However it is only useful in phase shift applications. The stub design of fig. 6.13(a) greatly enhances attenuation as shown by its frequency response of fig. 6.14.

6.5 DIFFERENTIAL PHASE SHIFT CHARACTERISTICS

6.5.1 Broadband matching technique: One of the most useful passive components of microwave integrated

circuits is the differential phase shifter which is frequently used to obtain phase shifts of 45, 90 and 180^{o}. Such a differential phase shifter can be conveniently obtained by connecting a meanderline circuit in series with a transmission line of prescribed electrical length. By comparing the insertion phase of the meanderline with that of the reference transmission line, a differential phase shift characteristic can be readily obtained where the phase difference of the two paths is the required phase shift.

If the electrical length of the meanderline is made 180 degrees at the centre frequency, the mid band electrical length of the reference transmission line will be 180 degrees plus the wanted phase shift. Thus it is possible to realize fixed wideband phase shifters for frequencies up to at least 18 GHz.

However, if the differential phase shifter is realized using microstrip lines, the circuit will not be matched because of the phase-velocity differences between the odd and the even modes of the coupled meanderline region and because of the discontinuity reactances discussed earlier. For the ideal TEM meanderline which has equal phase volocities of the odd and even modes, i.e. $\theta_o = \theta_e$, the product $Z_{in(e)} \cdot Z_{in(o)}$ is real and independent of frequency.

In the case of the microstrip meanderline, this product depends on frequency because of the difference in the phase velocities.

Although this difference in phase velocities is relatively small, it strongly deteriorates the maximum return loss which can be obtained with such a network. Hence some form of impedance matching is required at the input and output ports. A simple matching technique which allows one to obtain a return loss better than 30dB over a wide bandwidth is given in this section.

In this approach, the coupled sections of the meanderline is divided into two or more sections of equal electrical length but with different characteristic impedance values. The aim is to reduce the magnitude of the reflection coefficient at the input and output ports while maintaining the high transmission coefficient required for phase shift characteristics.

The impedance levels of the various sections were obtained using the program of appendix D. In the analysis, the meanderline was regarded as cascaded coupled sections. The effects of dispersion were included in the design. The dispersive model used was based on that of a parallel coupled transmission line[9]. The phase shift characteristics of the multi-sections was obtained by suitably modifying the expressions for the phase shift of a single section

meanderline - appendix E.

Six circuits were built on a 0.031 in-thick duroid substrates using two, three and four transforming sections. The ratio of the reference line to the main meadnerline was chosen to obtain a differential phase shift of 45^{o} and 90^{o} for the various sections. Table 6.1 shows the computed dimensions of the circuits. The configuration of the circuits are shown in figs. 6.15, 6.18 and 6.20.

Fig. 6.16 shows the measured return loss of a compensated and uncompensated phase shifters shown in fig. 6.15. For the uncompensated circuit, the maximum return loss was 23dB compared to the minimum value of 28dB obtained with the compensated circuit. The maximum insertion loss in each case was 4.1dB and 1.6dB respectively. The insertion phase of the two circuits are shown in fig. 6.17.

The results of a three and four sections are given in figs. 6.19 and 6.21. Though a higher (lower) return loss (insertion loss) was obtained with the three sections, only a maximum return loss of 16dB was obtained with the 4-sections. The reason for this is probably because as the number of the sections is increased, the mode impedances of some of the sections become too high in comparison to their adjacent neighbours. This effect is shown in fig. 6.20.

Table 6.1

N = 2

ϕ^{o}	R_z	$\lambda_{g(r)}$	Z_e^{1}	Z_e^{11}	Z_e^{111}	Z_e^{1v}
45	1.7	0.625	1.368	1.595	-	-
90	2.73	0.75	1.737	2.04	-	-

N = 3

45	1.7		1.317	1.25	1.591	-
90	2.73		1.654	1.557	2.08	-

N = 4

180	2.62		1.59	1.679	1.409	2.08

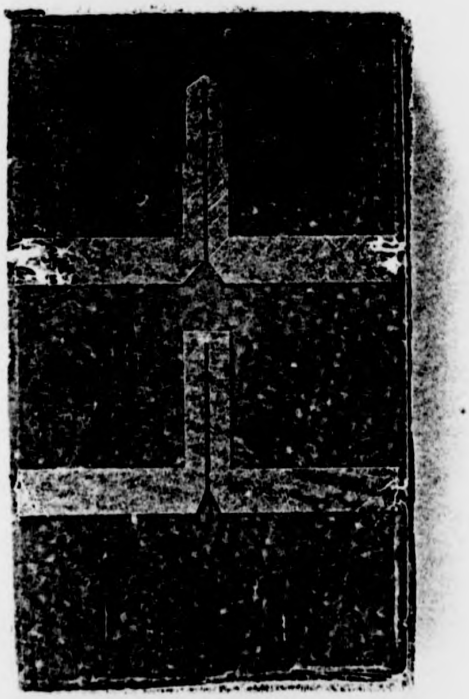

Compensated

Uncompensated

Fig.6.15 90 - degrees differential phase shifter

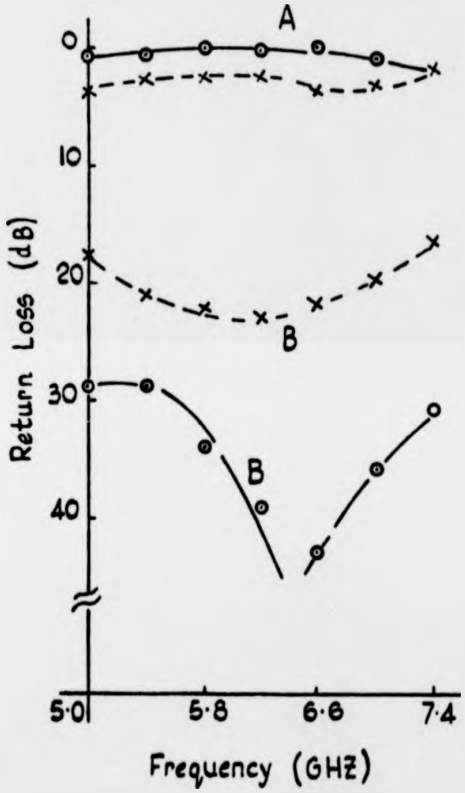

Fig.6.16 Insertion loss (A) and return loss (B) of fig.6.15.

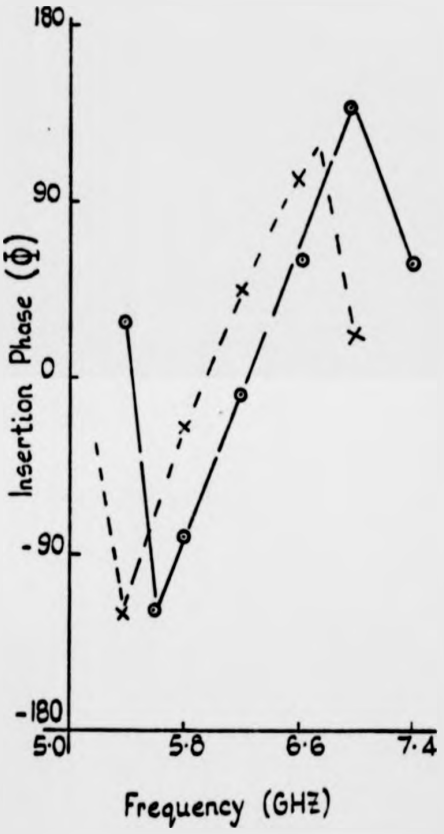

Fig.6.17 Insertion phase with frequency.

x---x Uncompensated

o——o Compensated.

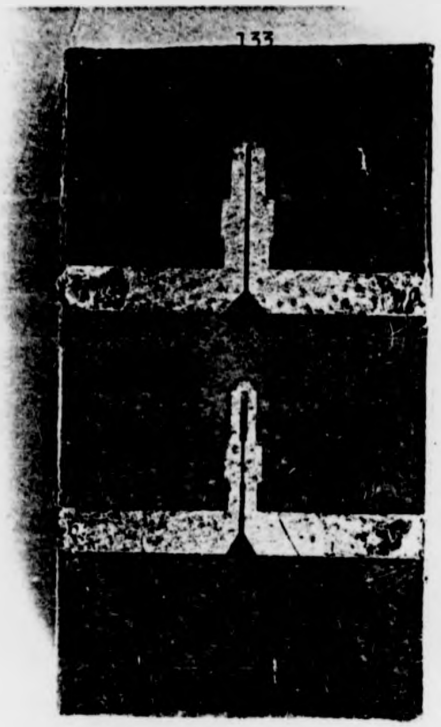

3 - sections 90 differential phase shifter.

3 - sections 45 differential shifter

Fig.6.18 3 - sections differential phase shifters.

180 differential phase shifter N=4

45 differential phase shifter N=2

Fig.6.20 4 and 2 - sections differential phase shifters.

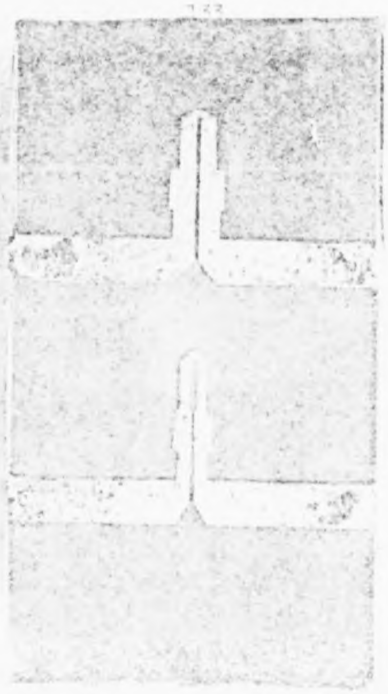

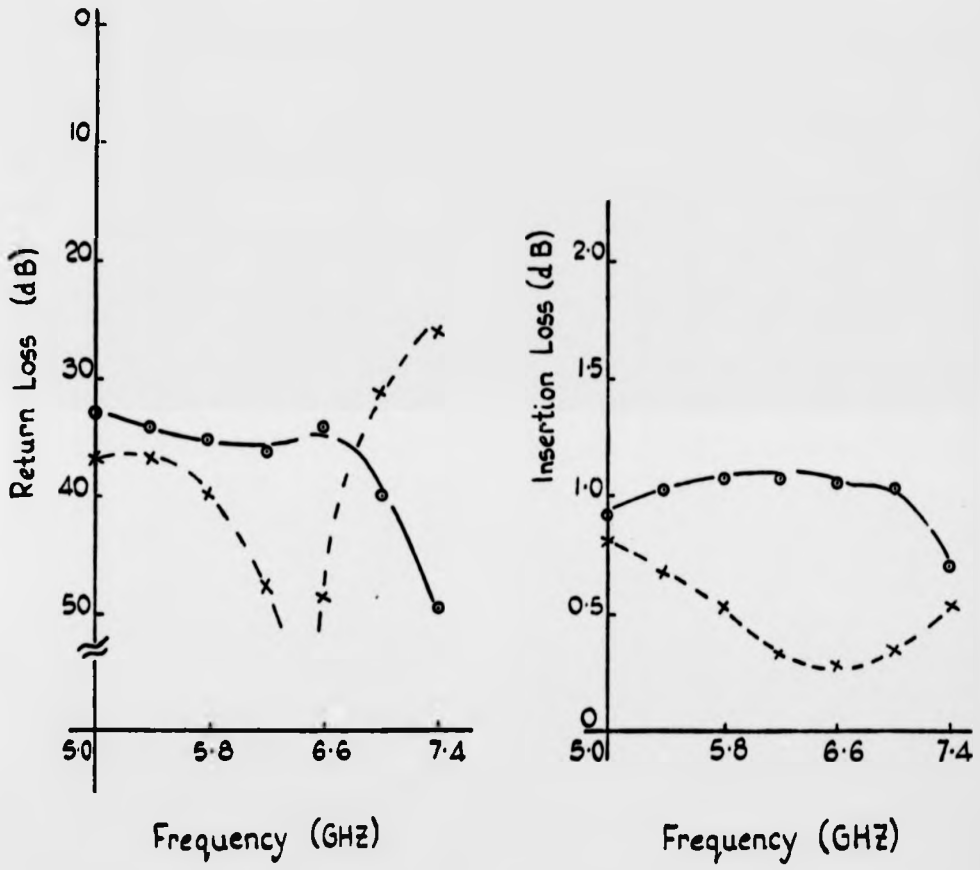

Fig. 6.19 Response of 3 - sections phase shifter.

●—● 45

×- -× 90

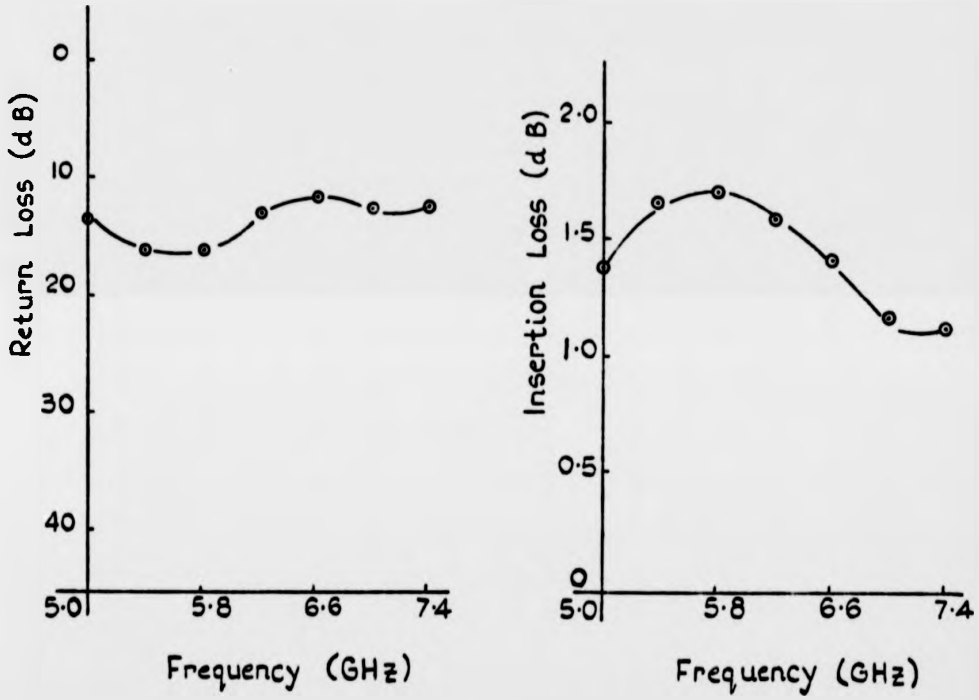

Fig. 6.21 Response of 4-section phase shifter.

REFERENCES

1. EFREMOV, YU. G. et al., "Filtering characteristics of meander transmission lines", Telecomms. and Radio Engineering, Vol. 32-33, pt. No. 11, 1978, pp.58-61.
2. RIZZOLI, V. and LIPPARINI, A, "Bloch-wave analysis of stripline and microstrip array slow-wave structures", IEEE Trans. Vol. MIT-29 Feb. 1981 , pp. 143-150.
3. ROOME, G. T., and HAIR, H. A., "Thin ferrite devices for MIC", IEEE Trans. MIT-16, 1968, pp. 411-420.
4. LIBBEY, W. M., "Characteristics of a microstrip two-meander ferrite phase shifter", IEEE Trans. Vd. MIT-21, 1973, pp. 483-487.
5. IWAKURA, H. et al, "A design method of meanderline type low-pass filter", Institute of Electronics and Comms. Engineers, Trans. Vol. E-62, No. 10, Oct 1979, pp. 684-685.
6. HOWE, H. A., Stripline circuit design, Artech House (Dedham Mass) 1974.
7. EASTER, B. et al., "Resonant techniques for the accurate measurement of microstrip properties and equivalent circuits", Proc. 1973 European microwave conference paper B7.5.
8. ANDERS, P. and ARNDT, F., "Moment method of designing matched microstrip bends", 1979 European microwave conference, digest of papers, pp. 430-434.
9. GUPTA, K. C. et al., Microstrip lines and slotlines, Artech House (Dedham Mass) 1979.
10. SCHIEK, B., and KOHLER, J., "A method for broadband matching of microstrip differential phase shifters", IEEE Trans. Vo. MIT-25, Aug. 1977, pp.666-671.

CHAPTER 7

MEANDERLINE NETWORKS INCORPORATING P.I.N. DIODES FOR DIGITAL MULTIPLEXING APPLICATIONS

7.1 INTRODUCTION

Recent advances in technology have resulted in the use of switched element filters in modern multiplexer design. These types of multiplexers are frequently used in telecommunications and electronic warfare applications. Their design can be accomplished by integrating a semiconductor device into a filter network. In this chapter this objective was achieved by incorporating p.i.n. diode device in a meanderline circuit.

It was shown in chapter 5 that the p.i.n. diode can be used to simulate an open or short circuit impedance depending on the bias applied to the device. With the terminals of such a diode connected across any transmission line it is possible to pass virtually all the microwave energy when the diode is reverse biased. Hence it approximates to an open circuit relative to the line impedance. On the other hand, if a forward bias signal is applied to the diode, most of the energy will be reflected hence approximating to a short circuit relative to the line

impedance. This principle of using the diode to simulate an open or short circuit condition was applied here in the design of the digital multiplexer.

The design uses the filtering characteristics of the meanderline. In this case, the meanderlines were loaded with p.i.n. diode terminated stubs inside the meander-loops. These secondary loads have the effect of changing the fundamental characteristics of the meanderlines. Secondly, at the frequency of operation, the p.i.n. diode loads will appear both transformed and shifted from its physical location by the stub length.

It was proved in section 5.3 that connecting p.i.n. diodes at the end of shunt stubs reverses the characteristics presented by the biased conditions of the diode. This means that the short circuit condition presented by the forward biased diode will be transformed to an open circuit condition. Similarly, the reverse biased characteristics are transformed to a short circuit condition. This character reversal together with the shift in the reference plane resulting from the stub introduces additional complexities in the design.

Thus the main design problems fall into four categories:

(i) To design a meanderline circuit which will give a bandpass filter characteristic when a TTL 'O' is applied to the diode, and will convert to a bandstop filter characteristic when the bias on the diode is a TTL '1'.

(ii) To modify the transformed impedance characteristics of the p.i.n. diode so that it approximates more closely to that of an ideal switch.

(iii) To compensate for the shift in the reference plane and hence reduce the mismatch and other measurement errors arising from it.

(iv) To cascade the filter circuits of (i) to form a digital multiplexer whose input can be switched to any of its outputs.

The techniques used in solving these problems are detailed in the following sections.

7.2 IMPEDANCE MATCHING

7.2.1 Matching techniques: The switching performance of the p.i.n. diode depends inherently upon the impedance levels presented by the diode in its two

switching states. These determine the transmission coefficients of the diode in the two states. An ideal transmission-reflection switch has scattering matrices in the "OFF" and "ON" states respectively of the form:-

$$\text{OFF}: \quad S = \begin{bmatrix} 0 & 0 \\ 0 & 0 \end{bmatrix}; \quad \text{ON}: \quad S = \begin{bmatrix} 0 & 1 \\ 1 & 0 \end{bmatrix}$$

In section 5.3, a single stub terminated diode was found to have transmission coefficient of $|S_{21}| = 0.87$ and $|S_{21}| = 0.21$ in the forward and reverse biased states respectively. These values do not compare favourably with that of the ideal case given above. Hence it was decided to modify the characteristics of the diode so that it approximates more closely to the ideal switch. This was achieved by introducing a matching network ahead of the diode termination.

Existing techniques for designing a diode matching network deal with the cases where the desired reflection coefficients in the two states have a magnitude ratio of unity and a prescribed phase angle[1,2]. Such cases are only applicable to phase shifting networks. In this particular case the diode is serving as a reflection modulator and thus the aim is to design a matching network such

that the reflection coefficients in the two states should have an amplitude ratio greater than one with no phase shift.

Like in the case of the phase shifters, the design parameters used here were based on the expression for the transformed reflection coefficient appearing at the input to any network when such a network is terminated by the two impedance states of the diode. The required diode impedances were obtained from the results of fig. 4.14. It was assumed that the matching network is lossless and reciprocal. This assumption made it possible to compute the parameters of an impedance which would be transformed to the system characteristics impedance by the matching network.

The second assumption made was that the diode is switched from one state to another without any phase shift. This allowed the impedance parameters to be written in terms of the magnitude of the reflection coefficients only (appendix F). By choosing a suitable value for the reflection coefficient in the "ON" state, the matching network which can give the corresponding reflection coefficients was easily computed. The dimensions of this network were then found from standard transmission line theory[3].

7.2.2 Design and results: From fig. 4.14, the measured reversed and forward biased impedances of the diode are $Z_1 = 1.5 + j0.5$ and $Z_2 = 0.032 - j0.662$ using bias signals of -30V and 50mA respectively. All the above values are normalised to the system characteristic impedance. The reflection coefficient in the "ON" state was arbitrarily chosen as 0.05. The virtual impedance and the resulting reflection coefficient in the "OFF" state were computed as $Z_m = R_m + jX_m = 77.34 + j40.21$ and $\Gamma_2 = 0.974$. The dimensions of the network to match this virtual impedance to the line characteristic impedance were found as $Z_t = 82.61$ ohms and $\theta_t = 8.8m$ where θ is the electrical length at 3.0 GHz.

To confirm the above technique, two models were made as shown in fig. 7.1. The diode was first biased by 50mA, and the reflection coefficient of the whole stripline circuit measured over the frequency range 2.0 - 4.4 GHz using the on-line computer corrected network analyzer. The results are shown in fig. 7.2. For model 1, the measured value was 0.98 at the centre frequency of 3.0 GHz. This compares favourably with the computed value of 0.974. However this is limited to a very narrow bandwidth of only 13.3%. Below 2.8 GHz and above 3.2 GHz the measured value decreases sharply to below 0.79.

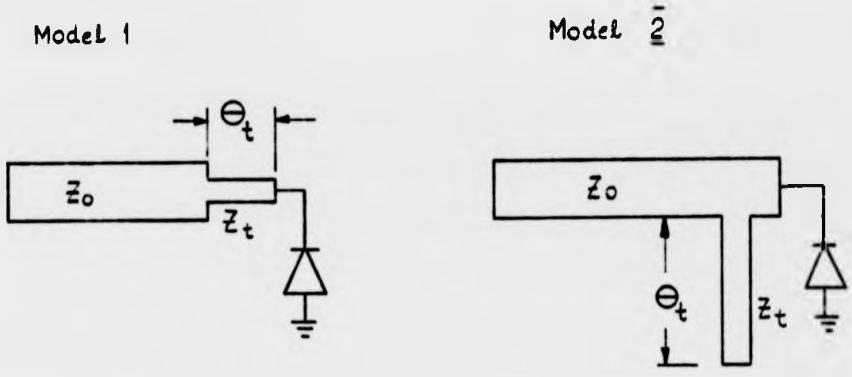

Fig.7.1 Impedance matching networks.

The results obtained for model 2 show a broad-band behaviour over the entire band. The minimum value obtained was 0.91 at 2.8GHz. The effect of changing the bias on the diode is also shown on the same figure. With a bias signal of 15 mA, the maximum value of $|\Gamma_2|$ obtained was 0.75. When the bias current was reduced to 10 mA, the value of $|\Gamma_2|$ obtained was 0.4. The reason for these poor performances obtained with low bias currents is obvious as it has been proved in section 5.2 that the diode impedance changes appreciably if the bias current falls below 15 mA. As long as the bias current is more than 25 mA, the changes in the diode impedance is negligible.

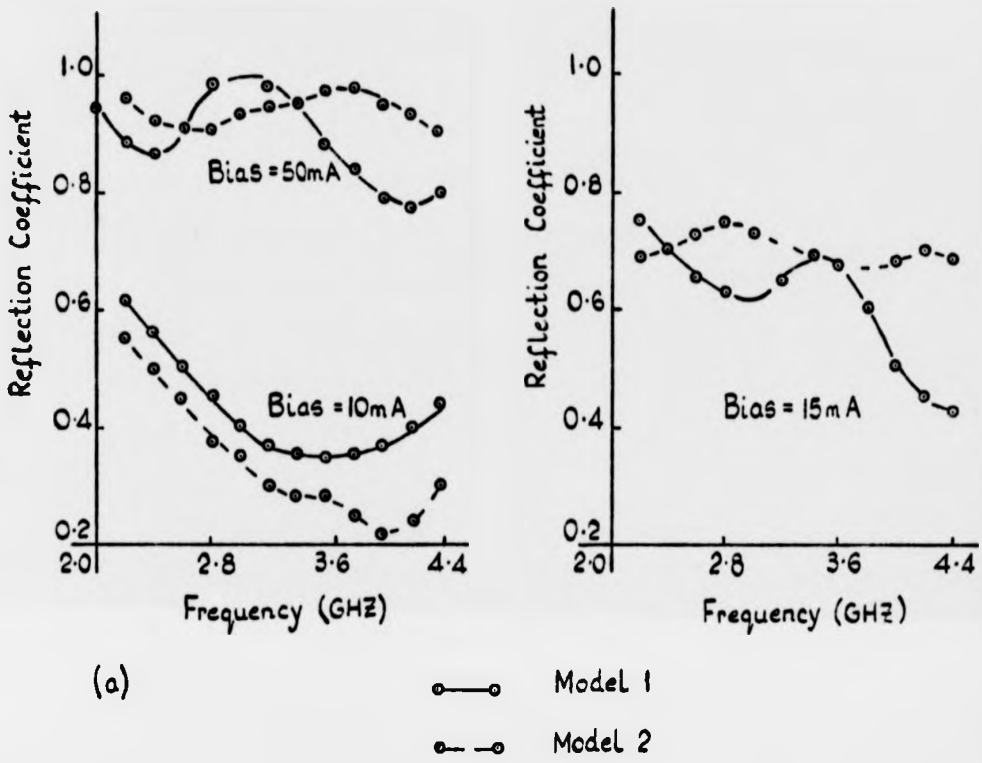

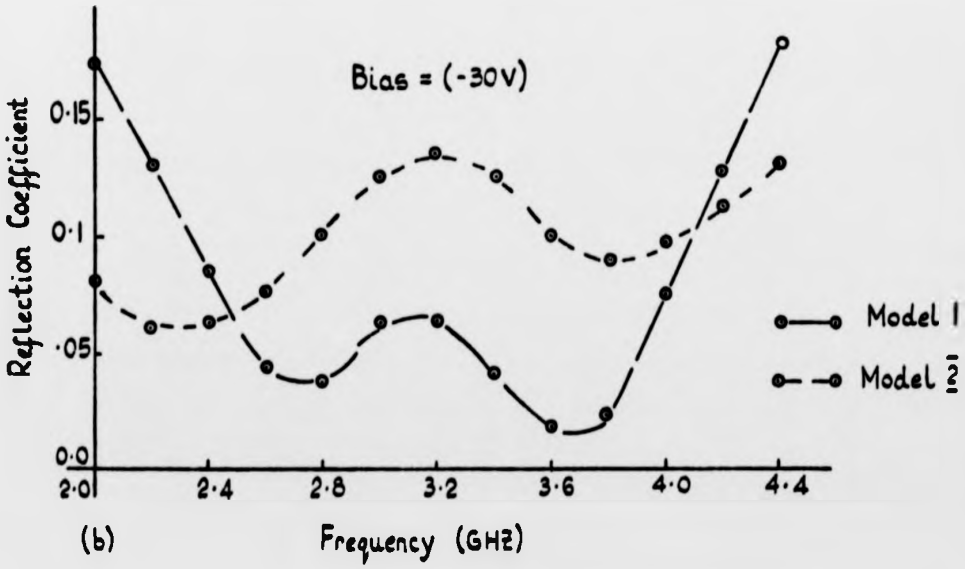

Fig.7.2 Variations of the magnitude of the reflection coefficient of the matched diode.

When the diode is reverse biased, the maximum reflection coefficient obtained with model 1 was 0.061 at 3.0 GHz. This value was obtained over a wide bandwidth. It was also found that changing the reverse bias signal does not affect the response of the compensated network significantly. The measured value of 0.061 compares well with the chosen value of 0.050.

The second problem to be combated in the design is the shift in the reference plane introduced by the stubs. The method of tackling this problem was explored in chapter three and the results obtained there were used here.

7.3 SINGLE CHANNEL "TWO-STATE" FILTERS

7.3.1 Synchronous design technique: The most essential step in the design of these types of filters is choosing the parameters of the meanderline circuit such that when the network converts from a bandpass filter to a bandstop filter, it should maintain the same bandwidth and band-edge characteristics. It was decided to start with a bandstop filter parameter (i.e. with the diodes reversed biased), and then to tailor down these parameters until they meet the specification required for a bandpass filter.

The diode matching network used was based on the approach of model 1 of fig. 7.1. A lower value

of reflection coefficient in the reverse biased state, $\Gamma_1 = 0.15$, was initially chosen. This gave a very wide bandwidth of 40 percent in the reverse biased state and only 17 percent in the forward biased state. The reflection coefficient and the matching network were then adjusted until the bandwidth in both states was 26.7 percent. Table 7.1 shows the computed coupling parameters of the filters while fig. 7.3 shows the photographic views of the filters.

The filters were made on duroid substrate using two or three diodes for each circuit. The diode stubs were synchronously centred at 3.0 GHz. The response of each filter was measured over the frequency band 2.0 - 4.0 GHz. The results are shown in figs. 7.4 - 7.7. In fig. 7.4, the computed and measured response of an uncompensated filter are compared. Here the effects of the T-junction were assumed negligible and no matching network was used. The results show that the centre frequency shifts from the designed value of 3.0 GHz to 2.4 GHz in the forward biased state and to 2.3 GHz in the reverse bias state. Moreover, the relative bandwidth increased substantially from the designed value of 26.7% to the measured value of 41%.

The response of the matched filter of fig. 7.3(a) is shown in fig. 7.5. This shows a good agreement between the measured and the computed

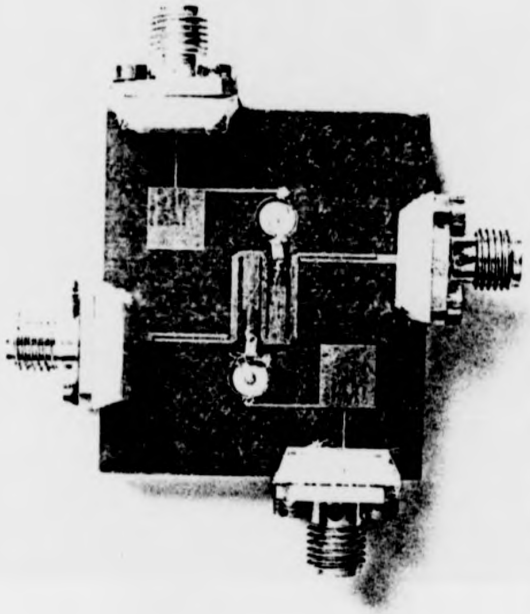

Fig. 7.3a Matched Filter

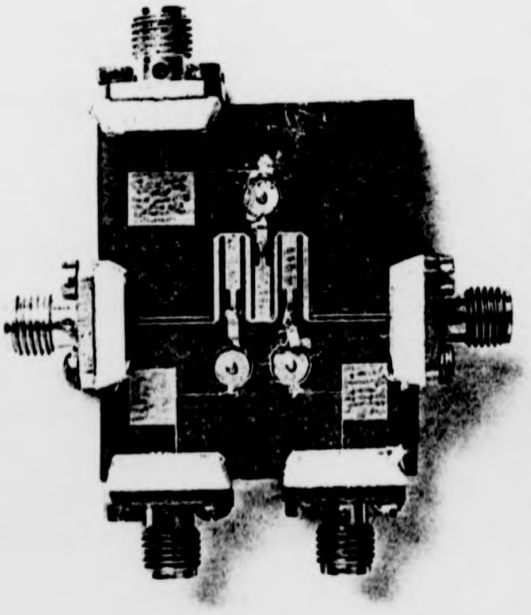

Fig. 7.3b 3 diodes synchronous filter.

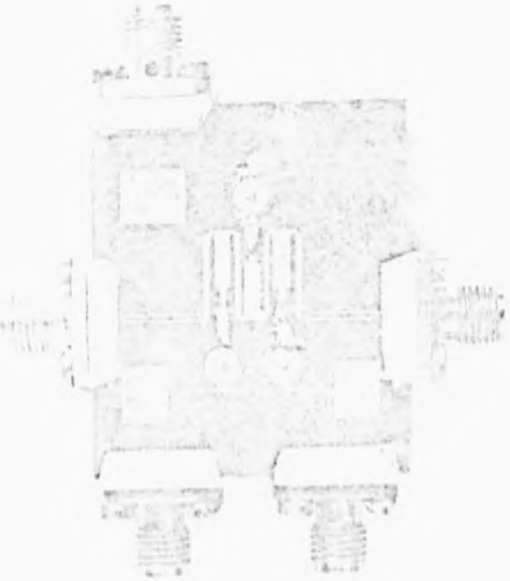

values. With a TTL'O' driving the diodes, the measured transmission coefficient at the centre frequency is 0.95 instead of the designed value of 0.97. The measured badnwidth was 25% compared to the computed value of 26.7%. With a TTL '1' applied an isolation of 35dB was achieved. However, the centre frequency shifted to 2.8 GHz. Attempts were made to correct this shift in frequency by decreasing the coupling of the inner conductors but it was found that doing this alsc increases the centre frequency of the '1'-state by the same amount.

Increasing the number of diodes to three (fig. 7.3(B)) results in greater isolation in the '1' state and improved transmission in the 'O' state as shown in fig. 7.7. However the bandwidth obtained was only 28%. This is not a significant improvement on the earlier results and another technique was explored as explained in the next section.

7.3.2 Stagger stub design: To increase the bandwidth in both states, the technique of staggering the stubs was used. Here the centre frequencies of the individual stubs were made different. The new centre frequencies were selected such that $5^{o} \leq \Delta\theta \leq 8.5^{o}$ where $\Delta\theta$ is the difference in electrical length between any two stubs. The diode impedances for each of these centre frequencies were obtained from fig.

4.14. Using these impedance values, the appropriate matching networks for these stubs were designed as shown in table 7.2. The configuration of the filter is shown in the attached photograph of fig. 7.8.

Fig. 7.9 shows the response of the filter. The maximum transmission coefficient in the '0' state was $|S_{21}| = 0.94$. However an intolerable 1.94dB ripple was obtained. In the '1' state the minimum transmission coefficient was $|S_{21}| = 0.13$ which corresponds to an isolation of 17.7dB. The measured bandwidth increased substantially to 38.9% compared to 25% obtained earlier.

The reason for the unacceptable ripple obtained in both states was due to the fact that the centre frequencies of the stubs could not be well aligned to obtain a maximally flat response. Another point noted from the results is that the two state filters cross-over at 5.1dB instead of the designed value of 3.0dB.

Table 7.1 Dimensions of filters

Diode Number	$K_{i,i+1}$	Spacing mm	Meanderlines W(mm)	Stubs W(mm) θ(mm)	Transformer W(mm) θ(mm)
	0.125	0.4	0.8	-	-
2	0.16	0.2	0.6	1.8, 5.4	0.8, 3.4
	0.16	0.2	0.8	1.8, 5.4	0.8, 3.4
	0.125	0.4	-	-	-
	0.125	0.40	0.8	-	-
	0.158	0.21	0.6	1.7, 5.4	0.8, 3.4
3	0.16	0.20	0.6	-	-
	0.155	0.23	-	1.8, 5.4	0.75, 3.4
	0.141	0.30	0.8	-	-
	0.125	0.40	-	1.7, 5.4	0.8, 3.4

Table 7.2 Dimensions of stagger stub filter

$K_{i,i+1}$	Spacing mm	Meanderlines W (mm)	Stubs W(mm)	Stubs θ(mm)	Transformer W(mm)	Transformer θ(mm)
0.125	0.40	0.8	-	-	-	-
0.16	0.20	0.6	1.8	4.4	0.8	3.0
0.157	0.22	0.8	1.77	5.3	0.75	2.1
0.125	0.40	-	-	-	-	-
0.158	0.21	0.7	1.82	6.4	0.8	1.1
0.132	0.38	0.8	1.8	5.5	0.76	1.9
0.16	0.20	-	-	-	-	-
0.125	0.40	-	-	-	-	-

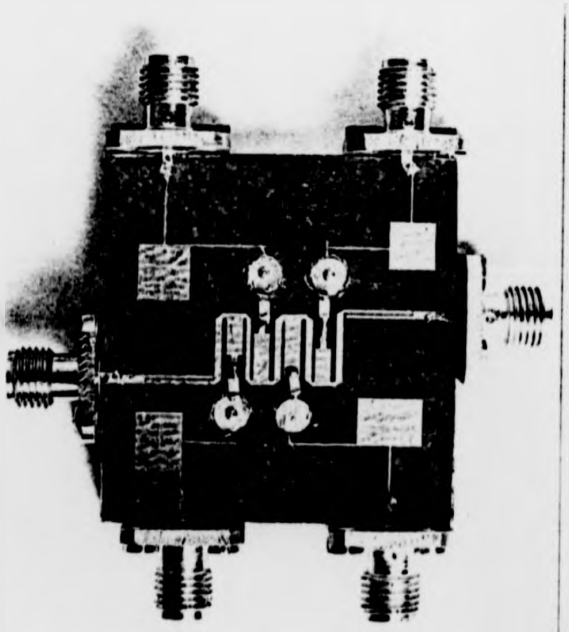

Fig.7.8 Photographic view of stagger stub filter.

Table 7.2 Dimensions of stagger stub filter

$K_{i,i-1}$	Spacing mm	Meanderlines W (mm)	Stubs W(mm)		Transformer W(mm)	
0.125	0.40	0.8	-	-	-	-
0.16	0.20	0.6	1.6	4.4	0.8	3.0
0.157	0.22	0.8	1.77	5.2	0.75	2.1
0.125	0.40	-	-	-	-	-
0.158	0.21	0.7	1.82	6.1	0.8	1.1
0.152	0.33	0.8	1.3	5.5	0.76	1.9
0.16	0.20	-	-	-	-	-
0.125	0.40	-	-	-	-	-

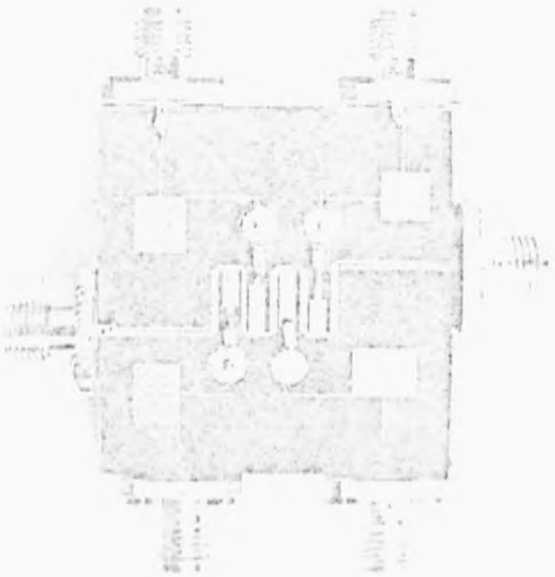

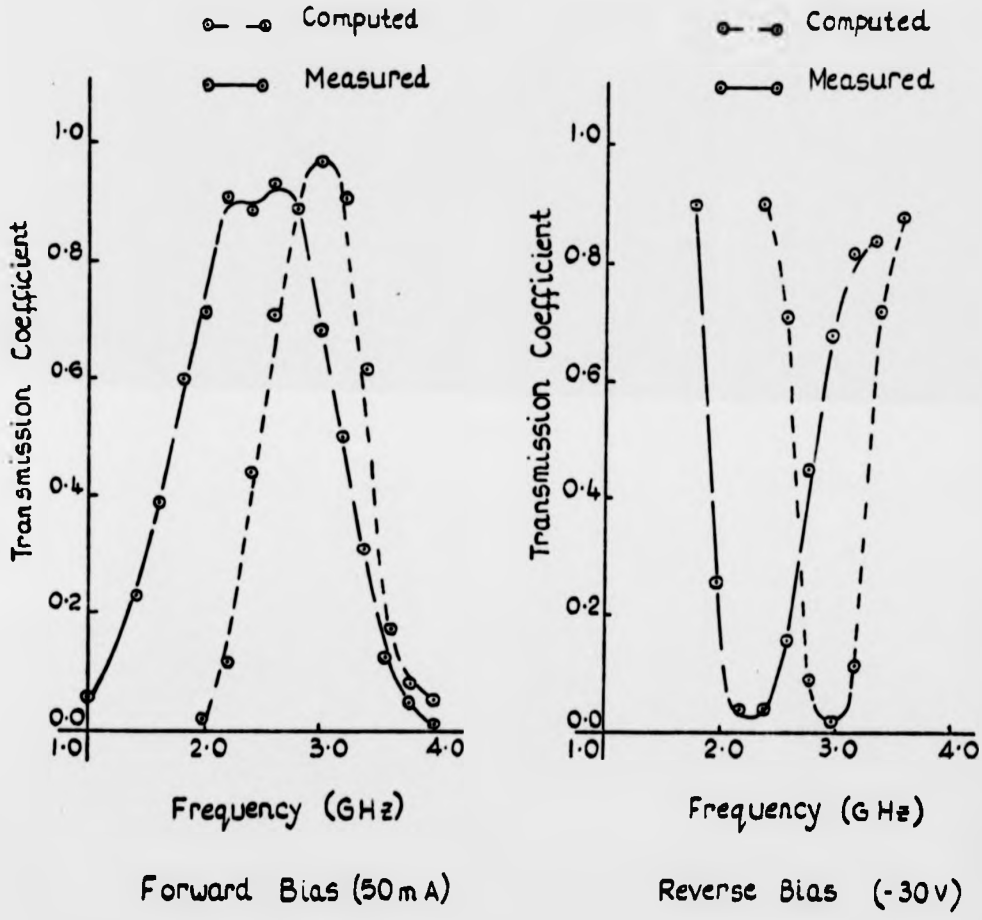

Fig.7.4 Response of uncompensated single - channel filter.

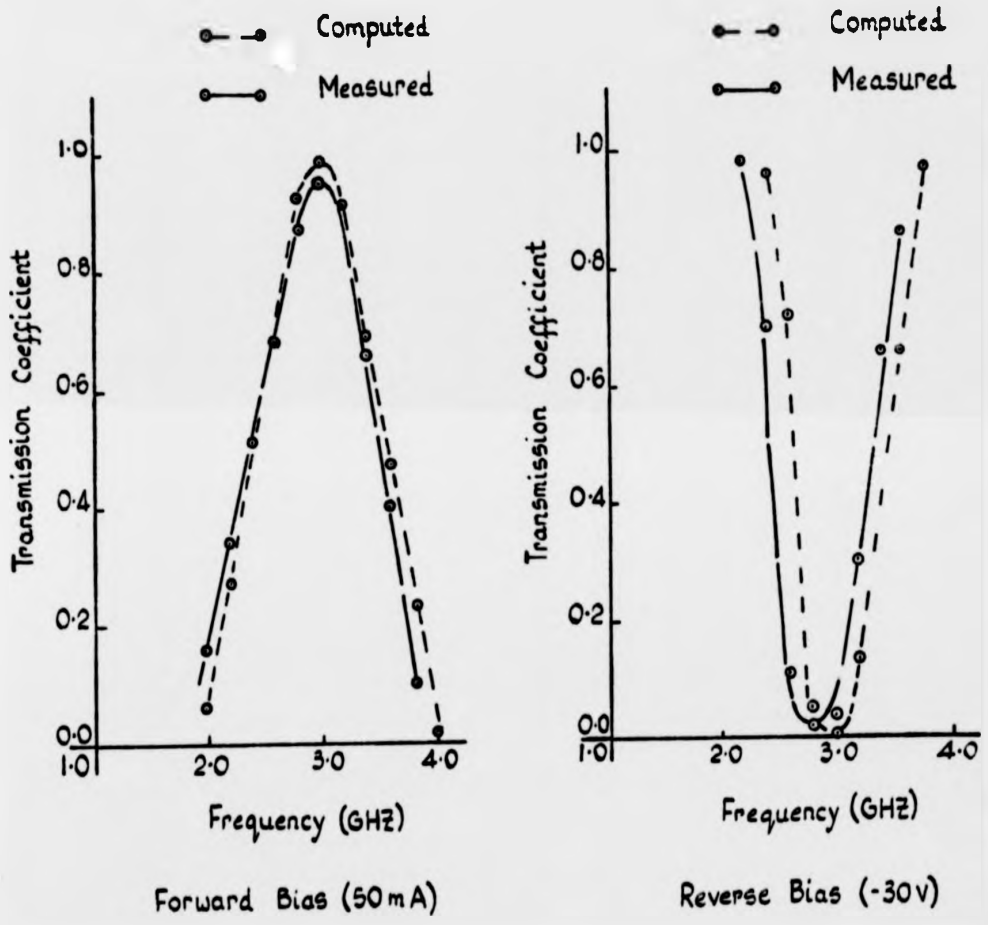

Fig.7.5 Response of matched channel filter.

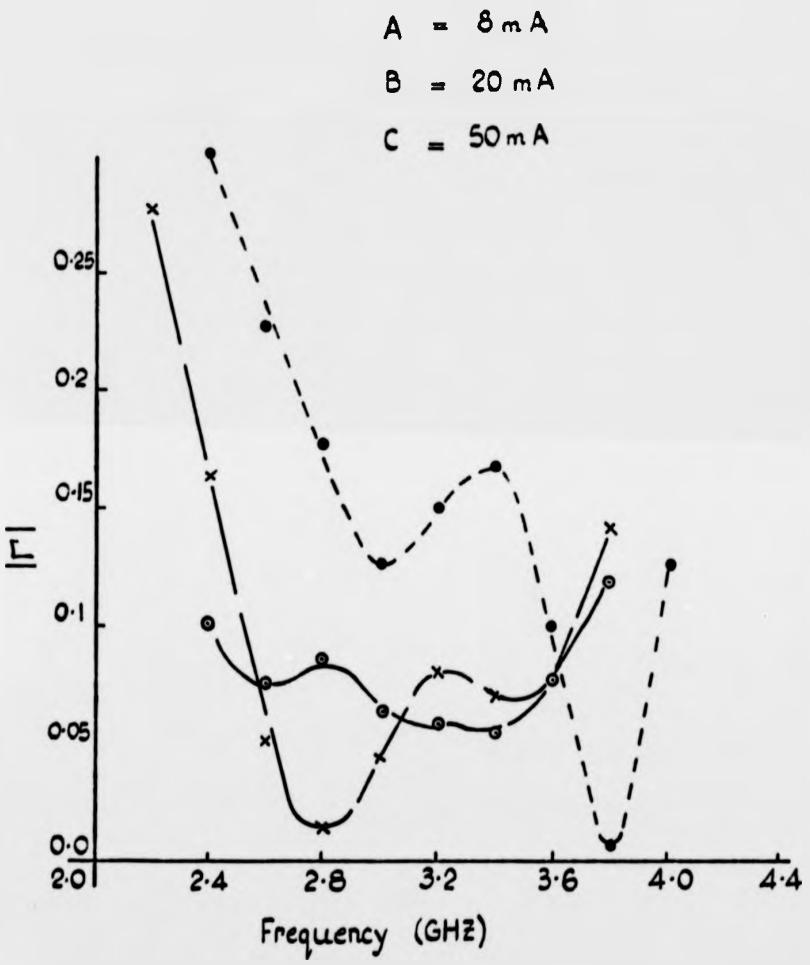

Fig.7.6 Variation of the magnitude of the reflection coefficient for various bais levels.

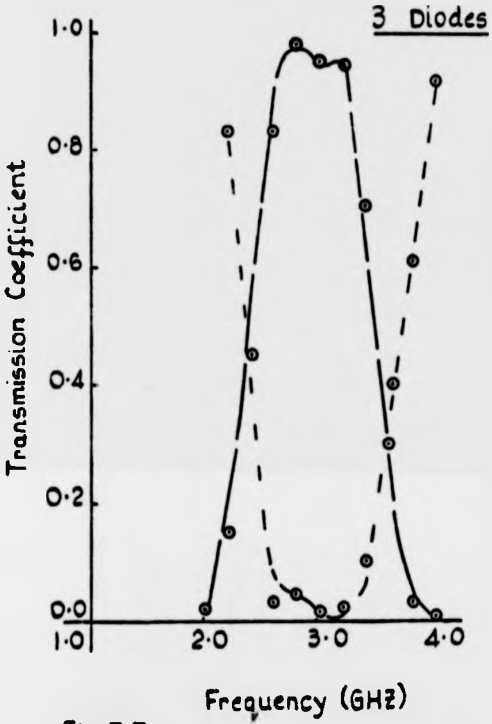

Fig. 7.7

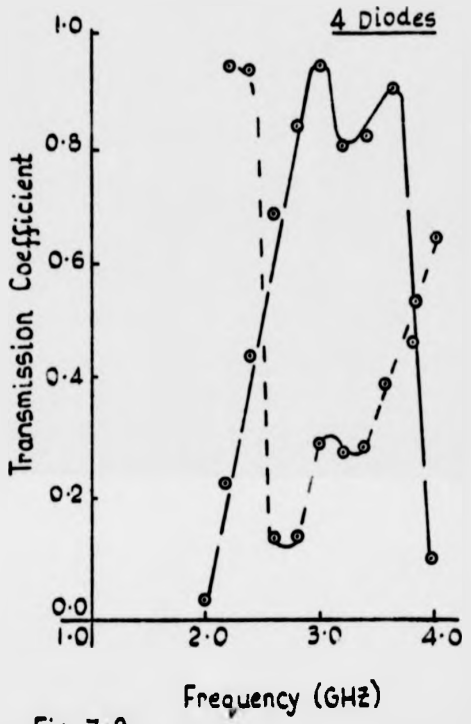

Fig. 7·9

o—o Forward Bias (50 m A)

o- -o Reverse Bias (-30V)

Fig.7.7 3 - diodes synchronous filter.

Fig.7.9 4 - diodes stagger - stub filter.

7.4 SWITCHABLE MULTIPLEXER DESIGN

7.4.1 Diplexer design: The techniques used in the last section were applied in the diplexer design. An assymmetric Y-junction was used instead of a T-junction. It was assumed that this junction has negligible effect on the network response. The angle between the Y-legs was arbitrarily made 139^{o}. This angle was wide enough to separate the adjacent resonators of the different channel filters such that no coupling exists between them. The electrical length of each leg was chosen to be a quarter-wavelength at the operating frequency of its connected filter.

Fig. 7.10 shows the photographic view of the diplexer. Its parameters are given in table 7.3. These parameters were obtained using the micro-3 program[4]. Since the diplexer is a 3-ports network, its matrix elements were measured by reducing the network to a series of equivalent two-ports networks. This was achieved by placing matched loads at all other ports except the input and k-th port (i.e. $a_i = 0$, $i \neq k$). The incident and reflected waves at the input and k-th port are then related as follows[5]:-

$$\begin{bmatrix} b'_1 \\ b'_k \end{bmatrix} = \begin{bmatrix} S'_{11} & S'_{1k} \\ S'_{1k} & S'_{kk} \end{bmatrix} \begin{bmatrix} a'_1 \\ a'_k \end{bmatrix} \qquad 7.1$$

The normalised scattering parameter S'_{11} ,S'_{1k} and S'_{kk} were then obtained using the network analyzer. This procedure was then carried out two times. The response of the diplexer is shown in fig. 7.11. With a TTL 'O' driving the diodes, the transmission coefficients measured for each filter were $|S_{21}| = 0.96$ and 0.93 for channels 1 and 2 respectively. The maximum reflection coefficients in this state were $|S_{11}| = 0.11$ and 0.091 respectively. When a TTL '1' was applied, isolations of 25.4dB and 20.8dB were obtained for the two cases.

The 'O' and '1' states of the filters cross-over at $|S_{21}| = 0.66$ (3.6dB) for channel 1 and $|S_{21}| = 0.62$ (4.1dB) for channel 2. The respective bandwidths were 23.5% and 21.8%. The measured centre frequencies of 6.4 GHz and 8.2 were slightly outside the designed values of 6.0 GHz and 8.0 GHz respectively.

7.4.2 Digital triplexer design: In this design, the most difficult problem encountered was the design of the common junction. For the triplexer to be matched, the input admittance at the common port must be real and constant all over the channels. For this case where the channel filters were connected directly to the main junction, a singly terminated minimum-suscpetance network could have been appropriate[6]. This type of design can provide an input admittance with a real

part which approximates to a constant value over the channel bandwidth. However the non-zero imaginary part had to be cancelled out using an annulling network and this introduces complexities in the design.

The technique used here was to modify the junction dimensions such that it approximates to an extended junction[7]. Fig. 7.12 shows the configuration of the triplexer while table 7.4 shows the computed dimensions. The measurement technique used is identical to that used for the diplexer, but here the procedure was carried out three times in order to determine all the coefficients of the triplexer. To determine the coupling between adjacent channels, the mutual coefficients of the filters were measured. The results are shown in figs. 7.13 - 7.15.

In the response of fig. 7.13, channel 1 and 2 show a good cross-over of 3.27dB at the designed corner frequencies of 4.2 and 4.4 GHz for channel 1 and 4.8 and 5.2 GHz for channel 2. However this is not the case for channel 3. Here the bandpass and bandstop filters do not fall within the same centre frequency. There is a shift in the centre frequency when the filter is switched to the reverse biased mode.

Another point noticed in fig. 7.13 is that the transmission coefficient of channel 2 is only $|S_{21}| = 0.91$ compared to $|S_{21}| = 0.97$ obtained for

Table 7.3 Dimensions of Diplexer

Channel	$K_{i,i+1}$	Spacing mm	Meanderline W(mm)	Stubs W(mm); θ(mm)	Transformer W(mm); θ(mm)
	0.125	0.4	-	-	-
1	0.16	0.2	0.80	1.8; 4.0	0.8; 2.0
	0.162	0.19	0.70	1.4: 4.0	0.6; 2.0
	0.129	0.39	0.80	-	-
	0.129	0.39	0.81	-	-
2	0.158	0.21	0.70	1.4; 4.0	0.8; 2.0
	0.157	0.22	0.80	1.3; 4.0	0.76; 2.0
	0.125	0.4			

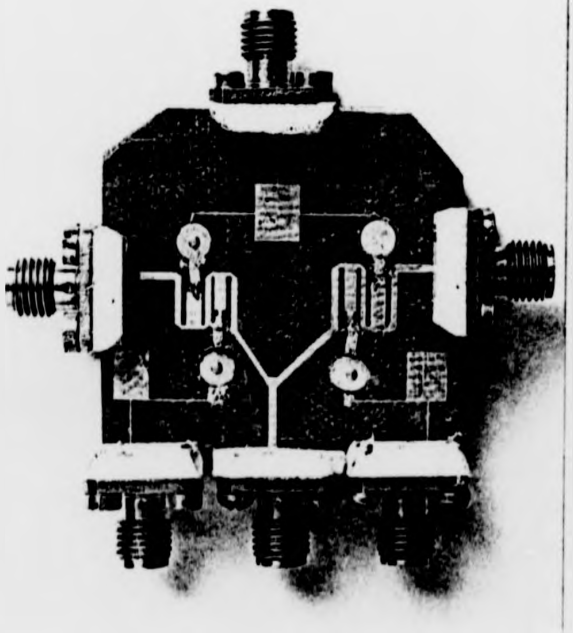

Fig.7.10 Photographic view of diplexor.

Table 7.3 Dimensions of Diplexer

Channel	$K_{i,i+1}$	Spacing mm	Meanderline W(mm)	Stubs W(mm); S(mm)	Transformer W(mm); S(mm)
1	0.125	0.4	-	-	-
	0.16	0.2	0.80	1.8; 4.0	0.8; 2.0
	0.162	0.19	0.70	1.4; 4.0	0.8; 2.0
	0.129	0.39	0.80	-	-
2	0.129	0.39	0.81	-	-
	0.158	0.21	0.70	1.4; 4.0	0.8; 2.0
	0.157	0.22	0.80	1.3; 4.0	0.73; 2.0
	0.125	0.4			

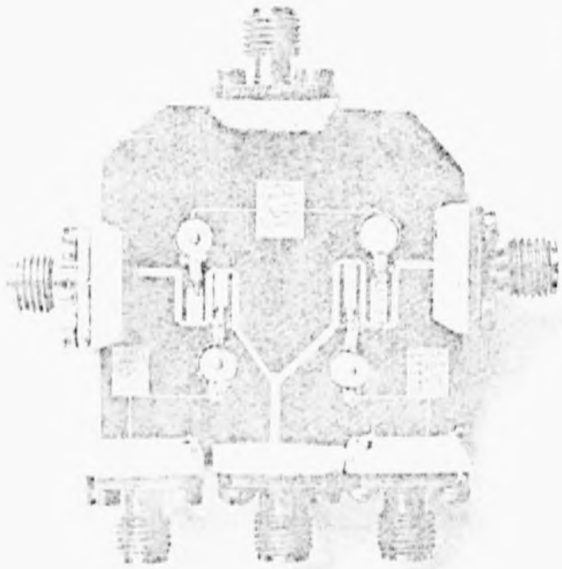

7.12 Photographic view of diplexer.

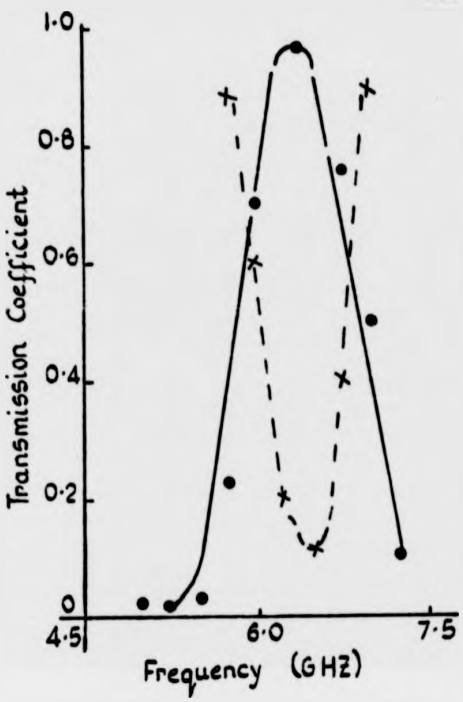

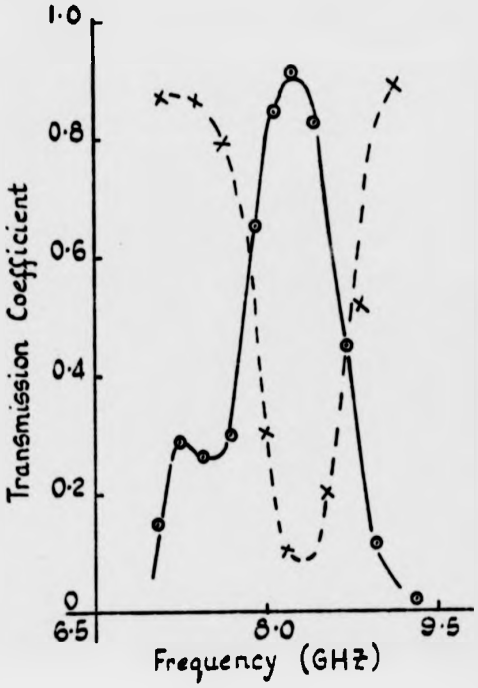

Chan. 1

Chan. 2

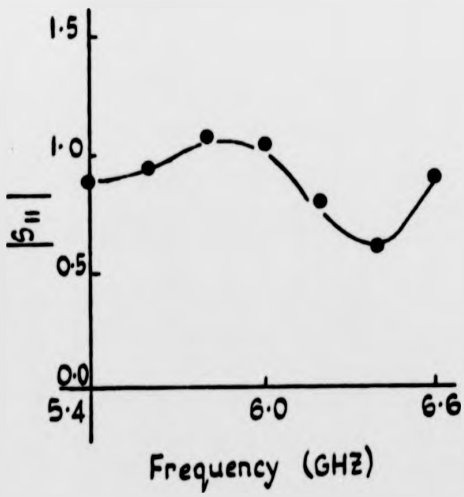

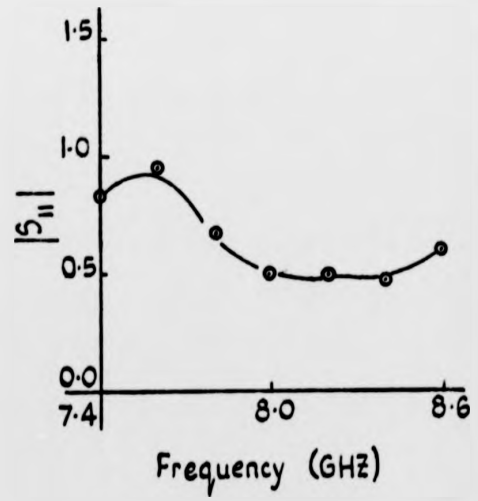

Fig.7.11 Response of diplexer.

o——o Forward

x - - - x Reverse

Table 7.4 Dimensions of Triplexer

Channel	$K_{i,i+1}$	Spacing mm	Meanderlines W(mm)	Stubs W(mm) θ(mm)	Transformer W(mm) θ(mm)
	0.125	0.4	0.8	-	-
1	0.158	0.21	0.8	1.4, 4.0	0.6, 2.0
	0.164	0.18	-	1.35, 4.0	0.6, 2.0
	0.131	0.38	0.78	-	-
	0.129	0.37	0.78	-	-
2	0.16	0.20	0.8	1.6, 3.9	0.58, 2.02
	0.162	0.19	-	1.58, 3.8	0.59, 1.9
	0.129	0.39	0.77	-	-
	0.125	0.4	0.79	-	-
3	0.162	0.19	0.81	1.2, 5.0	0.61, 3.0
	0.16	0.20	-	1.22, 5.0	0.60, 3.0
	0.125	0.40	0.8	-	-

the other two channels when a TTL - '0' is driving the diodes. When a TTL '1' is driving the diodes the worst result was obtained for channel 3. Here the measured transmission coefficient is $|S_{21}| = 0.06$ compared to $|S_{21}| = 0.01$ obtained for the other two channels. These values were obtained under matched conditions. Mismatching any of the ports degrades the circuit performance as shown in fig. 7.14. Fig. 7.15 shows the coupling between adjacent channels. The isolation between channels 1 and 2 was 21dB as compared to 10.45dB between 2 and 3.

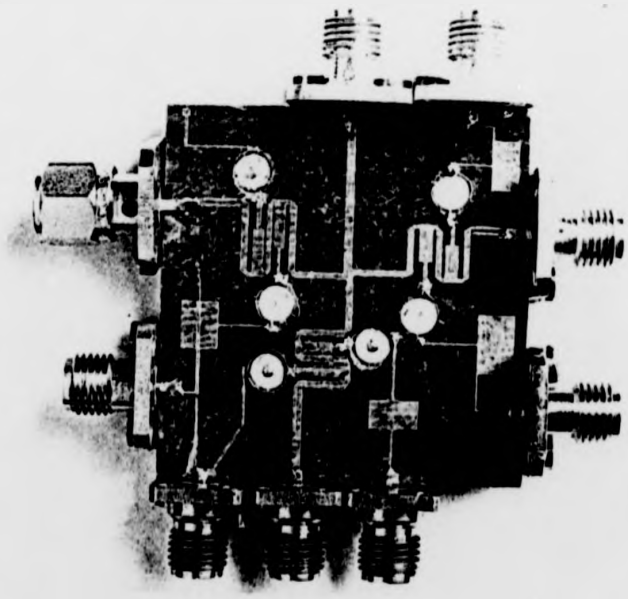

Fig.7.12 Photographic view of digital triplexer.

the other two channels when a TTL - '0' is driving the diodes. When a TTL '1' is driving the diodes the worst result was obtained for channel 3. Here the measured transmission coefficient is $|S_{21}| = 0.06$ compared to $|S_{21}| = 0.01$ obtained for the other two channels. These values were obtained under matched conditions. Mismatching any of the ports degrades the circuit performance as shown in fig. 7.14. Fig. 7.15 shows the coupling between adjacent channels. The isolation between channels 1 and 2 was 21dB as compared to 10.45dB between 2 and 3.

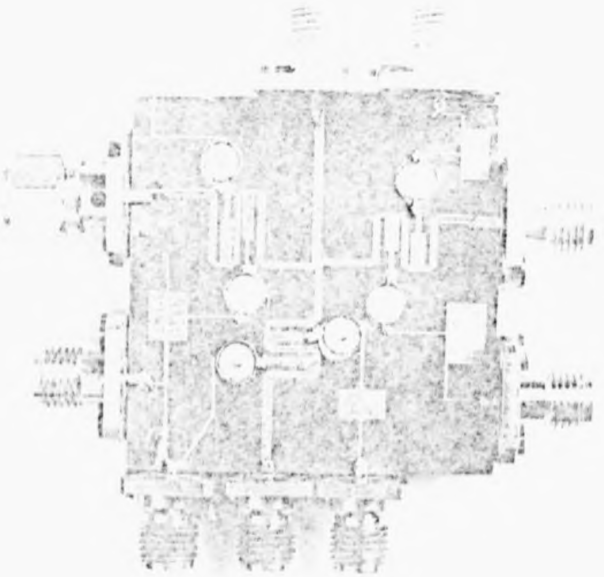

Fig.7.13 Photographic view of digital beamformer.

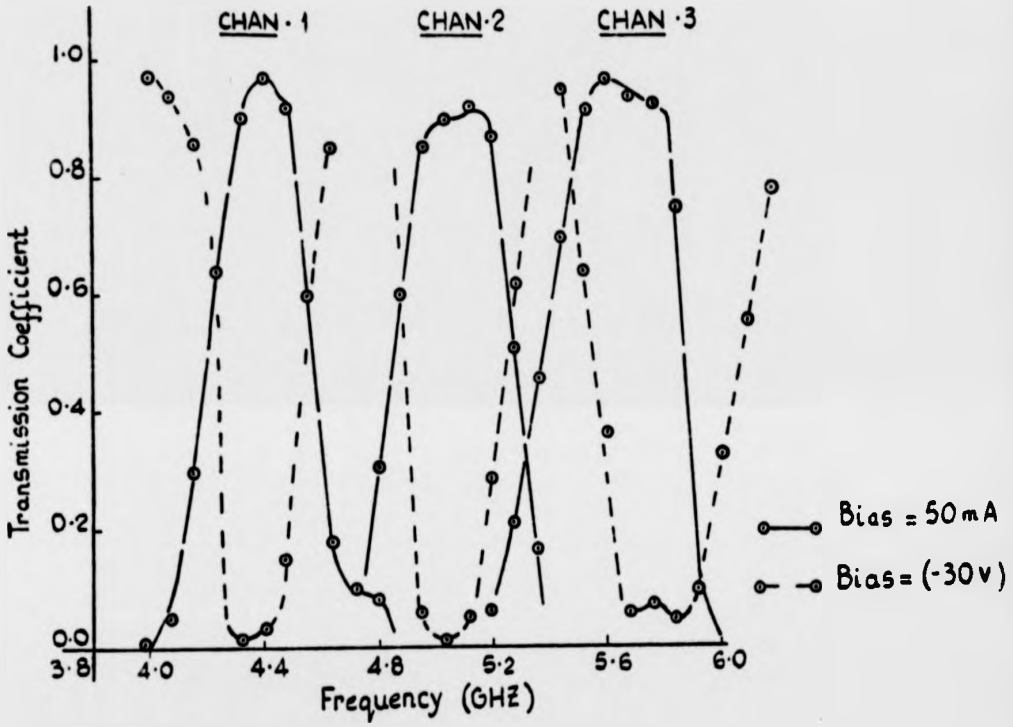

Fig.7.13 Response of 3 - channel multiplexer.

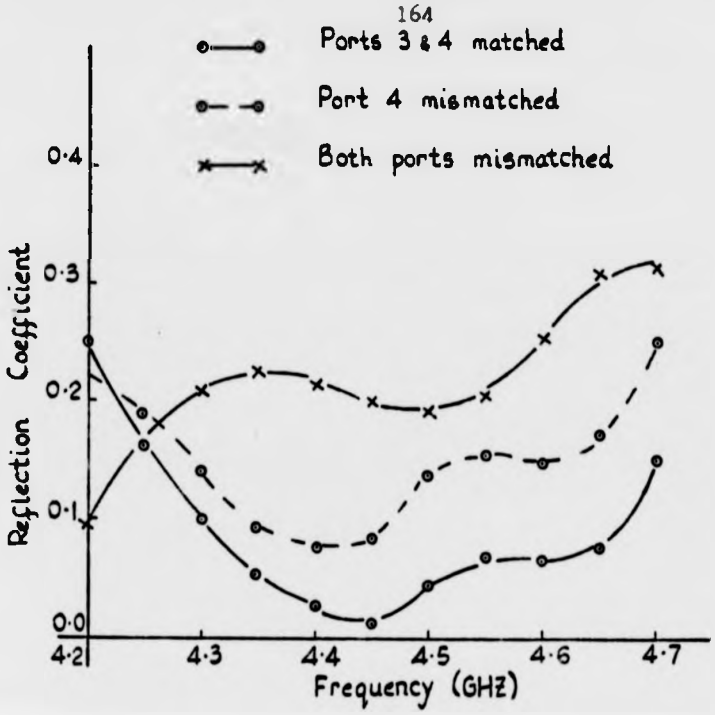

(a) Channel 1 (Bias = 50 mA)

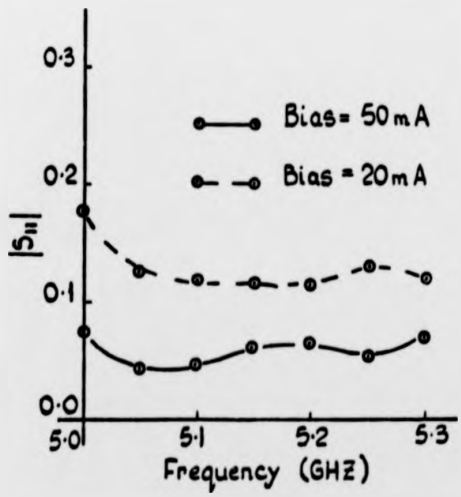

(b) Chan. 2

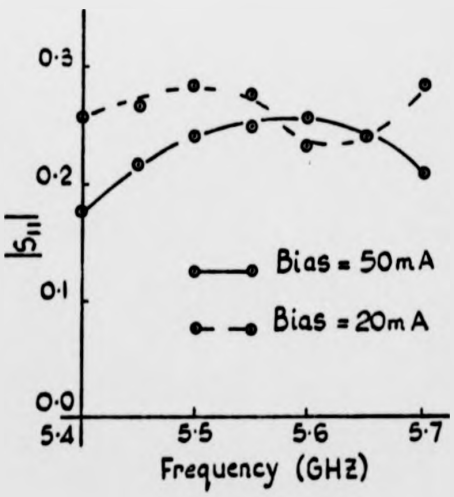

(c) Chan. 3

Fig.7.14 Variations of the magnitude of the reflection coefficient of the multiplexer.

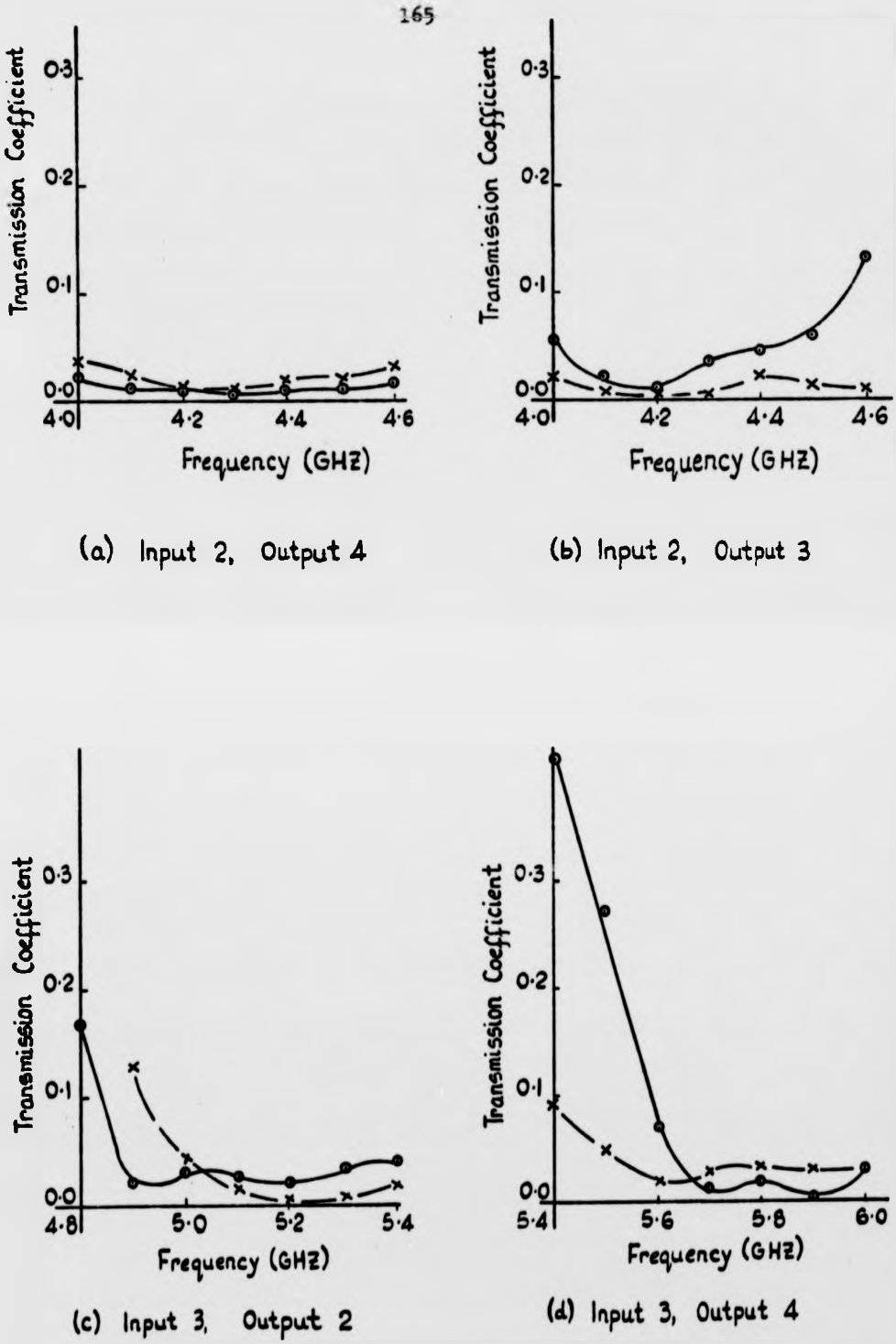

Fig.7.15 Coupling between adjacent channels.

REFERENCES

1. REHNMARK, S. "Meander-folded coupled lines", IEEE Trans. Vol. MTT-25 April 1977, pp.

2. KATO, S. et al, "A design method of meanderline type delay line", Electronics and Communications in Japan. Vol. 58-A, No. 4, 1975, pp.25-32.

3. KOWALSKI, G. "Microstrip meanderlines", AEU Vol. 29, 1975 pp.248-250.

4. EFREMOV, YU-G, et al, "Filtering characteristics of meander transmission lines", Telecomms and Radio Engineering, Vol. 32-33, No. 11, 1978, pp.58-61.

5. IWAKURA, H. et al, "A design method of meanderline type low-pass filters", IECE Trans. Vol. 62, No. 10, 1979, pp. 684-685.

6. KOMPA, G. and MEHRAN, R., "Planar waveguide model for calculating microstrip components", Electronics Letters, Vol. 11, 1975, pp.459-460.

7. GUPTA, K. C. et al, Microstrip lines and slotlines, Artech House, (Dedham Mass) 1979.

CHAPTER 8

CONCLUSIONS

A technique for realising a two-state multiplexer has been presented. The technique is based on the filtering characteristics of a meanderline and the switching actions of a p.i.n. diode. The designed two-state multiplexer makes it possible to combine the functions of time switching and frequency selection. The use of p.i.n. diodes in the design is one of the great advantages of this technique. This is because the switching speed of this device has not yet been equalled by other semiconductor devices.

The design was limited to only three channels for two main reasons. Firstly, only six diodes were available for the project and a minimum of two diodes are required for each channel. Secondly, the Kodak high resolution plates and the mask-liner exposure unit can handle a maximum circuit dimension of 4cm x 4cm. This limits the number of channels which can be realised.

The response of the multiplexers falls within an acceptable range. For the three channels multiplexer, the achieved minimum transmission coefficient

in the 'O' state was $|S_{21}| = 0.91$, corresponding to an insertion loss of 0.82dB (for channel 2). The maximum transmission coefficient in the '1' state for channel 3 of the same multiplexer was $|S_{21}| = 0.06$ corresponding to an isolation of 24.4dB. Knowing that the above values are for the worst case conditions, it can be concluded the response of the three channels multiplexer are acceptable for most applications.

The coupling between adjacent channels was greater than 20dB for both the two-channels and the three-channels multiplexers. The only exception being between channels 2 and 3 of the three channels multiplexer. In this particular case only an isolation of 10.45dB was obtained. In most of the channels, the two states of each filter cross-over at the 3-dB point. Maintaining this design criteria was one of the difficulties encountered throughout the design.

The use of stagger stub technique to increase the maximum achievable bandwidth could not be well perfected. Though a transmission coefficient of $|S_{21}| = 0.94$ (an insertion loss of 0.54dB) was obtained in the 'O' state, an unacceptable ripple of 1.94dB was also obtained in that state. Equally the isolation obtained in the '1' state was only

17.7dB, though it must be said that a bandwidth of 38.9 percent was obtained compared to only 28 percent obtained for the case when all the stubs were centred at the same centre frequency.

The technique given in chapter 6 for the anlaysis of a meanderline circuit is as simple as it is fast. The close agreement between the computed and the measured results shows the validity of the technique. The filtering properties of this structure were explored in detail. The results obtained show that the structure is not an all-pass network as earlier works suggested[1,2,3] though it should be mentioned that Efremov[4] and Iwakura[5] had recently showed these flitering properties using different methods.

Only little work was done on the differential phase shift characteristics of the meanderline but the matching technique presented was shown to give a very high return loss of 28dB. The dispersive model used in this design was that of a single coupled line. Owing to lack of time, the author could not conduct detailed investigation on the dispersive nature of the meanderline and further work in this area could prove fruitful.

All the discontinuities encountered in the project were evaluated by making input impedance measurements on open circuited lines containing the

appropriate discontinuity. This technique is by far simpler than the more rigorous full-wave analysis adopted by most authors[6]. The results obtained with the above simple technique have been shown to be comparable to that obtained using known techniques. In the case of step-in width discontinuity, the values obtained for the series inductance arms are within 5 percent of that obtained using the expressions of Gupta et al[7].

In the final sum up, it can be said that the use of p.i.n. diodes to realise a filter which can be switched from a '0' state to a '1' state and vice-versa has opened an avenue of expansion in the field of microwave switching and multiplexing applications. A great future lies for the ideas presented in this project.

REFERENCES

1. AITWATER, H., "Reflection coefficient transformation for phase shift circuits", IEEE Trans. Vol. MTT-28, June 1980, pp. 563-568.

2. KUROKAWA, K. and SCHLOSSER, W. O., "Quality factor of switching diodes for digital modulation", IEEE Trans. Vol. MMT-18, 1970, pp. 180-181.

3. EDWARDS, T. C., Foundations for microstrip circuit design, Wiley 1981.

4. MERCHENT, B., Micro-3 program, University of Warwick, Computer Unit.

5. FOX, S., Handbook of microwave measurements, Vol. 1, 3rd edition, Wiley, 1963.

6. MATTHAEI, G. L. et al, Microwave filters, impedance matching networks and coupling structures, Artech House (Dedham Mass) 1981.

7. TOURETTE, LA, P. M. and ROBERTS, J. L., "Extended junctions combline multiplexer", Int. microwave symposium digest 1978, pp. 214-216.

APPENDIX A

A1 - Microstrip lines: Microstrip is a transmission line which evolved conceptually from a parallel-wire line. The characteristic impedance of these lines were computed from

$$Z_{om} = \frac{377}{2\pi\sqrt{\epsilon_{re}}} \cdot \ln\left(\frac{8h}{W_e} + \frac{0.25W_e}{h}\right) \quad \text{for } \frac{W}{h} \leq 1 \qquad \text{A.1}$$

$$= \frac{377}{\sqrt{\epsilon_{re}}}\left[\frac{W_e}{h} + 1.393 + 0.667 \ln\left(\frac{W_e}{h} + 1.444\right)\right]^{-1}$$

$$\text{for } \frac{W}{h} \geq 1 \qquad \text{A.2}$$

$$\text{where } \frac{W_e}{h} = \frac{W}{h} + \frac{1.25}{\pi} \cdot \frac{t}{h}\left(1 + \ln\frac{4\pi W_e}{t}\right) \quad \text{for } \frac{W}{h} \leq \frac{1}{2\pi}$$

$$= \frac{W}{h} + \frac{1.25}{\pi} \cdot \frac{t}{h}\left(1 + \ln\frac{2h}{t}\right) \quad \text{for } \frac{W}{h} \geq \frac{0.5}{\pi} \qquad \text{A.3}$$

$$\epsilon_{re} = \frac{\epsilon_r+1}{2} + \frac{\epsilon_r-1}{2} \cdot F\left(\frac{W}{h}\right) - C \qquad \text{A.4}$$

$$C = \frac{\epsilon_r-1}{4.6} \cdot \frac{t/h}{(W/h)^{\frac{1}{2}}} \qquad \text{A.5}$$

$$f(W/h) = (1+12h/W)^{-\frac{1}{2}} + 0.04(1-W/h)^2 \quad \text{for } \frac{W}{h} \leq 1$$

$$= (1+12h/W)^{-\frac{1}{2}} \quad \text{for } \frac{W}{h} \geq 1 \qquad \text{A.6}$$

A.2 Triplate

$$Z_{ot}\sqrt{\varepsilon_r} = \frac{94.15}{(W/b)/(1-T/B) + (C_f/0.0885\varepsilon_r)} \qquad A.7$$

where $C_f = \frac{0.0885\varepsilon_r}{\pi}\left[2K\ln(K+1) - (K-1)\ln(K^2-1)\right]$

and $K = \frac{1}{1-T/B}$ A.8

Equations (3.7) through (3.8) yield data that is accurate to within 0.9 percent for $W/(B-T) > 0.35$.

For narrow strips, where $W/B < 0.35$

$$Z_{ot}\sqrt{\varepsilon_r} = 60 \ln\left(\frac{4B}{\pi D}\right) \qquad A.9$$

where the strip width, W, and thickness T, are related to a round centre conductor of diameter D by

$$D \approx W/2\left[1 + T/\pi W\left(1 + \ln\left[\frac{4\pi W}{T}\right] + 0.51\left[\frac{T}{W}\right]^2\right)\right] \qquad A.10$$

provided $T/W < 0.11$.

```
: GPED/11 (05/21/83)

C       MICROSTRIP IMPEDANCE
        WRITE(6,11)
11      FORMAT(1X,'MICROSTRIP PARAMETERS')
        WRITE(6,22)
22      FORMAT(3X,'INPUT  W  H  D  T  Z')
        READ(5,*)F,W,D,T,Z
        PI=3.14159265359
        IF(W.GT.0.0) GOTO 222
        A=.001
        W1=.001
        H=.01
        IF(Z.EQ.0.0) GOTO 222
33      A=(D-1.)/4.6*T/H+1./(SQRT(W/H))
        IF((W/H).GE.0.15915494) GOTO 44
        WEFF=W+1.25*T*(1.+ALOG(4.*PI*W/T))/PI
        GOTO 55
44      WEFF=W+1.25*T*(1.+ALOG(2.*H/T))PI
55      IF((W/H).GE.1.) GOTO 66
        F=1./SQRT(1.+12.*H/W)+(.04*(1.-(W/H))**2)
        DEFF=((D+1.)+(D-1.)*F)/2.
        DEFF=DEFF-A
        Z1=60.*ALOG((8.*H/WEFF)+(0.25*WEFF/H))/SQRT(DEFF)
        GOTO 77
66      F=1./SQRT(1.+12.*H/W)
        DEFF=((D+1.)+(D-1.)*F)/2.
        DEFF=DEFF-A
        G=WEFF/H+1.393+.667*ALOG(WEFF/H+1.444)
        Z1=120.*PI*1./(G*SQRT(DEFF))
77      IF((Z1-Z).LT.0.0) GOTO 88
        IF(ABS(Z1-Z).LE.F) GOTO 99
        W=W+W1
        GOTO 33
88      W=W-W1
        W1=W1/10.
        GOTO 33
99      Z1=Z
        WRITE(6,111)Z,DEFF,W
        GOTO 777
111     FORMAT(1X,'Z0=',F10.6,3X,'DEFF =',F5.3,3X,'WIDTH=',F6.5)
222     P=W/H
        IF((W/H).GE.0.15915494) GOTO 333
        WEFF=W+1.25*T*(1.+ALOG(4.*PI*W/T))/PI
        GOTO 444
333     WEFF=W+1.25*T*(1.+ALOG(2.*H/T))/PI
444     IF((W/H).GE.1.) GOTO 555
        F=1./SQRT(1.+12.*H/W)+.04*(1.-(W/H))**2)
        DEFF=((D+1.)+(D-1.)*F)/2.
        DEFF=DEFF-A
        Z1=60.*ALOG((8.*H/WEFF)+(0.25*WEFF/H))/SQRT(DEFF)
        GOTO 666
555     F=1./SQRT(1.+12.*H/W)
        DEFF=((D+1.)+(D-1.)*F)/2.
        DEFF=DEFF-A
        G=WEFF/H+1.393+.667*ALOG(WEFF/H+1.444)
        Z1=120.*PI*1./(G*SQRT(DEFF))
666     WRITE(6,222)Z1,DEFF,W
777     STOP
        END
```

```
: GREG/01 (05/21/82)

      C     STRIPLINE CHARACTERISTIC IMPEDANCE
            WRITE(6,17)
      17    FORMAT(1X,'STRIPLINE IMPEDANCE')
            WRITE(6,22)
      22    FORMAT(3X,'INPUT B  T  ER  D1 D2 D3')
            READ(5,*)B,T,ER,
            WRITE(6,44)
      44    FORMAT(1X,'ZO(OHMS) RANGE(START,STOP,STEP)')
            READ(5,*)D1,D2,D3
            IF(D1.LT.0.0001) GOTO 950
            WRITE(6,88)
      88    FORMAT(1X,'ZO      WIDTH')
            PI=3.1415926535
            ZO=D1
      99    IF(ZO.GT.D2) GOTO 777
            A=.01
            W=.001
            W1=.1
            G=1.(/(1.-T/B)
            F1=2.*G*ALOG(G+1.)
            F2=(G-1.)*ALOG((G**2.)-1.)
            C=1./PI*(F1-F2)
      111   D=.5*(1.+T/(PI*W)*(1.+ALOG((4.*PI*W)/T)+.51*PI*((T/W)**2)))
            Z=60./SQRT(ER)*ALOG(4.*B/(PI*D))
            IF(ABS(Z-ZO).LT.A) GOTO 500
            IF((Z-ZO).LT.0.0) GOTO 222
            IF(W.GT.B*0.35) GOTO 277
            W=W+W1
            GOTO 111
      222   W=W-W1
            W1=W/10.
            W=W+W1
            GOTO 111
      277   W1=.010
      333   Z=94.15/(SQRT(ER)*(((W/B)/(1.-T/B))+C))
            IF(ABS(Z-ZO).LT.A) GOTO 555
            IF((Z-ZO).LT.0) GOTO 440
            W=W+W1
            GOTO 333
      440   W=W-W1
            W1=W1/10.
            W=W+W1
            GOTO 333
      500   Z=(100.*Z+.5)/100.
      555   WRITE(6,666)ZO,W
      666   FORMAT(F10.1,F10.5)
            ZO=ZO+D3
            GOTO 99
      777   WRITE(6,888)
      888   FORMAT(/,/,/)
            GOTO 44
      950   STOP
            END
```

APPENDIX B

T-JUNCTION COMPENSATION TECHNIQUE

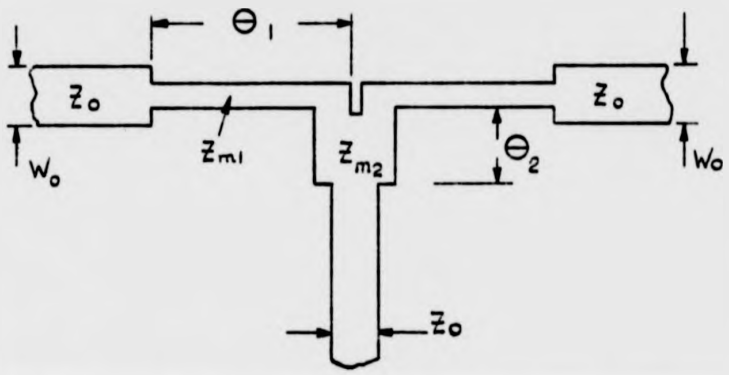

Fig. B·1 Compensated T- junction

$$Z_{m1} = [\Gamma_m Z_o^2 + X_a^2/(\Gamma_m - 1)]^{\frac{1}{2}} \qquad \text{B.1}$$

$$\theta_1 = \tan^{-1}[\Gamma_m - 1(1+\Gamma_m(\Gamma_m - 1)(Z_o/X_a)^2)]^{\frac{1}{2}} \qquad \text{B.2}$$

$$Z_{m2} = n[(n^2 X_b^2)/(n^2-1) + Z_o^2]^{\frac{1}{2}} \qquad \text{B.3}$$

$$\theta_2 = \tan^{-1}[(n^2-1)(1+\{n^2-1\}(Z_o/nX_b)^2)^{\frac{1}{2}}] \qquad \text{B.4}$$

where Γ_m is the minimum desired VSWR and

$$\frac{X_a}{Z_o} = -\frac{D_2}{\lambda_g}\left(\frac{n\pi}{4}\right)^2 \qquad \text{B.5}$$

$$\frac{X_b}{Z_o} = \frac{X_a}{2Z_o} + \frac{2D_1}{n^2\lambda_g}\left[\ln\left(\frac{1.43D_1}{D_2}\right) + 2\left(\frac{D_i}{\lambda_g}\right)^2\right] \qquad \text{B.6}$$

$$n = \mathrm{Sin}((\pi D_2/\lambda_g)/(\pi D_2/\lambda_g)) \qquad \text{B.7}$$

$$D = B\,(\mu_o)^{\frac{1}{2}}/2Z_o\varepsilon_o\varepsilon_r \qquad \text{B.8}$$

APPENDIX C

```
C     MICROWAVE CIRCUIT ANALYSIS BY GREG. A. DUDH
C     THIS PROGRAM ANALYZES MICROWAVE CIRCUITS USING ABCD MATRICES.
5     FORMAT("MICROWAVE CIRCUIT ANALYSIS PROGRAM",/)
20    FORMAT("ZL(RL,XL  OHMS) = ")
25    FORMAT("ZG(RG,XG  OHMS) = ")
35    FORMAT("F0,F1,F2,DELTA(IN GHZ.) =")
      COMPLEX ZL,ZG,ABCDS(20,2,2),ABCDT(2,2),ZIN
      DIMENSION IST(20),ST(20,4)
      WRITE(6,5)
      WRITE(6,20)
      READ(5,/)ZL
      WRITE(6,25)
      READ(5,/)ZG
      WRITE(6,35)
      READ(5,/)F0,F1,F2,DELTA
      CALL ELEMT(N,IST,ST)
      WRITE(6,150)
      F=F1
65    CALL ABCD(N,IST,ST,F,F0,ABCDS)
50    CONTINUE
      CALL TOTAL(N,ABCDS,ABCDT)
      CALL CALC(ABCDT,ZG,ZL,VSWR,ALOS,PHASE,ZIN)
      WRITE(6,195)F,VSWR,ALOS,PHASE,ZIN
150   FORMAT("FREQ-GHZ VSWR LOSS-DB",3X,"PHASE-DEG ZIN=(R), (JX)",/)
195   FORMAT(F7.3,F9.2,F9.2,F10.1,F11.1,F10.1)
      F=F+DELTA
      IF(F.GT.(F2+DELTA/2)) GOTO 230
      GOTO 65
230   END
C
C
C     SUBROUTINE ELEMT TO INPUT ELEMENT TYPES & THEIR PARAMETER VALUES
C
      SUBROUTINE ELEMT(N,IST,ST)
      DIMENSION IST(20),ST(20,4),NEW(4)
      DATA NEW/"LIN","SLG","PLG","STB"/
40    FORMAT(" HOW MANY ELEMENTS? ")
55    FORMAT("ELEM",I3,"TYPE & PARAMETERS = ")
      WRITE(6,40)
      READ(5,/)N
      DO 200 I=1,N
85    WRITE(6,55)I
      READ(5,/)IST(I),(ST(I,J),J=1,4)
      DO 150 K=1,4
150   IF(NEW(K).EQ.IST(I)) GOTO 200
      WRITE(6,155)
155   FORMAT(" NO SUCH ELEMENT, TRY AGAIN. ")
      GOTO 85
200   CONTINUE
      RETURN
      END
C
C
C     SUBROUTINE ABCD TO EVALUATE THE ABCD MATRIX OF ELEMENTS.
C
      SUBROUTINE ABCD(N,IST,ST,F,F0,ABCDS)
      COMPLEX ABCDS(20,2,2),Y,Z,GAMMAL,COSH,SINH
      DIMENSION IST(20),ST(20,4),KIND(20),NEW(4)
      DATA NEW/"LIN","SLG","PLG","STB"/
      TPI=6.2831853
```

```
      DO 960 I=1,N
C     DETERMINE ELEMENT KIND
      DO 50 K=1,4
      IF(IST(I).EQ.NEW(K)) KIND(I)=K
50    CONTINUE
      GOTO (100,200,300,400) KIND(I)
C     "LINE" ELEMENT(K=1),(Z0=OHMS,DEG=AT FO,LOSS=DB/AL   )
100   BETAL=(F/FO)*ST(I,2)/57.29578
      ALPHAL=(ST(I,3)/8.685889)*(BETAL/TPI)*SQRT(F/FO)
      GAMMAL=CMPLX(ALPHAL,BETAL)
      ABCDS(I,1,1)=CCOSH(GAMMAL)
      ABCDS(I,1,2)=ST(I,1)*CSINH(GAMMAL)
      ABCDS(I,2,1)=(1./ST(I,1))*CSINH(GAMMAL)
      GOTO 950
C     "SLC" SERIES LCR ELEMENT(K=2),(L=NH,C=PF,R=OHMS,   )
C     SHORT OUT A ZERO SERIES CAPACITANCE VALUE
200   IF(ST(I,2).LT.(1.E-15)) ST(I,2)=1.E+12
      Z=CMPLX(ST(I,3),(TPI*ST(I,1)-159.1549/(F*ST(I,2))))
      ABCDS(I,1,1)=CMPLX(1.,0.)
      ABCDS(I,1,2)=Z
      ABCDS(I,2,1)=CMPLX(0.,0.)
      GOTO 950
C     "PLC" PARALLEL LCR ELEMENT(K=3),(L=NH,C=PF,R=OHMS,   )
C     OPEN CIRCUIT ZERO VALUE SHUNT L OR R ELEMENTS
300   IF(ST(I,1).LT.(1.E-12)) ST(I,1)=1.E+12
      IF(ST(I,3).LT.(1.E-12)) ST(I,3)=1.E+12
      Y=CMPLX((1./ST(I,3)),((-1./(TPI*F*ST(I,1)))+(F*ST(I,2)/159.1549)))
      ABCDS(I,1,1)=CMPLX(1.,0.)
      ABCDS(I,1,2)=CMPLX(0.,0.)
      ABCDS(I,2,1)=Y
      GOTO 950
C     "STB" CAPACITANCE TERMINATED STUB(K=4),(Z0,DEG,LOSS),C   )
C     MAKE A ZERO CAPACITANCE FINITE
400   IF(ST(I,4).LT.(1.E-15)) ST(I,4)=1.E-15
C     STUB SUSCEPTANCE
      Y=CMPLX(0.,TPI*F*ST(I,4))
C     STUB PROPAGATION CONSTANT
      BETAL=(F/FO)*ST(I,2)/57.29578
      ALPHAL=(ST(I,3)/8.685889)*(BETAL/TPI)*SQRT(FO/F)
      GAMMAL=CMPLX(ALPHAL,BETAL)
C     TRANSFORM C ALONG STUB
      CALL SHUNTP(Y,GAMMAL,ST(I,1),Y)
      ABCDS(I,1,1)=CMPLX(1.,0.0)
      ABCDS(I,1,2)=CMPLX(0.,0.0)
      ABCDS(I,2,1)=Y
950   ABCDS(I,2,2)=ABCDS(I,1,1)
960   CONTINUE
      RETURN
      END
C
C
C     SUBROUTINE TOTAL TO FIND THE TOTAL ABCD MATRIX OF N NETWORKS
C
      SUBROUTINE TOTAL(N,ABCDS,ABCDT)
      COMPLEX ABCDS(20,2,2),ABCDT(2,2),NEXT(2,2)
      ABCDT(1,1)=ABCDS(N,1,1)
      ABCDT(1,2)=ABCDS(N,1,2)
      ABCDT(2,1)=ABCDS(N,2,1)
      ABCDT(2,2)=ABCDS(N,2,2)
      IF(N.EQ.1) GOTO 10
      DO 30 I=1,(N-1)
      NEXT(1,1)=ABCDS((N-I),1,1)
      NEXT(1,2)=ABCDS((N-I),1,2)
```

```
      DO 960 I=1,N
C     DETERMINE ELEMENT KIND
      DO 50 K=1,4
      IF(IST(I).EQ.NEM(K)) KIND(I)=K
50    CONTINUE
      GOTO (100,200,300,400) KIND(I)
C     "LINE ELEMENT(K=1),(Z0=OHMS,DEG=AT FO,LOSS=DB/AL   )
100   BETAL=(F/F0)*ST(I,2)/57.29578
      ALPHAL=(ST(I,3)/8.685889)*(BETAL/TPI)*SQRT(F/F0)
      GAMMAL=CMPLX(ALPHAL,BETAL)
      ABCDS(I,1,1)=CCOSH(GAMMAL)
      ABCDS(I,1,2)=ST(I,1)*CSINH(GAMMAL)
      ABCDS(I,2,1)=(1./ST(I,1))*CSINH(GAMMAL)
      GOTO 950
C     "SLC" SERIES LCR ELEMENT(K=2),(L-NH,C-PF,R-OHMS,   )
C     SHORT OUT A ZERO SERIES CAPACITANCE VALUE
200   IF(ST(I,2).LT.(1.E-15)) ST(I,2)=1.E+12
      Z=CMPLX(ST(I,3),(TPI*ST(I,1)-159.1549/(F*ST(I,2))))
      ABCDS(I,1,1)=CMPLX(1.,0.)
      ABCDS(I,1,2)=Z
      ABCDS(I,2,1)=CMPLX(0.,0.)
      GOTO 950
C     "PLC" PARALLEL LCR ELEMENT(K=3),(L-NH,C-PF,R-OHMS,   )
C     OPEN CIRCUIT ZERO VALUE SHUNT L OR R ELEMENTS
300   IF(ST(I,1).LT.(1.E-12)) ST(I,1)=1.E+12
      IF(ST(I,3).LT.(1.E-12)) ST(I,3)=1.E+12
      Y=CMPLX((1./ST(I,3)),((-1./(TPI*F*ST(I,1)))+(F*ST(I,2)/159.1549)))
      ABCDS(I,1,1)=CMPLX(1.,0.)
      ABCDS(I,1,2)=CMPLX(0.,0.)
      ABCDS(I,2,1)=Y
      GOTO 950
C     "STB" CAPACITANCE TERMINATED STUB(K=4),(Z0,DEG,LOSS,C   )
C     MAKE A ZERO CAPACITANCE FINITE
400   IF(ST(I,4).LT.(1.E-15)) ST(I,4)=1.E-15
C     STUB SUSCEPTANCE
      Y=CMPLX(0.,TPI*F*ST(I,4))
C     STUB PROPAGATION CONSTANT
      BETAL=(F/F0)*ST(I,2)/57.29578
      ALPHAL=(ST(I,3)/8.685889)*(BETAL/TPI)*SQRT(F0/F)
      GAMMAL=CMPLX(ALPHAL,BETAL)
C     TRANSFORM Y ALONG STUB
      CALL SMITH(Y,GAMMAL,ST(I,1),Y)
      ABCDS(I,1,1)=CMPLX(1.,0.)
      ABCDS(I,1,2)=CMPLX(0.,0.)
      ABCDS(I,2,1)=Y
950   ABCDS(I,2,2)=ABCDS(I,1,1)
960   CONTINUE
      RETURN
      END
C
C
C     SUBROUTINE TOTAL TO FIND THE TOTAL ABCD MATRIX OF N NETWORKS
C
      SUBROUTINE TOTAL(N,ABCDS,ABCDT)
      COMPLEX ABCDS(20,2,2),ABCDT(2,2),NEXT(2,2)
      ABCDT(1,1)=ABCDS(N,1,1)
      ABCDT(1,2)=ABCDS(N,1,2)
      ABCDT(2,1)=ABCDS(N,2,1)
      ABCDT(2,2)=ABCDS(N,2,2)
      IF(N.EQ.1) GOTO 10
      DO 90 I=1,(N-1)
      NEXT(1,1)=ABCDS((N-I),1,1)
      NEXT(1,2)=ABCDS((N-I),1,2)
```

```
      NEXT(2,1)=ABCDS((N-1)*2+1)
      NEXT(2,2)=ABCD_((N-1)*2+2)
      CALL MAT(NEXT,ABCDI,ATOT)
50    CONTINUE
100   RETURN
      END
C
C
C     SUBROUTINE CALC TO CALCULATE THE RESPONSE OF THE NETWORK
C
      SUBROUTINE CALC(ABCD,ZG,ZL,VSWR,ALOS,PHASE,ZIN)
      COMPLEX ABCD(2,2),ZG,ZL,ZIN,REFL,RATIO,A,B,C,D
      A=ABCD(1,1)
      B=ABCD(1,2)
      C=ABCD(2,1)
      D=ABCD(2,2)
C     INPUT IMPEDANCE
      ZIN=(A*ZL+B)/(C*ZL+D)
C     REFLECTION COEFFICIENT
      REFL=(ZIN-ZG)/(ZIN+ZG)
C     INPUT VSWR
      VSWR=(1.+CABS(REFL))/(1.-CABS(REFL))
C     RATIO OF MAXIMUM AVAILABLE TO ACTUAL LOAD VOLTAGE(V0/V2)
      RATIO=0.5*((ZIN+ZG)/ZIN)*(A+(B/ZL))
C     INSERTION LOSS IN DB
      ALOS=10.*ALOG10(CABS(RATIO*RATIO)*REAL(ZL)/REAL(ZG))
C     TRANSMISSION PHASE(-ARG(V0/V2))
      X=REAL(RATIO)
C     PRECAUTION TO AVOID DIVISION BY ZERO
      IF(ABS(X).LT.(1.E-5)) X=1.E-8
      Y=AIMAG(RATIO)
C     CALCULATION OF TRANSMISSION PHASE(RADIANS)
      PHASE=-ATAN(Y/X)
C     CONVERSION OF PHASE FROM RADIANS TO DEGREES
      PHASE=PHASE*57.2957804
      RETURN
      END
C
C
C     SUBROUTINE HYPCS TO CALCULATE COMPLEX HYPERBOLIC COSINE & SINE
C
      COMPLEX FUNCTION CCOSH(Z)
      COMPLEX Z
      CCOSH=(CEXP(Z)+CEXP(-Z))/2.
      RETURN
      END
C
C
      COMPLEX FUNCTION CSINH(Z)
      COMPLEX Z
      CSINH=(CEXP(Z)-CEXP(-Z))/2.
      RETURN
      END
C
C
C     SUBROUTINE MAT FOR COMPLEX 2X2 MATRIX MULTIPLICATION.
C
      SUBROUTINE MAT(A,B,C)
C     COMPLEX ELEMENT, 2X2 MATRIX MULTIPLICATION
      COMPLEX A(2,2),B(2,2),C(2,2),D(2,2)
      D(1,1)=A(1,1)*B(1,1)+A(1,2)*B(2,1)
      D(1,2)=A(1,1)*B(1,2)+A(1,2)*B(2,2)
      D(2,1)=A(2,1)*B(1,1)+A(2,2)*B(2,1)
```

```
      D(2,2)=A(2,1)*B(1,2)+A(2,1)*B(2,1)
      DO 10 I=1,2
      DO 10 J=1,2
      C(I,J)=D(I,J)
10    CONTINUE
      RETURN
      END
C
C
C     SUBROUTINE SMITH TO PERFORM LOSSY LINE SMITH CHART TRANSFORMATION
C
C     SMITH CHART TRANSFORMATION ALONG A LOSSY LINE
      SUBROUTINE SMITH(YL,GAMMAL,ZC,YIN)
      COMPLEX YIN,GAMMAL,CCOSH,CSINH,YL,A,B
      IF(ZC.LT.1.E-12) ZC=1.E-12
      A=YL*CCOSH(GAMMAL)+(1./ZC)*CSINH(GAMMAL)
      B=CCOSH(GAMMAL)+YL*ZC*CSINH(GAMMAL)
      IF(CABS(B).LT.1.E-12) B=CMPLX(1.E-12,0.0)
      YIN=A/B
      RETURN
      END
```

APPENDIX D

```
C       PROGRAM TO COMPUTE COUPLING PARAMETERS
C       COMPUTED VALUES ARE DIMENSIONLESS
C       VALUES ARE NORMALISED TO FREE SPACE PERMITIVITY
C       PROGRAM CAN BE USED FOR EITHER TRIPLATE OR MICROSTRIPLINES
C       THE CONDITION W=0 DEFINES A BALANCED STRIPLINE (TRIPLATE)
C
C
C       PROGRAM COMPUTES COUPLING VOLTAGE,KT, IN TERMS OF SPACING,S.
C
        REAL KEFF,KM,KFE,KFO,KG,KP,KT
        WRITE(6,10)
10      FORMAT(1X,'COUPLED PARAMETERS')
        WRITE(6,16)
16      FORMAT(3X,'INPUT H T KEFF W C01 C02 C03')
        READ(5,*)H,T,KEFF,W,C01,C02,C03
        IF(C01.LT.0.0001) GOTO 999
        WRITE(6,22)
22      FORMAT(1X,'KM      S')
        PI=3.1415926535
        KTO=C01
50      IF(KTO.GT.C02) GOTO 777
        P=0.01
        S=0.001
        S1=0.010
        X=(PI*S)/(2.*H)
        TANH(X)=(1.-EXP(-2.*X))/(1.+EXP(-2.*X))
        COTH(X)=1./TANH(X)
        D1=ALOG(1.+TANH(X))
        D2=ALOG(1.+COTH(X))
        R=1./(1.+T/H)
        F1=2.*R*ALOG(R+1.)
        F2=(R-1.)*ALOG((R**2.)-1.)
C
C
        CFD=1./PI*(F1-F2)
        CDD=2.*KEFF*0.4427/PI
        CFOD=2.*KEFF*D2/PI
        CFEV=2.*KEFF*D1/PI
        KFE=CFD*CFEV/CDD
        KFO=CFD*CFOD/CDD
        KP=2.*W/(H-T)
C
C
        KG=2.*(KFE*KP*CFD)
        KM=KFO-KFE
54      KT=KM/(KG+KM)
        IF(ABS(KT-KTO).LT.P) GOTO 500
        IF((KT-KTO).LT.0.0) GOTO 121
        IF(S/T.GE.10.) GOTO 270
        S=S+S1
        GOTO 54
121     S=S-S1
        S1=S/10.
        S=S+S1
        GOTO 54
270     KFO2=CFOD*(KEFF*T/S)
300     KM=KFO2-KFE
        KT=KM/(KG+KM)
        IF(ABS(KT-KTO).LT.P) GOTO 555
        IF((KT-KTO).LT.0.0) GOTO 440
```

APPENDIX D

```
C     PROGRAM TO COMPUTE COUPLING PARAMETERS
C     COMPUTED VALUES ARE DIMENSIONLESS
C     VALUES ARE NORMALISED TO FREE SPACE PERMITIVITY
C     PROGRAM CAN BE USED FOR EITHER TRIPLATE OR MICROSTRIPLINES
C     THE CONDITION W=0 DEFINES A BALANCED STRIPLINE (TRIPLATE)
C
C
C     PROGRAM COMPUTES COUPLING VOLTAGE,KT, IN TERMS OF SPACING,S.
C
      REAL KEFF,KM,KFE,KFO,KO,KP,KT
      WRITE(6,10)
10    FORMAT(1X,'COUPLED PARAMETERS')
      WRITE(6,16)
16    FORMAT(3X,'INPUT H T KEFF W C01 C02 C03')
      READ(5,*)H,T,KEFF,W,C01,C02,C03
      IF(C01.LT.0.0001) GOTO 999
      WRITE(6,22)
22    FORMAT(1X,'KM     S')
      PI=3.14159265359
      KTO=C01
50    IF(KTO.GT.C02) GOTO 777
      P=0.01
      S=0.002
      S1=0.010
      X=(PI*S)/(2.*H)
      TANH(X)=(1.-EXP(-2.*X))/(1.+EXP(-2.*X))
      COTH(X)=1./TANH(X)
      D1=ALOG(1.+TANH(X))
      D2=ALOG(1.+COTH(X))
      R=1./(1.-T/H)
      F1=2.*H*ALOG(R+1.)
      F2=(R-1.)*ALOG((R**2.)-1.)
C
C
      CFD=1./PI*(F1-F2)
      CDD=2.*KEFF*0.4427/PI
      CFOD=2.*KEFF*D2/PI
      CFEV=2.*KEFF*D1/PI
      KFE=CFD*CFEV/CDD
      KFO=CFD*CFOD/CDD
      KP=2.*W/(H-T)
C
C
      KO=2.*(KFE+KP+CFD)
      KM=KFO-KFE
54    KT=KM/(KO+KM)
      IF(ABS(KT-KTO).LT.P) GOTO 500
      IF((KT-KTO).LT.0.0) GOTO 121
      IF(S/T.GE.10.) GOTO 270
      S=S+S1
      GOTO 54
121    S=S-S1
      S1=S/10.
      S=S+S1
      GOTO 54
270   KFO2=CFOD*(KEFF*T/S)
300   KM=KFO2-KFE
      KT=KM/(KO+KM)
      IF(ABS(KT-KTO).LT.P) GOTO 555
      IF((KT-KTO).LT.0.0) GOTO 440
```

```
      S=S+S1
      GOTO 300
400   S=S+S1
      S1=S1/10.
      S=S+S1
      GOTO 300
500   KT=(100.*K+0.5)/100
555   WRITE(6,711)KT,S
711   FORMAT(1X,'KT = ',F1%.4,3X,'S = ',F5.6)
      KT=KT+003
      GOTO 50
777   WRITE(6,833)
833   FORMAT(/,/)
      GOTO 500
999   STOP
      END
```

APPENDIX E

PHASE SHIFT OF MULTI-SECTION MEANDERLINE

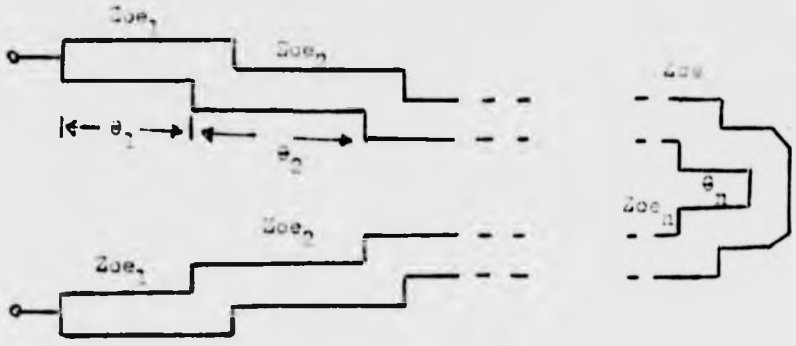

Fig.E.1 Multi-section differential phase shifter

The phase shift of a signal which has passed through a single section meanderline is given by:

$$\phi_{(n)} = \cos^{-1}\left[\frac{K - (\tan\theta_{e,o})^2}{K + (\tan\theta_{e,o})^2}\right] \qquad \text{E.1}$$

where $K = Z_{oe}/Z_{oo}$ and $\tan\theta_{e,o} = \tan\theta_e \tan\theta_o$.

For two sections

$$\phi_{(n=2)} = \cos^{-1}\left[\frac{K_1 - (\tan\theta^1_{1(e,o)})^2}{K_1 + (\tan\theta^1_{1(e,o)})^2}\right] \qquad \text{E.2}$$

where $\phi_1^1 = \phi_1 + \tan^{-1}(Z_{oo_2} \quad Z_{oo_1})\tan\theta_2$

for three sections

$$\phi_{(n=3)} = \text{Cos}^{-1}\left[\frac{K_1 - (\tan\theta^1_{1(e,o)})^2}{K_1 + (\tan\theta^1_{1(e,o)})^2}\right] \qquad \text{E.3}$$

where $\theta_1' = \theta_1 + \tan^{-1}\left[(Z_{oo_2} \; Z_{oo_1})\tan\theta_2'\right]$

and $\theta_2' = \theta_2 + \tan^{-1}\left[(Z_{oo_3} \; Z_{oo_2})\tan\theta_3\right]$

Thus for n sections

$$\theta_n = \text{Cos}^{-1}\left[\frac{K_1 - (\tan\theta'_{1(e,o)})^2}{K_1 + (\tan\theta'_{1(e,o)})^2}\right] \qquad \text{E.4}$$

where $\theta_1' = \theta_1 + \tan^{-1}(a_{12}\tan\theta_2')$

$\theta_2' = \theta_2 + \tan^{-1}(a_{23}\tan\theta_3')$

$\theta_{n-1}' = \theta_{n-1} + \tan^{-1}(a_{(n-1)n}\tan\theta_n')$

$\theta_n' = \theta_n$

and $a_{i,i+1} = Z_{oe_i} \; Z_{oe_{(i+1)}} = Z_{oo_{(i+1)}} \; Z_{oo_i}$

APPENDIX F

In a two-port network characterized by the voltage relations:-

$$V_1 = AV_2 - BI_2$$
$$I_1 = CV_2 - DI_2 \qquad \text{F.1}$$

the matrix of the general circuit parameters

$$M = \begin{pmatrix} A & B \\ C & D \end{pmatrix}$$

has the property that if the network is considered loss-less and reciprocal, then M may be written as

$$M = \begin{pmatrix} a & jb \\ jc & d \end{pmatrix} \quad \text{where a, b, c and d are real} \qquad \text{F.2}$$

If the impedance transformer is described by a generalized ABCD matrix, the transformed impedance is given by

$$Z_K' = (aZ_K + jb)/(jcZ_K + d);\ K = 1, 2 \qquad \text{F.3}$$

The reflection coefficient of any network of impedance Z_K' is given by:-

$$\Gamma_K(Z_K') = (Z_K'-Z_O)/(Z_K'+Z_O) \qquad \text{F.4a}$$

Equation F.4a is equivalent to

$$(\Gamma_K-1)aZ_K + jb(\Gamma_K-1) + j(\Gamma_K+1)cZ_OZ_K + (\Gamma_K+1)dZ_O = 0 \qquad \text{F.4b}$$

Introducing the reflection variable R, where e is given by:-

$$e_K = (\Gamma_K-1)/(\Gamma_K+1) \qquad \text{F.5}$$

Hence from F.4: $ae_K Z_K + je_K b + jcZ_o Z_K + dZ_o = 0$ F.6

The complex form of e_K and Z_K may be written as

$$e_K = e_K' + je_K''$$

$$Z_K = R_K + jX_K$$

When these forms are introduced into F.6, the real and imaginary parts separate and the result is:-

Real: $(e_K' R_K - e_K'' X_K)a - e_K'' b - cZ_o X_K + dZ_o = 0$ F.7

Imag: $(e_K'' R_K + e_K' X_K)a + e_K' b - CZ_o R_K = 0$ F.8

When F.7 and F.8 are written for cases K = 1 and 2, the result is a set of four homogeneous equations in the network constants a, b, c, d. These equations will have a unique solution only if the determinant of their coefficient vanishes. This determinant is

$$\begin{vmatrix} (e_1' R_1 - e_1'' X_1) & -e_1'' & -Z_o X_1 & Z_o \\ (e_2' R_2 - e_2'' X_2) & -e_2'' & -Z_o X_2 & Z_o \\ (e_1'' R_1 + e_1' X_1) & e_1' & Z_o R_1 & 0 \\ (e_2'' R_2 + e_2' X_2) & e_2' & Z_o R_2 & 0 \end{vmatrix} = 0 \qquad \text{F.9}$$

Expanding F.9 produces the result

$$\frac{(X_1 - X_2)^2 + (R_1 - R_2)^2}{R_1 R_2} = \frac{(e_1' - e_2')^2 + (e_1'' - e_2'')^2}{e_1' e_2'}$$

This equation may be written more compactly in the form

$$\frac{|Z_1 - Z_2|^2}{R_1 R_2} = \frac{|e_1 - e_2|^2}{e_1' e_2'} \qquad \text{F.10}$$

Equation F.10 is a necessary condition for the existence of a solution for the network constants of an impedance transformer which produces complex reflection coefficients Γ_1 and Γ_2 when terminated with impedances Z_1 and Z_2.

Solution for the network parameter Z_m

Equation F.3 may be written as

$$\Gamma_K(Z_K') = \frac{Z_K - Z_m}{Z_K + Z_m^*} \cdot \frac{(a - jcZ_o)}{(a + jcZ_o)} = \frac{Z_K - Z_m}{Z_K + Z_m^*} \cdot n \qquad \text{F.11}$$

where $Z_m = (dZ_o - jb)/(a - jcZ_o)$ and n is a phase factor of unit amplitude ($n = \exp(2j\tan^{-1}(-cZ_o/a))$.

The version of F.11 for cases K = 1 and K = 2 may be combined

$$\frac{1}{n} = \frac{1}{\Gamma} \cdot \frac{Z_1 - Z_m}{Z_1 + Z_m^*} = \frac{1}{\Gamma_2} \cdot \frac{Z_2 - Z_m}{Z_2 + Z_m^*} \qquad \text{F.12}$$

The solution for Z_m^* is

$$Z_m^* = \frac{VZ_m + U}{Z_m + W} \qquad \text{F.13}$$

where

$$V = -\frac{(\Gamma_1 Z_1 - \Gamma_2 Z_2)}{(\Gamma_1 - \Gamma_2)} \qquad \text{F.14}$$

$$W = -\frac{(\Gamma_1 Z_2 - \Gamma_2 Z_1)}{\Gamma_1 - \Gamma_2} \qquad \text{F.15}$$

$$U = Z_1 Z_2 \qquad \text{F.16}$$

The allowable values of Γ_1 and Γ_2 are restricted by a condition which arises from F.4b. When F.4b is written for cases K = 1, 2; the real and imaginary parts separate. The result is a set of four homogeneous equations in the unknown network parameter. The equation will have a solution only if the determinant of their coefficient vanishes. The vanishing of the determinant leads to the relation

$$\frac{|G_1 - G_2|^2}{G_1 G_2} = \frac{|Z_1 - Z_2|^2}{R_1 R_2} = Q^2 \qquad \text{F.17}$$

where G_1, G_2 are reflection variables defined by

$$G_1 = (\Gamma_1 - 1)/(\Gamma_1 + 1); \qquad G_2 = (\Gamma_2 - 1)/(\Gamma_2 + 1) \qquad \text{F.18}$$

Substitution of F.18 into F.17 yields

$$\frac{4|\Gamma_1 - \Gamma_2|^2}{(|\Gamma_1|^2 - 1)(|\Gamma_2|^2 - 1)} = \frac{|Z_1 - Z_2|}{R_1 R_2} = Q^2 \qquad \text{F.19}$$

By choosing a suitable value of Γ_1, the value of Γ_2 was found from the above as

$$|\Gamma_2| = |R \pm (S + T^2)^{\frac{1}{2}}| \qquad \text{F.20}$$

where $R = (|\Gamma_1| \mathrm{Cos}\psi)/(1 + P^2)$

$S = (P^2 - |\Gamma_1|^2)/(1 + P^2)$

$P^2 = \frac{1}{4} Q^2 (1 - |\Gamma_1|^2)$

Equation F.13 may be solved for Z_m by taking its complex conjugate and substituting back into itself. This leads to the solution:-

$$Z_m = -\alpha \pm (\beta + \alpha^2)^{\frac{1}{2}} \qquad \text{F.21}$$

where $$\alpha = \frac{(V.V^* - W.W^* + U-U^*)}{2(U + W^*)} \qquad \text{F.22}$$

$$\beta = \frac{W.U^* + V^*.U}{(V + W)} \qquad \text{F.23}$$

The dimensions of the matching network are then computed using the ground equation

$$Z_T = \left[Z_o \left| \frac{R_m Z_o - (R_m^2 + X_m^2)}{Z_o - R_m} \right| \right]^{\frac{1}{2}} \qquad \text{F.24}$$

$$\theta_T = \tan^{-1} \left[\left(\frac{Z_o - R_m}{Z_o X_m^2} \right) \left(R_m Z_o - \left[R_m^2 + X_m^2 \right] \right) \right] \qquad \text{F.25}$$

PUBLICATIONS

1 Electronics Letters Vol.17 No.19 1981 pp.702 - 703

2 Colloquium on Microwave filters. 14th Jan. 1982
pp.2.1 - 2.3

and H-type waveguide circulators, the operational principle is dominated by the transverse magnetic-field components.) The field pattern in Fig. 1*a*, which is inherent to a correctly adjusted circulator, is rotated by 90° in comparison to that of a conventional circulator.

Possible solutions for mounting the ferrite resonator are shown in Figs. 1*b–d*. Up to now, the single-puck structure of Fig. 1*d* yielded the best results. Notice that the slots of the unilateral fin-lines open at the resonator surface! The inner circulator is matched to standard *X*-band waveguides by exponential tapers. Optimising the parameters yielded a bandwidth of 4%. The symmetrical mounting of the ferrite disc turned out to be very critical. It must be centred with a tolerance of less than 0·1 mm. As for a conventional waveguide circulator, the shape of the waveguide housing largely influences the performance. Tuning plungers above and below the disc had to be properly adjusted, although one surface of the ferrite disc was metallised.

A vast increase in bandwidth can be achieved by replacing the tapers by quarter-wave transformer sections and by optimising the distance to the ferrite resonator. Fig. 2*a* depicts a bandwidth of 10%, and an insertion loss of about 0·5 dB. No efforts had, however, been undertaken to minimise the loss. A triangular ferrite disc has also been tried but with a slightly worse performance. The bandwidth was about 9% (Fig. 2*b*). Tuning screws had, however, to be used in addition to the quarter-wave transformer.

In conclusion, a successful operation of an E-type fin-line circulator has been demonstrated. Further investigations should be directed towards increasing the frequency into the lower millimetre-wave region. The experiments have also shown the need for a theoretical investigation in order to reduce the number of parameters. A first step could be a computer-aided design of the matching circuits following the ideas developed in Reference 4.

Acknowledgment: The authors are indebted to Dr. Friedrich of AEG-Telefunken, Backnang, for supplying the ferrite material and the Deutsche Forschungsgemeinschaft for financial support.

M. BRAAS
C. SCHIEBLICH
Institut für Hochfrequenztechnik
Technische Universität
Postfach 3329, D-3300 Braunschweig, West Germany

21st July 1981

References

1 OHASAWARA, S., and KAJI, M.: 'Coplanar-guide and slot-guide junction circulators', *Electron. Lett.*, 1977, **7**, (9), pp. 220–221
2 MEYER, A., and SOLBACH, K.: 'Fin-line ferrite isolator for integrated millimeter-wave circuits', IEEE international microwave symposium digest, 1981, pp. 296–298
3 MEYER, A., and WOLFF, I.: 'Fin-line ferrite isolator and circulator for the K-band'. To be presented at 11th European microwave conference, Amsterdam, 1981
4 HUFFNAWY, D., and SCHÜNEMANN, K.: 'Computer-aided design of semiconductor mounts in fin-line technology', IEEE international microwave symposium digest, 1981, pp. 307–309

0013-5194/81/190701-02$1.50/0

PIN DIODES IN MEANDER-LINE FILTERS FOR MULTIPLEXING APPLICATIONS

Indexing terms: Semiconductor devices and materials, Multiplexing, PIN diodes

A new application of PIN diodes is described in terms of a meander-line switchable filter. With the diodes forward-biased, bandpass properties result, but under reverse bias the passband is converted into a stopband. These filters are intended for use in multiplexing systems.

Introduction: Based on parallel-coupled transmission line theory,[1] the meander line is considered as a particular form of multiline system incorporating a series of end connections. Using nodal analysis, the voltage coupling ratio may be found for the meander line and this ratio is in turn used in calculating the even and odd mode characteristic impedances.[2] These, together with a knowledge of the electrical lengths involved, enable the transmission coefficient to be calculated as a function of frequency. For the purpose of switching, however, PIN diodes are mounted at the ends of quarter-wavelength stub arms, which are connected to the meander loop, as illustrated in Fig. 1. Design equations are then obtained by introducing the concept of an *admittance inverter parameter*.

Analysis: The meander line is divided into pairs of elements and each pair subjected to standard procedures, yielding the even and odd mode characteristic impedances Z_{0e} and Z_{0o} from which the spacing and width may be determined. The stub arms containing the diodes act as impedance inverters. Using the results of Makimoto and Yamashita,[3] for an electrical angle of $\pi/2$, leads to the equations:

$$\frac{Z_{0e}}{Z_0} = 1 + \frac{J}{Y_0} + \left(\frac{J}{Y_0}\right)^2 \quad (1)$$

$$\frac{Z_{0o}}{Z_0} = 1 - \frac{J}{Y_0}\left(1 - \frac{J}{Y_0}\right) \quad (2)$$

The admittance inverter parameter J is obtained, using the results of Kato *et al.*:[4]

$$J_{0,1} = Y_0\sqrt{\frac{2B_1\theta}{G_0 G_1}} \quad (3)$$

$$J_{i,i+1} = Y_0\sqrt{\frac{2B_i\theta}{G_i G_{i+1}}} \quad (4)$$

where B_i and G are the relative bandwidth and conductance values, respectively, and i signifies a particular element of the meander line.

The above analysis does not allow for the coupling capacitances of the meander sections, which can be related to the even and odd mode characteristic impedances,[5] leading to the design equations:

$$Z_0\sqrt{\left(\frac{1 + Co_{i,i+1}}{1 - Co_{i,i+1}}\right)} = 1 + \frac{J}{Y_0} + \left(\frac{J}{Y_0}\right)^2 \quad (5)$$

and

$$Z_0\sqrt{\left(\frac{1 - Co_{i,i+1}}{1 + Co_{i,i+1}}\right)} = 1 - \frac{J}{Y_0}\left(1 - \frac{J}{Y_0}\right) \quad (6)$$

where Co is expressed in terms of Cm, mutual capacitance between adjacent conductors and Cg, capacitance to ground, by

$$Co = \frac{Cm_{i,i+1}}{(Cg_i + Cm_{i,i+1})(Cg_{i+1} + Cm_{i,i+1})} \quad (7)$$

Design and construction: Polyguide triplate of 1·59 mm thickness was used as the substrate material, the diodes being

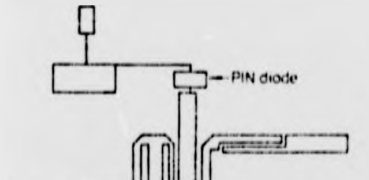

Fig. 1 *PIN diode switchable filter*

MEDL type DC 2418A. Each diode package was located in a slot milled into the substrate at a depth permitting the connecting leads to be aligned with the triplate conductors. Filter elements were designed for a bandwidth of 2·6–3·4 GHz.

In order to characterise the stub meander line accurately, it is necessary to compensate for the effects of the discontinuity capacitance caused by the T-junction which is formed by the stub and the main arms of the meander line. If neglected, the effects of this discontinuity cause the centre frequency of the network to deviate by about 5%.[6] The discontinuity capacitance is compensated by changing the line widths near the junction, as shown in Fig. 2. The dimensions of the impedances Z_1 and Z_2 are evaluated in terms of the designed values using the empirical expression derived by Dydyk.[7]

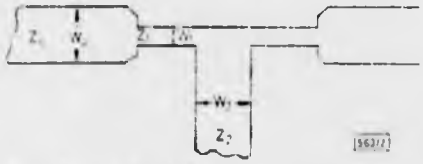

Fig. 2 *Compensated T-junction*

Low thermal impedance was ensured by backing with aluminium plates. Chip ceramic capacitors were used for tuning and served to provide DC blocking also.

Results: The computed response in terms of $|S_{21}|$ for a 4-element filter of the above design is shown in Fig. 3. It will be noted that the crossover for forward and reverse bias occurs when $|S_{21}| = 0{\cdot}707$, at the 3 dB designed corner frequencies of 2·6 and 3·4 GHz.

Experimental results obtained for this filter are shown in Fig. 4, which indicates a fair measure of overall agreement but with serious discrepancies in detail. Principal of these are shifts

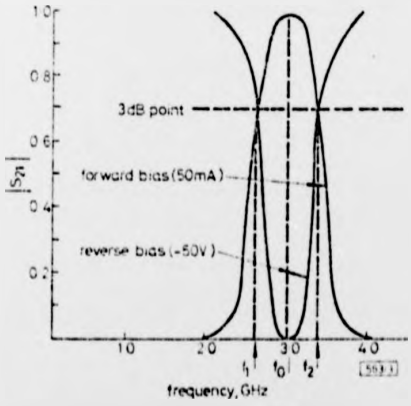

Fig. 3 *Computed response of filter shown in Fig. 1*

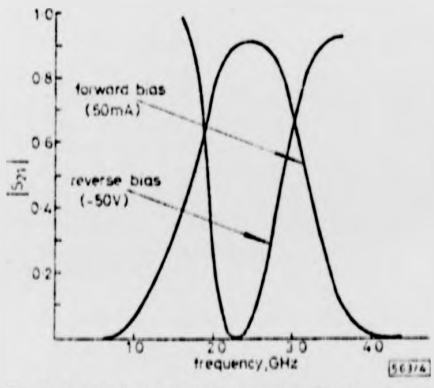

Fig. 4 *Measured response of filter shown in Fig. 1*

in centre frequency from a designed value of 3 GHz for both states to approximately 2·4 GHz for the stopband and 2·6 GHz for the passband. The measured bandwidths are correspondingly 41% and 33%, compared with the designed value of 26·7%. Further, the maximum transmission is only 0·92 for the bandpass state but reaches 0·99 in the bandstop condition.

Comments: There are several factors contributing to the discrepancies observed, including imperfections of connectors (Scalectro SMA 645 4575), neglect of line losses and the effect of the meander-line bends. Preliminary investigations indicate that these are significantly frequency-dependent, mitred bends, as used in the example, being superior to simple right-angled bends but not so good as others having a circular curvature.

Acknowledgment: This work was supported by the Nigerian Ministry of Communications.

G. N. O. UGWUAGU
H. V. SHURMER

Department of Engineering
University of Warwick
Coventry CV4 7AL, England

17th July 1981

References

1 ZYSMAN, G. I., and JOHNSON, A. K.: 'Coupled transmission line networks in an inhomogeneous dielectric medium', *Proc. IEEE*, 1969, **MTT-17**, pp. 753–758
2 COHN, S. B.: 'Shielded coupled strip transmission line', *ibid.*, 1955, **MTT-3**, pp. 29–38
3 MAKIMOTO, M., and YAMASHITA, S.: 'Bandpass filters using parallel coupled stripline stepped impedance resonators', *ibid.*, 1980, **MTT-28**, pp. 1413–1417
4 KATO, S., SEMOTO, Y., SATO, R., and SAGASAWA, T.: 'A design method of meander-line type delay line' *IECE Trans.*, 1975, **58-A**, pp. 25–32
5 HOWE, H.: 'Stripline circuit design' (Artech, Dedham, 1974)
6 GUPTA, K. C., GARG, R., and BAHL, I. J.: 'Microstrip lines and slotlines' (Artech, Dedham, 1979)
7 DYDYK, M.: 'Master the T-junction and sharpen your MIC design', *Microwaves*, 1977, **16**, pp. 184–186

0013-5194/81/190702-02$2.50/0

$In_{0.53}Ga_{0.47}As$ CONTACT LAYER FOR 1·3 μm LIGHT-EMITTING DIODES

Indexing terms: Light-emitting diodes, Semiconductor devices and materials

Measurements of the specific contact resistance on epitaxially grown layers of p-$In_{1-x}Ga_xAs_yP_{1-y}$ as a function of composition demonstrate the resistance minimum of 7×10^{-8} Ωcm² for $In_{0.53}Ga_{0.47}As$. Growth procedures for the preparation of InGaAsP/InP double-heterostructure LED wafers incorporating such a ternary InGaAs contact layer are described. This contacting technique allows fabrication of high-performance devices with reproducibly low series resistance.

The performance of optical communication systems based on light-emitting diodes (LEDs) can be greatly improved with devices fabricated out of $In_{1-x}Ga_xAs_yP_{1-y}$ alloys lattice-matched (i.e. with $y/x \approx 2{\cdot}2$) to InP. Data rates as high as 274 Mbit/s (T4) and repeater distances of many kilometres have been achieved with LEDs operating near 1·3 μm.[1] This spectral region corresponds to the dispersion minimum of silica-based fibres, and the quaternary LEDs, unlike their $Ga_{1-x}Al_xAs$ ($\lambda = 0{\cdot}82$ μm) counterparts, are power-limited in most of the applications at present envisaged. The high power launched into optical fibre required for system applications can be achieved by decreasing the size of the light-emitting area and increasing the drive current. This presents ever more stringent demands on the *p*-type metallisation since the light spot is

MEANDER-LINE FILTERS INCORPORATING P I N DIODES

G.N.O. Ugwuagu and H.V. Shurmer

INTRODUCTION

Technological advances in the utilization of microwave frequencies for air surveillance, communications and other aspects of telecommunication have resulted in a growing interest in the development of rf filters which can be used in frequency discrimination and selection. Such filters when connected in series or parallel are often needed in order to split a single channel carrying many frequencies into a number of channels carrying narrower band of frequencies. In this paper a compact stripline structure which can be used for a wide band switchable multiplexer is discussed. The basic element is a meander-line incorporating p·i·n diodes inside the meander loops. The diodes serve to provide either open or short circuit terminations to the meander stubs, depending on the bias applied to them. With the diodes forward biased, a bandpass filter results, but under reverse bias, the bandpass is converted to bandstop. A cascade of these filters is used in a 3-channel frequency multiplexer.

ANALYSIS & DESIGN

The meander-line is analysed in terms of the coupling capacitances between the lines. Knowledge of the voltage coupling ratio enables the even and odd mode characteristic impedances and hence the dimensions of the lines to be determined. The lines are quarter wavelength at the centre frequency. For switching purposes, the pin diodes are mounted at the ends of the stubs which are connected inside the meander-loops. In an earlier design[1], stagger tuning techniques were employed to obtain maximum isolation and hence minimum impedance termination when the diodes are forward biased. Choice of the respective resonant frequencies to give the required ripple response proved a problem. Here the p·i·n diodes are made to approximate more closely to an ideal open and short circuit termination by transforming the reflection coefficient appearing at the input to the stub network when it is terminated by the respective forward and reverse bias impedance states of the diode.

Figure 1(a) shows the configuration of a single channel 4-element filter employing two diodes. Using the measured forward and reverse biased impedances of the diodes, the appropriate transforming circuits were designed using the procedures outlined by Atwater[2] for the case of an amplitude modulator. The reflection coefficient magnitude (Γ_1) for the low-level state of the diode is arbitrarily assigned a value of 0.01. It is assumed that an amplitude transition with no phase-shift exists between the reflection coefficient magnitudes in the "OFF" and "ON" states respectively. For the example of fig. 1(a), the computed

G.N.O. Ugwuagu and H.V. Shurmer are with the Department of Engineering, University of Warwick, Coventry.

reflection coefficient magnitude in the high-level state was 0.97 giving a switching ratio of more than 39dB. An appropriate matching transformer to achieve this value was computed to have the following dimension:- ℓ_m = 32.6 ℓ_m = 8.8mm. It must be remembered that in all cases the total length of the stub and the transformer must be equal to $\lambda_g/4$.

The right angle bend at each meander junction is chamfered to compensate for the parasitic reactances associated with that discontinuity. The effects of the discontinuity caused by the T-junction formed by the stubs and the main arms of the meander-line were characterized using the empirical expressions of Garg and Bahl[3]. Polyguide triplate of 1.59mm thickness was used as the substrate material. The diodes used are MEDL type DC 2418A. Each diode package was located in a slot milled into the substrate to a depth permitting the connecting leads to be aligned with the conductors. Good heat transfer was ensured by the aluminium backing the substrate. Bias signal is applied to the diodes via a three-section low-pass filter. Chip ceramic capacitors were used as DC blocks.

RESULTS

The computed response of the single-channel filter of fig.1(a) in terms of $|S_{21}|$ is shown dotted in fig. 1(b). It will be noted that the crossover for the forward and reverse bias states occurs when $|S_{21}| = 0.707$ i.e. at the 3dB designed corner frequencies of 2.6 and 3.4 GHz. Experimental result for this filter indicates a fair measure of the overall agreement. The measured bandwidths are correspondingly 41% and 33% compared to the designed value of 26.7%. Further the transmission is only 0.92 in the bandpass state and 0.02 in the bandstop state as compared to the computed values of 0.97 and 0.015 respectively. The computed response of the 3-channel multiplexer is shown in fig.2.

REFERENCES

1. UGWUAGU, G.N.O.; and SHURMER, H.V.; "P•i•n Diodes in Meander-line filters for multiplexing applications", Electronics Letters, Vol.17, No.19 Sept. 1981 pp.702-703.

2. ATWATER, H.A.; "Impedance transformation for the generalized reflection modulator", IEEE Trans. 1981 Vol. MTT-29, No.3 pp.229-234.

3. GARG, R.; and BAHL, I.J.; "Microstrip Discontinuities", Int. J. Electronics, Vol.45 July 1978 pp. 81-87.

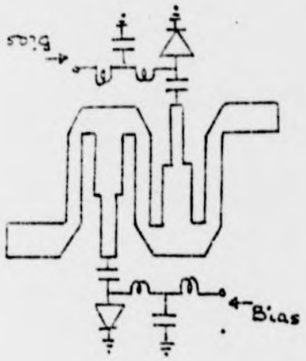

Fig. 1(a) PIN Diode Switchable Filter

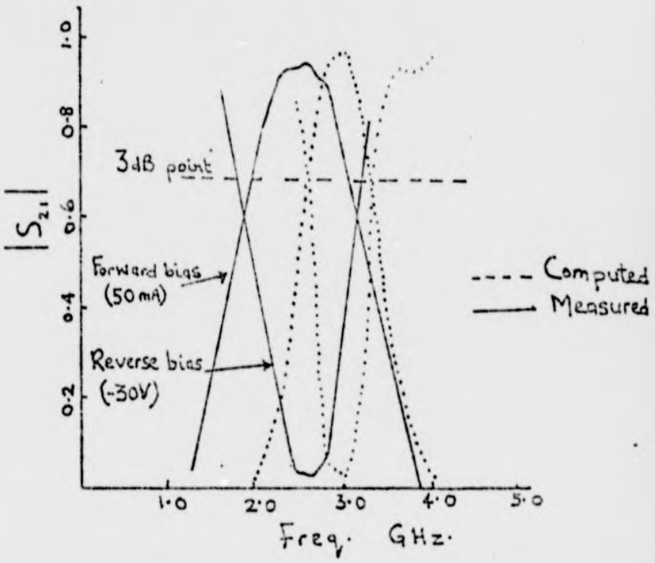

Fig. 1(b) Computed & Measured response

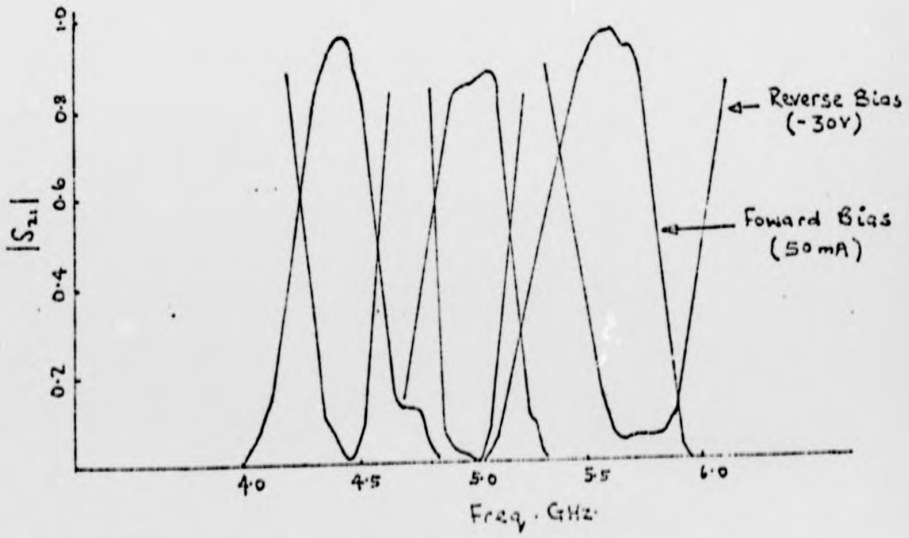

Fig. 2. Response of 3-Channel Filter

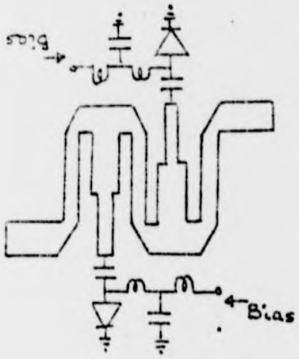

Fig. 1(a) PIN Diode Switchable Filter

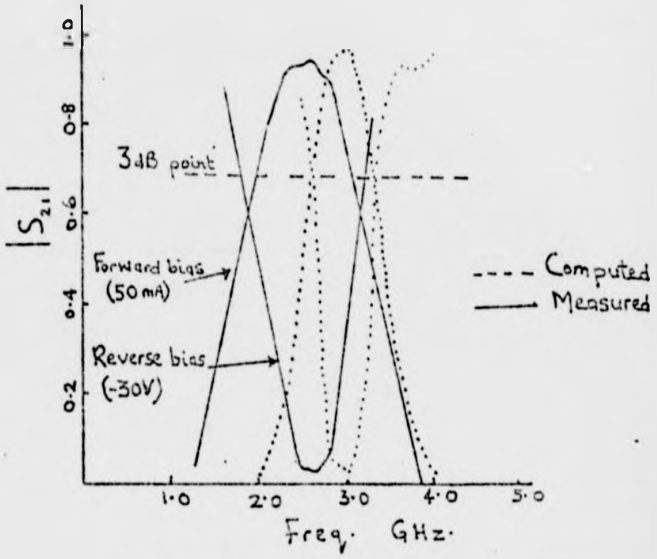

Fig. 1(b) Computed & Measured response

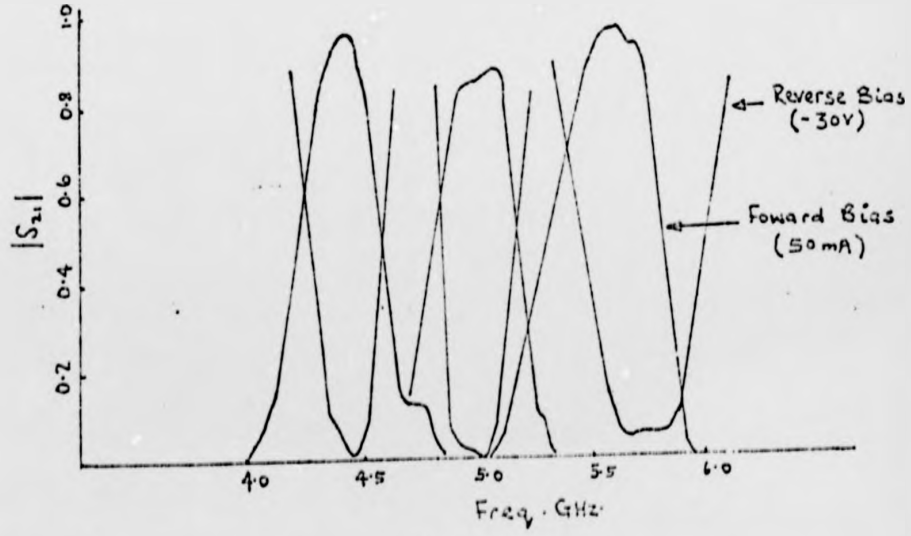

Fig. 2. Response of 3-Channel Filter